HEINRICH HEINE
UNIVERSITÄT DÜSSELDORF

Role of C2 domain protein EHB1 in Arabidopsis iron uptake

Inaugural-Dissertation

zur Erlangung des Doktorgrades
der Mathematisch-Naturwissenschaftlichen Fakultät

der Heinrich-Heine-Universität Düsseldorf

vorgelegt von

Imran Khan

Aus Malakand, Pakistan

Düsseldorf, April 2018

aus dem Institut für Botanik

der Heinrich-Heine-Universität Düsseldorf

Gedruckt mit der Genehmigung der
Mathematisch-Naturwissenschaftlichen Fakultät der

Heinrich-Heine-Universität Düsseldorf

Berichterstatter:

1. Prof. Dr. Petra Bauer

2. Prof. Dr. Rüdiger Simon

Tag der mündlichen Prüfung:

Acknowledgements

Firstly, I would like to express my sincere gratitude to my supervisor **Prof. Dr. Petra Bauer** for the continuous support of my Ph.D study and related research, for her patience, motivation, and immense knowledge. Her guidance helped me in all the time of research and writing of this thesis. I could not have imagined having a better advisor and mentor for my Ph.D study. She kindly helped me to obtain financial support during my prolongation.

I am also thankful to **Prof. Dr. Rüdiger Simon** for accepting of my Ph.D supervision and for the correction of my dissertation.

I would like to thank the German Academic Exchange Service (Deutscher Akademischer Austausch Dienst, **DAAD**) for their financial support granted through my Ph.D.

My special thanks goes to **PD.Dr. Rumen Ivanov** for his kind support and guidance throughout my studies. Without his mentorship this journey would be a lot difficult and long.

I thank **Dr. Hans-Joerg Mai** and **Dr. Tzvetina Brumbarova** who were always there to assist me and answer all of my questions. Many thanks to all my colleagues and members of my group for all the nice time and special occasions. Special thanks goes to my colleague **Heithem** for help and encouragement during my studies. Thanks to my bachelor student **Lara Genders** for helping in the BiFC experiment. Thanks to **Ulrike, Angelika, Elke, Ginte** and **Kai** for all the technical support.

A very special thanks to my father and role model **Salah-u-din** for his support and trust. Thanks to my master thesis supervisor **Dr. Muhammad Sayyar Khan** for his guidance in obtaining Ph.D funding.

Thanks to my siblings, friends and all family members for supporting me spiritually throughout my studies and in my life in general.

Last but not the least, I want to thank my wife **Afshan Khan** for her consistent help and support during all my hard times.

I dedicate this thesis to my Late mother **Johar Sani**.

Abbreviations

AHA2	Arabidopsis H^+-ATPase 2
A. thaliana	*Arabidopsis thaliana*
ATM1p	ABC Transporter Mitochondria 1 Protein
bHLH	Basic Helix Loop Helix
BiFC	Bimolecular fluorescence complementation
BTS	BRUTUS
C2	Conserved 2
CAR	C2-DOMAIN ABSCISIC ACID-RELATED
CBL	Calcium binding loops
Co-IP	Co-immunoprecipitation
CPL1	C-TERMINAL DOMAIN-LIKE PHOSPHATASE 1
DW	Dry weight
EDTA	Ethylenediaminetetraacetic acid
EE	Early endosome
EHB1	ENHANCED BENDING 1
EIL1	EIN3-LIKE1
EIN3	ETHYLENE INSENSITIVE 3
ET	Ethylene
FeNa-EDTA	Ferric Sodium EDTA
FER	FERRITIN
FIT	FER-Like Iron Deficiency Induced Transcription Factor
FRD3	Ferric chelate Reductase Defective 3
FRO2	FERRIC REDUCTASE OXIDASE 2
FW	Fresh weight
GA	Gibberellic acid
GAP1	GTPase-activating protein 1
GE	Genetic engineering
GFP	Green fluorescent protein
GPI	Glycosylphosphatidylinositol
GRF11	GENERAL REGULATORY FACTOR 11
HA	Hemagglutinin

IAA	Auxin
ICP-OES	Inductively coupled plasma optical emission spectrometry
IDF1	IRT1 DEGRADATION FACTOR 1
IPTG	Isopropyl *β*-D-1-thiogalactopyranoside
IRT1	IRON REGULATED TRANSPORTER 1
MA	Mugineic acid
MATE	Multidrug and Toxic compound Extrusion
MCTPs	Multiple C2 domain and transmembrane region proteins
MED	Mediator
MYB	Myeloblastosis
NA	Nicotianamine
NRAMP	NATURAL RESISTANCE-ASSOCIATED MACROPHAGE PROTEIN
PC	Phosphatidylcholine
PCC	Pearson's correlation coefficient
PCR	Polymerase Chain Reaction
PH	Pleckstrin homology
PI	Phosphoinositide
PKC	Protein kinase C
PLD	Phospholipase D
PM	Plasma membrane
PS	Phytosiderophores
PtdIns(4)P	Phosphatidylinositol 4-phosphate
Ptdlns(4,5)P2	Phosphatidylinositol 4, 5-bisphosphate
Ptdlns(3,4,5)P3	Phosphatidylinositol 3, 4, 5 trisphosphate
PX	Phox
PYE	POPEYE
QKY	QUIRKY
RCF3	REGULATOR OF CBF GENE EXPRESSION 3
ROS	Reactive oxygen species
RT-qPCR	Reverse transcription quantitative PCR
SDS-PAGE	Sodium dodecyl sulfate-polyacrylamide gel electrophoresis
SKB1	SHK1-BINDING PROTEIN1

SNX1	SORTING NEXIN 1
STA1	STARIK 1
TF	Transcription factor
TGN	Trans Golgi network
TOM1	Transporter of mugineic acid 1
TMDs	Transmembrane domains
VIT1	Vacuolar iron transporter 1
WT	Wild type
WHO	World health organization
Y2H	Yeast two-hybrid screen
YS1	Yellow stripe 1
YSL	Yellow stripe 1-like
ZIP	ZRT, IRT-like Protein

Table of content

Statement of declaration:

I, **Imran Khan**, hereby declare that I have fully and independently written the submitted dissertation without additional unauthorized support and consultation beyond that permitted and specified in the dissertation to include the necessary and appropriate cited literary resources. I confirm that this thesis presented for the degree of has not been submitted for any other degree or professional qualification. I played a major role in the preparation of the experimental work, data analysis, Interpretation, preparation of figure and writing of dissertation.

The work was done under the guidance and the supervision of **Prof. Dr. Petra Bauer** at the Institute of Botany HHU, Dusseldorf, Germany.

Düsseldorf, April 10, 2018

Abstract

Iron is an essential constituent of many important proteins involved in a number of metabolic processes. Its ability to change its redox state is an important aspect of its function. The IRON-REGULATED TRANSPORTER1 (IRT1) a member of an evolutionarily ancient ZIP family of divalent metal zinc and iron permeases, controls the entry of iron into roots of the model plant Arabidopsis (*Arabidopsis thaliana*). Monitoring of the activity of IRT1 is critically important for the prevention of oxidative stress for plant survival. Here, we present the characterization of the IRT1-interacting peripheral membrane protein ENHANCED BENDING1 (EHB1). Using different approaches, we show that EHB1 interacts via its signature domain with specific helices in the cytosolic variable region of IRT1. We demonstrate the cytoplasmic localization of EHB1 and its colocalization with plasma membrane markers. In addition, we could show that EHB1 also colocalized with IRT1. Furthermore, we report that EHB1 binds membrane phospholipids. Plants with loss of EHB1 function, show elevated responses to iron deficiency and enhanced acquisition and storage of iron. These data show that EHB1 suppresses the import of apoplastic iron and seed iron content of the plant. EHB1 loss-of-function changes the expression pattern of iron deficiency-related genes. All these observations strongly suggest that EHB1 plays a role in negatively regulating IRT1-mediated iron acquisition. EHB1 may achieve this by direct and specific inhibition of IRT1 capacity to import iron into the cell. Inhibition of IRT1-mediated iron import is important because overaccumulation of iron can cause significant damage to the plant cell.

Zusammenfassung

Eisen ist ein essentieller Bestandteil vieler wichtiger Proteine, die in unterschiedlichen Stoffwechselprozessen involviert sind. Die Fähigkeit von Eisen, seinen Redoxstatus zu ändern, ist eine seiner wichtigsten Eigenschaften. Die Metal/Zink Permease IRON-REGULATED TRANSPORTER1 (IRT1), ein Mitglied der ZIP Familie, kontrolliert die Aufnahme von Eisen in die Wurzel der Modellpflanze Arabidopsis (*Arabidopsis thaliana*).

Die Kontrolle der Transporteraktivität von IRT1 ist wichtig, um die Pflanze vor oxidativem Stress zu schützen. In dieser Arbeit wird das mit IRT1 interagierende periphere Membranprotein ENHANCED BENDING1 (EHB1) vorgestellt und untersucht.

Unter Anwendung verschiedener Methoden konnte gezeigt werden, dass die Signaturdomäne von EHB1 mit bestimmten Bestandteilen der variablen Region von IRT1 interagiert. Wir zeigen die ztoplasmatische Lokalisation von EHB1 und dessen Kolokalisation mit Plasmamembran-Markern. Zusätzlich konnte gezeigt werden, dass EHB1 mit IRT1 kolokalisiert und Membranphospholipide bindet.

Pflanzen mit EHB1 Funktionsverlust zeigen eine starke Antwort auf Eisenmangel und speichern mehr Eisen als Pflanzen mit intaktem EHB1. Der Verlust der Funktion von EHB1 führt zu veränderter Expression von Genen, die an der Eisenmangelantwort beteiligt sind. Außerdem zeigen einige Daten, dass funktionales EHB1 die Aufnahme von Eisen aus dem Apoplasten und die Einlagerung von Eisen in den Samen verhindert.

Dies weist darauf hin, dass EHB1 als negativer Regulator eine wichtige Rolle in der Eisenaufnahme von IRT1 spielt. Dies könnte durch direkte und spezifische Hemmung des Eisentransports durch IRT1 geschehen. Die Regulation des Eisentransports durch IRT1 ist essentiell für die Pflanze, da eine zu hohe Konzentration von Eisen toxisch ist und die Pflanzenzelle schädigen könnte.

1. Introduction

1.1 Physiological Importance of iron for living beings

It is of vital importance that living organisms get enough nutrients in the diets for survival and to remain healthy. According to the definition, nutrients are chemicals that are required by living organisms to pursue their survival (Holst and Williamson, 2008). Different foods that humans eat in their daily routine contain different nutrients which provide minerals and vitamins to perform the daily tasks properly. Animals rely on different sources to obtain the major nutrients like carbohydrates, proteins, lipids, minerals, and vitamins (Holst and Williamson, 2008; Gropper and Smith, 2012).

Lack of essential nutrients in the human diets leads to many health-related issues, therefore, a balanced nutrition is very important. The condition in which the intake of essential nutrients is non-proper or completely lacking is called undernourishment (Naranjo-Arcos and Bauer, 2016). Undernourishment (Malnutrition and micronutrient deficiencies) continues to be a major problem regarding public health in the third world or developing countries. The daily diets in these countries are very often deficient in macro- and micronutrients which is a risk factor for illness and death globally. The major malnutrition in these countries are deficiencies in iodine, Zn, Fe, and vitamin A. These deficiencies cause impaired physical and brain development particularly in pregnant women, infants and young children (Müller and Krawinkel, 2005).

According to the WHO 2010 figures, around 104 million young children globally are underweight due to malnutrition (WHO, www.who.int/nutrition/challenges/en/). 13 million children are born prematurely or with low birth weight due to maternal undernourishment and other related factors which are very common in many developing countries. Maternal undernourishment is also a primal cause of poor fetal development and of many other complications during pregnancy (De Onis et al., 2012). As of 2012 WHO figures an estimated 162 million children under age 5 were stunted. Lack of indispensable vitamins and minerals in the diet largely affect immunity and healthy development and it can lead to irreversible mental and physical damage (Hoddinott et al., 2008). So, undernourishment in every form, causing significant threats concerning human health.

Currently, around 795 million people or 1 out of 9 in the world do not have enough food to live an active and healthy life. Out of these 795 million, 98% (525.6 million) people belong to developing countries of Asia, and they are facing the worst hunger condition, 214 million in Sub-Saharan Africa and 37 million people in Latin America and the Caribbean are also suffering from hunger (FAO).

Hunger sets poverty traps, the victims of poverty do not have the opportunities to enhance their lives because they are affected physically and psychologically. They find themselves trapped in a vicious cycle of hunger-poverty-hunger. People living in poverty live on less than $1.90 USD per day struggle to afford a healthy food to feed themselves (Ferreira et al., 2015). Majority of the poor people are farmers who entirely depend on cereal crops (rice or maize) which are poor sources of key mineral nutrients (Zhu et al., 2007). This cycle of hunger and poverty needs to be broken to improve the economic status of the poor people of the world. Ultimately which will help them to improve their living standards and they will get rid of the food insecurity (malnutrition) and with this, the society can become healthy.

1.1.1 Impact of iron malnutrition

According to world health organization, Iron-deficiency is one of the most frequent nutritional disorders in humans threatening health worldwide (Benoist et al., 2008). Anaemia, one of the fatal disease for humans is caused due to lack of iron. It is one of the central factors causing disability (in all age groups) and death globally. In total, over 1.6 billion people (24.8% of the world's population) are affected by iron-deficiency. The highest prevalence has been observed in preschool-age children and the lowest prevalence has been found in men (Organization, 2015). The risk of iron deficiency is very high especially in the poor countries of the world where it leads to significant health issues like poor pregnancy outcome and due to the poor health condition of the population, it also causes severe economic problems (Zimmermann and Hurrell, 2007).

There are three main strategies to tackle malnutrition: increase in diversity of food intake, food supplementation and biofortification of food crops (Gómez-Galera et al., 2010). The easy way to control malnutrition will be to increase the diversity in food intake i.e. to give people access to have diverse food in their diet. But unfortunately, this is impractical in many developing countries due to the bad economic status of the societies. Secondly, food supplementation is also not an ideal approach because

it has certain limitations, such as it needs a fast and robust distribution infrastructure. and the in-country resources available to develop the infrastructure which can help deliver the supplemented food to the consumers living in the remote areas in the developing countries are not enough (Hotz and Brown, 2004).

Finally, biofortification of food crops with metals can be performed, which are able to accumulate additional nutrients (Zhu et al., 2007). Biofortification of plants can be achieved by increasing the level of nutrients in fertilizers. This approach has been successfully practicing to augment the availability of Zn and Se (Lyons et al., 2003). Unfortunately, this strategy is not suitable to fortify iron in plants, because it depends on the mobility of the metal in soil and iron tends to be present in the soil in immobilized form (Gómez-Galera et al., 2012; Zhu et al., 2013). Conventional plant breeding can be used to obtain such a traits which might have elevated level of metals or other important organic nutrients (vitamins and essential amino acids) but the problem with conventional plant breeding is it needs a lot of time and it would take many generations to introgress these traits into the local varieties (Welch and Graham, 2005; Pérez-Massot et al., 2013).

An alternative and the most suitable approach to fortify organic nutrients of plants is genetic engineering (GE) technology. GE can be used to introduce genes from any other source to generate either transgenic (the introduced gene comes from another species) or cisgenic plants (the introduced gene comes from the same species) (Schouten et al., 2006; Pérez-Massot et al., 2013). Transgenic strategies to improve the mineral content of crop plants are mainly used for fortification of Fe and Zn which are considered to be the most prominent and frequently occurring deficiencies in human diets. In transgenic biofortification of iron and other minerals, it is important to not only improve the efficiency of uptake and transport to edible plant parts but to enhance the amounts of bioavailable minerals for assimilation in humans (Zhu et al., 2007; Naranjo-Arcos and Bauer, 2016).

Iron-deficiency symptoms can normally be treated and reversed easily by medical iron supplement and by consuming iron-rich solid foods, such as red meat and legumes (European Food Information Council, www.eufic.org). However, in poor countries, people with low income cannot afford such a diet. For them plants are the main source for fulfilling their nutritional requirements of iron, In this context, using

biofortification to increase the iron content of crops is a helpful strategy to facilitate supply of adequate amount of this micronutrient to people in the developing world (Meenakshi et al., 2010; Schuler et al., 2012).

The primary crops which are currently being biofortified for iron and other minerals include some very important staple crops in the developing countries: rice (*Oryza sativa*) (Qu et al., 2005; Masuda et al., 2013), wheat (*Triticum*) (Borrill et al., 2014) and cassava (*Manihot esculenta*) (Ihemere et al., 2012). To date, rice is the main focus for biofortification with iron. Rice has been engineered to express genes which are involved in iron accumulation or with genes which encodes iron storage protein, ferritin. This results in a many-fold increase in iron accumulation and storage (Vasconcelos et al., 2003; Qu et al., 2005; Masuda et al., 2013). Another important crop, which is subjected to biofortification is cassava. After rice and maize, cassava is the third largest source of calories for more than 800 million people worldwide and it serves as a staple crop for 300 million people in sub-Saharan Africa (Moser, 1989; Sayre et al., 2011). The iron content in cassava storage root has been increased from 10 to 36 ppm by introducing an iron assimilatory gene (*FEA1*) from green algae to cassava. This amount is sufficient to cover the minimum daily requirement of iron in 500 g meal (Ihemere et al., 2012).

It is known that both, deficiency and overexposure to certain elements, have noticeable effects on living organisms (humans, plants, and microorganisms). As iron can produce reactive radicals (reactive oxygen species, ROS), its concentration in tissues must be tightly regulated because the excessive amount can lead to tissue damage (Abbaspour et al., 2014). ROS can damage DNA, lipids (degradation of unsaturated lipid components) and proteins which leads to the damage of membranes and various cellular organelles (Peterson, 1991; Brewer, 2009).

1.1.2 Effects of iron-deficiency in plants

The majority of iron that plants acquire comes from the rhizosphere. Besides the fact that iron is the fourth most abundant metal in the earth's crust it is not readily available for the plant to be taken up (Connolly and Guerinot, 1998). Iron availability is controlled by the redox potential and pH of the soil. Soil having high pH oxidizes the iron easily and convert it to the insoluble ferric oxides. When the pH decreases, ferric iron is liberated from the oxide and it becomes available and reduced (ferrous)

for the plant roots to be taken up (Morrissey and Guerinot, 2009). Increasing the pH by a single unit can lower the iron solubility by 1000 times (Lindsay, 1995).
Iron is considered a very important element for almost every living being. In plants, it is present in many enzymatic systems essential for metabolism (Martínez-Cuenca et al., 2017). These include cytochrome complex, involved in the transport of energy in the redox system of chloroplasts and mitochondria (Marschner, 1995), ferredoxin an electron acceptor in photosynthesis and nitrate reduction (Marschner, 1995; Lawlor, 2004) and many others. Apart from this, iron is also important for DNA synthesis, photosynthesis, and respiration (Rout and Sahoo, 2015).

Iron deficiency can affect plants in many ways such as it can induce morphological and cytological changes in both shoot and roots. In non-graminaceous plants, iron starvation leads to increased root hair formation and thickness of the root cortex (Kramer et al., 1980; Landsberg, 1986). Electron microscopy showed that following 24-48 h of iron-deficiency, the rhizodermal cells of *Helianthus annuus* were differentiated into transfer cells, which are characterized by a dense cytoplasm (having many mitochondria, extensive rough endoplasmic reticulum, and large leucoplast) and a protruded mazy cell wall. Transfer cells are capable of promoting mineral absorption because of having a high internal plasmalemma surface (Kramer et al., 1980). Transfer cells are not present in graminaceous plants (Römheld and Kramer, 1983).

In shoots, the obvious symptoms of iron deficiency are yellowing of younger leaves, also known as leaf chlorosis. Chlorosis of leaves occurs due to the impaired formation of chloroplast pigments (Gruber and Kosegarten, 2002). Structural studies suggest that the chloroplast becomes disorganized because the number of grana and stroma decreases (Spiller and Terry, 1980; Yamaguchi-Iwai et al., 1995). Due to Iron starvation, the structure of mitochondria also becomes disorganized. Sycamore (*Acer pseudoplatan s L*) cells grown for 10 days in iron-deficiency condition showed disorganized mitochondria (Pascal and Douce, 1993). Such a phenomenon of mitochondrial disorganization was also observed for maize plantlets (Briat et al., 1995).

Limited iron conditions affect plants biochemically and physiologically by altering its metabolism. The change in metabolic activity could be due to low Fe but also, the

increased concentration of other minerals like Zn, Mn and Cu in roots and shoots. The increase in the concentration of these metals could either be due to increase in their uptake by metal-transporter or could be due to the low biomass production of plants (Welch et al., 1993; von Wirén et al., 1994). It has been shown that the exudation of organic compounds by roots is enhanced during iron-limited conditions (Marschner, 2011). Among these, phenolics are the most prominent compounds secreted by non-graminaceous dicots and monocots (Dakora and Phillips, 2002; Neumann and Römheld, 2007). It has been speculated that these compounds could contribute to iron reduction because they exhibit the ability of chelation and reduction (Rodríguez-Celma et al., 2013a).

1.2 Fe uptake strategies of plants

To date, at least two iron uptake strategies exist in the plant kingdom which helps them in iron mobilization in the rhizosphere and uptake (Marschner et al., 1986).

1.2.1 Reduction-based strategy (Strategy I)

All dicots and monocots except grasses have adopted Strategy I for iron mobilization and uptake from the immediate rhizosphere. In the model plant *Arabidopsis thaliana* the acquisition of iron takes place through Strategy I (Fig. 1.1 left.). Arabidopsis is a small flowering plant belonging to Brassicaceae family and is used as a model system in the field of plant biology. It has a small genome size, fully sequenced genome, short life cycle and it produces a large number of seeds. Beside these, it can be transformed easily and a large number of mutant lines are available commercially (TAIR, www.arabidopsis.org). Strategy I in Arabidopsis is a three-step process and is based on the activity of plasma membrane proteins in root epidermis cells. In the first step, the iron in soil has to be solubilized. This happens via proton extrusion by the plasma membrane (PM) localized Arabidopsis H^+-ATPase (AHA2) which leads to the acidification of the local rhizosphere (Santi and Schmidt, 2009; Brumbarova et al., 2015). *AHA2* belongs to the multigene family encoding an H^+-ATPase. In Arabidopsis, this family consists of 12 genes (Palmgren, 2001). It has been reported that with each unit of increase in the pH the solubility of iron decreases up to 1000-fold (Lindsay, 1995). Thus the acidification of the root vicinity by *AHA2* can have a substantial effect on iron solubility (Santi and Schmidt, 2009).

The solubilized iron is present in the ferric state (Fe^{3+}). To be imported into the plant by IRON-REGULATED TRANSPORTER 1 (IRT1), it has to be reduced to ferrous

iron (Fe^{2+}). This reaction is catalyzed by the FERRIC REDUCTASE OXIDASE (FRO) family protein FRO2. The mutant (*frd1*) which lacks *FRO2* activity has the ability to acidify the rhizosphere but it does not have the ability to reduce Fe^{3+} during iron deficiency (Yi and Guerinot, 1996; Robinson et al., 1999). In Arabidopsis, the FRO family of genes consists of 8 members (Mukherjee et al., 2006). This step of iron acquisition is assumed to be the rate-limiting one (Robinson et al., 1999). The import of reduced iron is performed by a member of the ZIP (Zinc-regulated transporter, Iron-regulated transporter-like Protein) family of metal transporters, (IRT1) (Eide et al., 1996; Vert et al., 2002).

The two steps of iron reduction and its import are greatly facilitated when Fe exists in a chelated form. Chelators are released by the roots to achieve this state. The type of chelator is species-specific. Arabidopsis mainly uses phenolic compounds like scopoletin which are exported by the ABC family transporter ABCG37 (Rodríguez-Celma et al., 2013a; Fourcroy et al., 2014; Schmid et al., 2014).

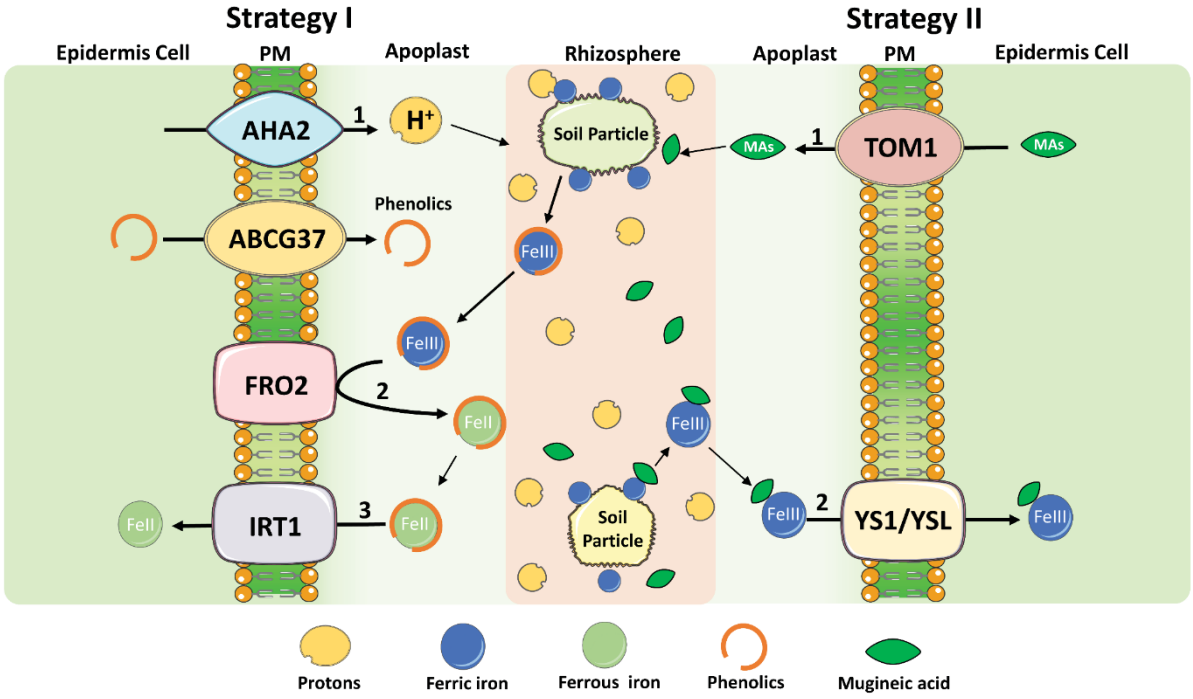

Figure 1.1. Iron uptake strategies in plants. On the left is Strategy I in non-graminaceous plants and on the right, is Strategy II in graminaceous plants. Different shapes represent different genes, transporters, and enzymes which plays important roles in these strategies. Abbreviations; PM, Plasma membrane; AHA2, Arabidopsis H^+-ATPase 2; FRO2, FERRIC CHELATE REDUCTASE OXIDASE; IRT1, IRON-REGULATED TRANSPORTER 1; YS1/YSL, YELLOW STRIPE 1/YELLOW STRIPE 1-like; TOM1, transporter of mugineic acid 1; MAs, mugineic acid (Eide et al., 1996; Kobayashi and Nishizawa, 2012; Fourcroy et al., 2014; Brumbarova et al., 2015).

1.2.2 Chelation-based strategy (Strategy II)

Members of the Poacea family employ a chelation-based strategy, named Strategy II. For chelation of ferric iron, the plants synthesize and secrete small metabolites called Phytosiderophores (PS). The chelator makes a complex with Fe^{3+} and this complex is then transported into the cell via a specific plasma membrane-localized transporter (Fig. 1.1 right.). The PS are synthesized from methionine and usually belong to the mugineic acid family (MAs) (Mori and Nishizawa, 1987). 9 types of MAs have been identified until now, all of which are synthesized from *S*-adenosyl-L-methionine (Shojima et al., 1990; Bashir et al., 2006). The MAs are transported to the rhizosphere through transporter of mugineic acid family phytosiderophores 1 (TOM1) (Nozoye et al., 2011). The MAs in the rhizosphere solubilize Fe^{3+} by making complexes with them (chelation). These MAs-Fe^{3+} complexes are transported into the root epidermal cells via the plasma membrane-localized YELLOW STRIPE 1 (YS1) in maize and by YELLOW STRIPE 1 LIKE (YSL) in barley (Fig. 1.1 right.) (Curie et al., 2001; Murata et al., 2006).

Despite being a Strategy II plant, rice also has the ability to take up Fe^{2+} because it also possesses the OsIRT1 transporter. The ferric chelate reductase activity in rice is very low compared to Strategy I plants suggesting that it can only transport the already reduced Fe^{2+} which is present in large quantity in aerobic and submerged conditions (Ishimaru et al., 2006).

Since our research was based on the model plant *Arabidopsis thaliana*, we focused on the regulation of iron homeostasis in Strategy I plants.

1.3 Long-distance transport of iron

Following the initial uptake into the root epidermal cells, iron must be transported to the shoots through the xylem (Conte and Walker, 2011). To prevent precipitation of iron in vascular tissues and to hinder it from taking part in the generation of hydroxyl radicals, it is believed that iron forms complexes with various chelators in the root vasculature (Kim and Guerinot, 2007; Morrissey and Guerinot, 2009). The binding of the chelator with iron is dependent on its surrounding environment, in the xylem at pH 5.5-6 iron binds with citrate and in the phloem, at pH 7.5 it binds nicotianamine (NA) (Kim and Guerinot, 2007; Curie et al., 2009).

In root epidermal cells, Fe^{2+} forms complexes with the chelator NA. This Fe^{2+}-NA complex then moves towards the xylem symplastically through intercellular connections in root cells due to a concentration gradient (Stephan et al., 1996;

Marschner, 2011). Once it reaches the pericycle, Fe^{2+} is effluxed into the xylem. The mechanism of Fe efflux to the xylem is still not clearly understood (Kim and Guerinot, 2007). Upon entering the xylem, Fe is oxidized to Fe^{3+} and then this oxidized form (Fe^{3+}) is chelated by citrate (Tiffin, 1966). The transfer of iron from NA to citrate occurs at pH 5.5-6 resulting in the formation of iron-citrate transport species (López-Millán et al., 2000). From the xylem iron moves towards the shoot along the transpiration stream (Morrissey and Guerinot, 2009).

Citrate appears to be transported into the xylem by FRD3 (Ferric chelate Reductase Defective 3), which belongs to the Multidrug And Toxic compound Extrusion (MATE) transporter family that is involved in the transport of small molecules (Rogers and Guerinot, 2002; Durrett et al., 2007). The expression of *FRD3* occurs in the pericycle and vascular cylinder of the root, which is an indication of its possible role in the efflux of citrate into the xylem vessels (Green and Rogers, 2004). The loss-of-function mutant *frd3* shows constitutive iron deficiency responses and severe chlorosis. It has been shown that the shoot Fe content of *frd3* mutants is lower than in wild type and Fe remains in the root vasculature due to impaired translocation (Rogers and Guerinot, 2002; Lahner et al., 2003; Durrett et al., 2007).

1.3.1 Sub-cellular storage of iron

To cope with scarcity or toxicity of iron, it is crucial for plants to properly manage iron storage and buffering at sub-cellular level. So, it is important to immediately compartmentalize the arrived iron in the cell for the sake of storage, otherwise it can cause extensive cellular damage due to its propensity to form free hydroxyl radicals (Kim et al., 2006; Briat et al., 2007).

Apart from storage in the apoplast, organelles like vacuoles and plastids are considered to play a key role in the intracellular compartmentalization of iron (Briat et al., 2007). Leaves are considered to be the major sink of iron in plants (Briat et al., 2005). In leaf cells, more than 90% of the iron is localized to chloroplasts (bound to ferritin), where it is needed for the maintenance of the structural and functional integrity of thylakoid membranes (Terry and Abadía, 1986; Marschner, 1995). In plastids, ferritins can store a considerable amount of cellular iron. During development and under iron limitation, ferritins play a key role in iron homeostasis through iron storage (Briat et al., 2006).

Currently, some membrane proteins which are involved in the transport of Fe into various cell organelles have been characterized. In Arabidopsis efflux of iron from mitochondria occurs through ABC-type transporter STARIK 1 (STA1) proteins which is a homolog of the yeast ATM1p (ABC Transporter Mitochondria 1 Protein) localized to the inner mitochondrial membrane. ATM1p is required for the assembly of Fe-S cluster in cytosolic proteins and is thought to export clusters from mitochondrial matrix to the cytoplasm (Lill and Kispal, 2000; Kushnir et al., 2001).

Seeds also contain stored iron where it supports embryogenesis. Iron is moved to the seeds partially using the phloem. The newly developing seeds receive iron from the senescing leaves and roots (Grusak, 1994; Stacey et al., 2008). In Arabidopsis seeds, only 5% of the total seed iron is associated with ferritin and around 50% of the seed iron is concentrated in the vacuoles of the surrounding cells of the vasculature (Kim et al., 2006; Ravet et al., 2009; Mary et al., 2015). For the development of young germinating seedlings, it is really important to mobilize the pools of stored iron in seeds. Recent advances have made it possible to identify the transporters that are involved in iron influx and efflux in the vacuole (Briat et al., 2007). Efflux of iron from vacuole to cytosol requires the activity of NATURAL RESISTANCE-ASSOCIATED MACROPHAGE PROTEIN 3 (AtNRAMP3) and AtNRAMP4 transporters. This mobilization of vacuolar iron pools is needed for proper germination. *nramp3, nramp4* double mutants lack the ability of iron retrieval from the vacuoles and therefore its germination is arrested under low iron nutrition (Lanquar et al., 2005; Mary et al., 2015). For iron influx into the vacuole, the activity of VACUOLAR IRON TRANSPORT 1 (VIT1) transporter is needed. VAT1 is an Arabidopsis ortholog of yeast CCC1p which transfer iron into the vacuole. *vit1* mutants lead to the mislocalization of iron (Kim et al., 2006).

1.4 The ZIP family

Metal ions are required for certain physiological processes like plant growth/development, nutrition and signal transduction (Eng et al., 1998b). Since trace elements are present in the natural environment in exceedingly low amounts or in inaccessible forms, plants need to use high-affinity transport systems to acquire these elements (Guerinot, 2000). Arabidopsis has devoted 5% of its genome for encoding membrane transport proteins which are involved in metal transport (Mäser et al., 2001). In plants, a novel metal transporter ZIP gene family was identified,

different members of which are capable of transporting various cations like Fe, Mn, Zn, Cu and Cd (Guerinot, 2000; Hall and Guerinot, 2006). Functional complementation of mutant yeast defective in many metal uptake showed that member of the ZIP family transporters can complement the defective yeast (Schachtman and Schroeder, 1994; Kampfenkel et al., 1995; Eide et al., 1996). The family was named after its founding members ZRT1, ZRT2 and IRT1 [ZRT, IRT-like Protein (ZIP)-family] (Mäser et al., 2001). To date, more than 100 members of this family have been identified in many different organisms (Hall and Guerinot, 2006) including bacteria, fungi, protozoa, plants, insects, and animals (Mäser et al., 2001). The member genes of the family have been divided into four main subfamilies based on amino acid sequence similarity: Subfamily I, Subfamily II, LIV-1 subfamily of ZIP zinc Transporters (LZT) and Gene of Unknown Function A (gufA) (Gaither and Eide, 2001; Taylor and Nicholson, 2003).

ZIP family proteins are predicted to be integral membrane proteins by having eight transmembrane domains (TMDs) and the same membrane topology: Amino and carboxy-terminal ends of the protein are located on the extra-cytoplasmic face of the membrane. The protein is consisting of 309-476 amino acids depending on the length between TMDs III and IV which is known as variable cytoplasmic loop region (Eng et al., 1998b; Guerinot, 2000; Eide, 2006; Nishida et al., 2008).

There are 18 predicted *ZIP* genes in Arabidopsis which belong to Subfamily I (Mäser et al., 2001; Ivanov and Bauer, 2017). One obvious question which arises is why does Arabidopsis have so many ZIP transporters? It is known that metals have to be taken up from the soil into the roots, and then to distribute it throughout the plant it should cross cellular and organellar membranes. Thus, it might be expected that different ZIP transporters might be functioning in various tissues and at different membranes. Besides, some of the ZIP transporters have different substrate specificity and affinities for metals: high-affinity transporters are activated in metals starved situations and low-affinity transporters perform its function when metals are present in abundance (Guerinot, 2000; Hall and Guerinot, 2006). In Arabidopsis, *ZIP* genes are upregulated in response to the depletion of specific metals. *AtIRT1* is induced in roots of iron-starved plants and the *AtZIP* transporter genes are induced during zinc deficient conditions (Eide et al., 1996; Zhao and Eide, 1996)

At the moment, a fair amount of details for understanding the function and role of only three Arabidopsis ZIP transporters (AtIRT1, AtIRT2, and AtIRT3) is available. Among which AtIRT1 has been studied extensively over the last 2 decades based on its role in iron uptake from the rhizosphere (Eide et al., 1996; Varotto et al., 2002; Vert et al., 2002; Lin et al., 2009; Vert et al., 2009).

1.4.1 IRT1

Eide et al (1996) performed functional complementation of *Saccharomyces cerevisiae* to identify a probable candidate gene for Fe^{2+} uptake. For this reason, they expressed Arabidopsis cDNA library in *fet3fet4* double mutant yeast strain which is sensitive to Fe deficiency. *fet3fet4* is incapable of iron import due to the lack of functional multicopper oxidase FET3 and a bivalent iron transporter FET4. They have successfully isolated an Arabidopsis gene designated as IRON-REGULATED TRANSPORTER 1 (IRT1), which complemented the defective yeast strain for iron uptake (Eide et al., 1996).

IRT1 is the major Fe transporter in Arabidopsis roots and exhibits high affinity for Fe^{2+}, in addition to this IRT1 is also capable of transporting Zn, Mn, and Cd (Eide et al., 1996; Korshunova et al., 1999; Rogers et al., 2000; Lin et al., 2009; Pedas et al., 2009; Greco et al., 2012).

Based on upregulation in response to iron deficiency and sequence homology to AtIRT1, orthologs of IRT1 have been identified in other organisms as well: tomato (*Solanum lycopersicum*), rice (*Oryza sativa*), pea (*Pisum sativum*), apple (*Malus xiaojinensis*), Chlamydomonas (*Chlamydomonas reinhardtii*) and others (Cohen et al., 1998; Eckhardt et al., 2001; Ishimaru et al., 2006; Li et al., 2006; Urzica et al., 2012; Ivanov and Bauer, 2017).

1.4.1.2 *irt1* mutants

When plants are grown under iron-limited conditions *AtIRT1* expression is upregulated in roots, suggesting its role in iron uptake. This has been demonstrated by characterizing *irt1* knock-out mutants (Eide et al., 1996; Connolly et al., 2002; Vert et al., 2002). The *irt1* mutant plants have a chlorotic phenotype and showed severe growth defects, which leads to death before producing the seeds. The *irt1* mutation is lethal and no other ZIP family member can compensate for its loss. Exogenous supply of iron can rescue this defect. In addition, *irt1* mutant loses the ability to take up other cation like Zn, Mn, Cd, and Co when grown under iron deficient condition,

this is in agreement with the suggestion that in addition to Fe IRT1 can also take up other divalent cations (Korshunova et al., 1999; Vert et al., 2002). The fact that AtIRT1 is the major iron transporter at the root surface is supported by the outcomes from the characterization of *irt1* mutant and by the plasma membrane localization of IRT1 in root epidermal cells (Vert et al., 2002). The in planta function of IRT1 has also been confirmed by characterizing two other independently obtained *irt1* mutant lines (Henriques et al., 2002; Varotto et al., 2002). Henriques et al (2002) observed a reduced number of chloroplast thylakoids stacking into grana, less vascular bundles in stems and abnormal endodermal and cortex cells in the roots (Henriques et al., 2002). The photosynthetic efficiency of *irt1* mutants is drastically decreased due to the reason that the proteins which are needed in abundance in photosynthetic apparatus and in chlorophyll decrease remarkably (Varotto et al., 2002).

1.4.1.3 Predicted structure of IRT1

The IRT1 protein is 347 amino acids in length (36.7 kDa) and like other ZIP family members, IRT1 also consists of eight TMDs which span the entirety of plasma membrane (Fig. 1.2.). It contains a large cytoplasmic loop, referred to as the variable region between TMD III and IV. The region contains a probable metal binding motif which is rich in histidine residues. The IRT1 histidine motif is HGHGHGH (Fig. 1.2). This proposed metal binding site is not conserved in all ZIP family members but in some (Eng et al., 1998b; Guerinot, 2000). The function of this particular region in the transport of metals is ambiguous because *IRT1* with mutated histidines was able to complement the *irt1* loss-of-function in Arabidopsis and the iron uptake-deficient yeast strain *fet3fet4* (Kerkeb et al., 2008). The variable region contains potential regulatory sites. Therefore it has been hypothesized that it might play an important role in the regulation of IRT1 activity (Ivanov and Bauer, 2017).

Other potential metal binding sites are also reported, the loop between TMD II and III located towards the extracellular space is shown to coordinate with Zn^{2+}, mutation in this loop leads to change in the substrate specificity of the transporter (Rogers et al., 2000; Potocki et al., 2013). A conserved histidyl residue is found on the hydrophobic side of TMD IV that together with the adjacent polar residues could function as a site for an intramembranous metal binding site (Eng et al., 1998b).

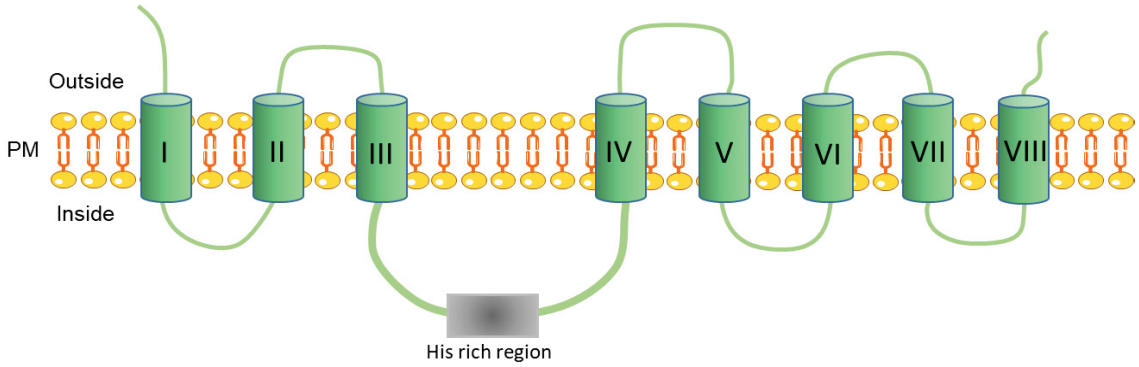

Figure 1.2. Overview of the predicted structure of IRT1. The eight predicted transmembrane domains (TMDs) numbered I-VIII spanning the plasma membrane are shown in the green, the large cytoplasmic loop (Variable region) between TMD III and IV is shown below. The grey box in the variable region represents the Histidine-rich region: a probable site for metals binding. PM: Plasma membrane, outside: the extra-cytoplasmic face of the membrane, inside: cytoplasmically exposed side (Guerinot, 2000; Kerkeb et al., 2008; Potocki et al., 2013).

1.4.1.4 Mechanism of transport

Recently the crystal structure of a prokaryotic ZIP from *Bordetella bronchiseptica* (BbZIP) gram-negative bacterium has been resolved (Zhang et al., 2017). They showed that it contains eight transmembrane helices (TMs). The structural analysis reveals that the eight TMs are arranged in such a way that they form a tight helix bundle. TMs 2, 4, 5, and 7 make an inner bundle which is surrounded by the rest of the TMs. They reported that the transporter contains potential binuclear metal centers (M1-M4) with conserved amino acid residues. The authors proposed a metal transport pathway, according to them, there are two negatively charged cavities in the transporter an entrance cavity on the outer extracellular surface and an exit cavity towards the cytoplasm. The metals enter through the entrance cavity and bind to the conserved binuclear metal center (M1 and M2). This binding stabilizes the inward-open bundle conformation and finally, the metals are released to the cytoplasm by the exit cavity through a chain of conserved metal chelating residues. There are multiple weak metal binding sites at the exit cavity that make a metal sink which largely facilitates the release of metals from the binuclear center to the cytoplasm. They demonstrate that two conserved aspartic acid metal chelating residues (D113 and D305) in the entrance cavity might play a crucial role in the recruitment of metals. An invariable serine (S106) which is located at the bottom of the entrance cavity is important for guiding metals into the transport pathway (Zhang et al., 2017).

After further inspection of the structure, they suggest that, four TMs namely TM1, TM4, TM5, and TM6 associate closely and forms a tight helix bundle. This bundle of 4-TMs associates weakly with the rest of the 4-TMs. The metal-bound binuclear metal center (M1 and M2) is held on the 4-TMs bundle. A slight rocking-like movement of this helix and the coordinating movement of the other TMs helps to expose the metals alternatingly to the extracellular space and to the cytoplasm (Antala et al., 2015; Zhang et al., 2017).

1.5 Iron uptake regulation

The balance should be strictly maintained between low bioavailability of iron, which can lead to iron deficiency in the plant and high amount of iron uptake, which can cause iron toxicity that can affect physiological processes of the plant. The regulation of Fe uptake is important for the proper development and growth of plant (Connolly and Guerinot, 2002; Walker and Connolly, 2008). Plants have evolved regulatory mechanisms for induction and repression of genes at both transcriptional and translational level to cope with fluctuating environmental changes.

1.5.1 Transcriptional regulation

The genes which encode for the essential Strategy I iron acquiring proteins are upregulated during iron-limited condition, meaning that transcription is a key step in the regulation of corresponding genes (Brumbarova et al., 2015). Many transcription factors are involved in the transcriptional regulation of iron uptake in Arabidopsis but, the basic Helix Loop Helix (bHLH) transcription factor (TF) FIT (FER-Like Iron Deficiency Induced Transcription Factor) is the central transcriptional regulator. *FIT* is an ortholog of the tomato *FER* gene, the expression of which is repressed under iron sufficient situation in roots at the post-transcriptional level (Ling et al., 2002; Colangelo and Guerinot, 2004; Brumbarova and Bauer, 2005).

Under limited iron condition, FIT plays an essential role in the induction of the key iron uptake genes *AHA2, FRO2* and *IRT1* (Colangelo and Guerinot, 2004; Ivanov et al., 2012). Under iron sufficiency, Constitutive overexpression of *FIT* is not enough to induce the downstream genes (Colangelo and Guerinot, 2004; Jakoby et al., 2004; Wang et al., 2013) this suggests that FIT needs an iron deficiency-induced interacting partner. So, to exert its proper function in transcription, FIT interact with the proteins of bHLH subgroup-Ib and forms heterodimers with one of the four members (Yuan et al., 2008; Wang et al., 2013) (Fig. 1.3.). In Arabidopsis, the bHLH

subgroup-Ib TF consists of four bHLH genes, namely *bHLH38*, *bHLH39*, *bHLH100* and *bHLH101* (Pires and Dolan, 2010). These four bHLH's share a partially redundant function in iron homeostasis (Wang et al., 2007). Analysis of the overexpressing lines showed that FIT interacts with at least bHLH38 or bHLH39. This heterodimerization is effective in the upregulation of *FRO2* and *IRT1* which ultimately results in higher iron content in shoots (Yuan et al., 2008).

FIT regulates a large number of iron-deficiency related genes, the prime examples are *FRO2* and *IRT1*. *MTPA2, CYP82C4 and KELCH REPEAT PROTEIN* are among others (Jakoby et al., 2004; Bauer and Blondet, 2011; Schuler et al., 2011; Maurer et al., 2014). On the contrary, the four bHLH's are not regulated by FIT but they are rather upregulated by limited iron supply (Wang et al., 2007). They are co-regulated together with the other known genes (*BTS, PYE, NAS4 and NRAMP4*) which are involved in iron homeostasis in FIT independent manner (Buckhout et al., 2009; Ivanov et al., 2012).

The FIT regulatory network is not the only network involved in the regulation of iron acquisition genes. Apart from FIT regulatory network, another set of transcriptional changes occurs in the root vasculature due to iron deficiency which might represent another transcriptional network (Hindt and Guerinot, 2012) (Fig. 1.3.). Recently, two genes from this additional network have been identified and studied in more detail, one of which is the bHLH transcription factor *bHLH047* named *POPEYE* (*PYE*) and the other one is *BRUTUS* (*BTS*), an E3-ubiquitin ligase. Both of these genes are induced in the root pericycle of iron-starved plants (Long et al., 2010). Both *PYE* and *BTS* are involved in iron homeostasis as they are upregulated in response to iron deficiency and are co-regulated. However, they appear to perform opposite functions. *PYE* positively regulates the iron status of the plant while *BTS* might affect negatively the *PYE* network (Long et al., 2010; Ivanov et al., 2012; Selote et al., 2015; Matthiadis and Long, 2016) (Fig. 1.3.). PYE plays a critical role in root growth under iron starvation, in addition, to be chlorotic, *pye* mutants displayed altered root architecture characterized by short and swollen primary and lateral roots due to decreased elongation of cortical and epidermal cells. PYE is involved in the regulation of *FRO3*, *NAS4,* and *ZIF1* which are known to encode proteins that play a role in iron transport (Long et al., 2010).

BTS belongs to the RING E3 ligases. The BTS protein has the capability to bind Zn and Fe owing to its hemerythrin domain (Kobayashi et al., 2013). The partial loss-of-function *bts-1* mutant exhibits increased root length and high rhizosphere acidification activity compared to wild-type during iron-deficient conditions. This suggests that BTS might negatively regulate the iron deficiency response (Long et al., 2010). Yeast two-hybrid experiments suggested that both BTS and PYE interact with PYE-like (PYEL) proteins including ILR3 (bHLH105), bHLH104 and bHLH115, they belong to the bHLH TF subgroup IVc (Fig. 1.3.). The interaction of BTS and PYE with PYELs demonstrated that PYELs plays an important role in iron homeostasis regulation (Long et al., 2010; Zhang et al., 2015) *pyel* mutants showed altered responses during iron deficiency and showed more sensitivity to iron starvation (Zhang et al., 2015; Matthiadis and Long, 2016).

Additionally, MYB72 and MYB10 are among the other important transcription factors which are critical regulators of the iron uptake. They are members of myeloblastosis (MYB) family of transcription factors, both genes are upregulated during low iron conditions and work redundantly (Palmer et al., 2013b). MYB72 is a direct target of FIT and is involved in the regulation of *NAS4* suggesting that it plays a role in iron redistribution (Fig. 1.3.). Double mutant *myb10myb72* was unable to induce transcription of *NAS4* and showed seedling lethality at iron deficiency (Sivitz et al., 2012; Palmer et al., 2013b). A β-glucosidase encoding gene *BGLU42* which is involved in the production and export of phenolics is also regulated by MYB72 (Van der Ent et al., 2008; Zamioudis et al., 2014) (Fig. 1.3.). Phenolic compounds are excreted by the roots which help in the mobilization of insoluble rhizospheric iron (Rodríguez-Celma et al., 2013a). This demonstrates the role of MYB72 in iron uptake on one hand and on the other hand in iron redistribution (Zamioudis et al., 2014; Brumbarova et al., 2015).

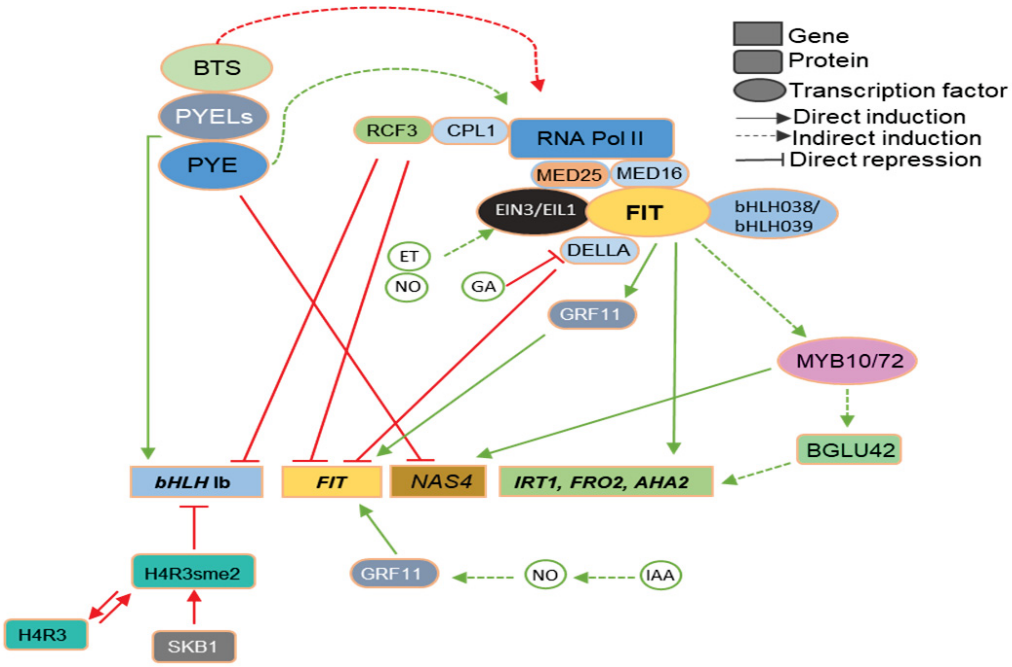

Figure 1.3. Iron uptake regulatory network in *A. thaliana*. Target genes are represented as filled rectangles; proteins are depicted as filled rounded corners rectangles; filled ovals represents the transcription factors. Upstream signaling molecules are shown in empty circles. Green arrows show direct induction, broken red and green arrows represents indirect negative and positive regulation respectively. Red lines with blunt end show direct repression.

The mediator (MED) complex plays a critical role in transcription regulation, it serves as a bridge by connecting transcription factors with RNA polymerase II during transcription initiation (Chadick and Asturias, 2005). Recently the role of, MED has been shown in the regulation of iron-dependent gene expression. The *YID1* gene which encodes the MED16 protein has been investigated, plants with MED16 loss of function showed hypersensitivity to iron deficiency and low level of expression of iron deficiency response marker genes; *FIT*, *IRT1,* and *FRO2*. MED16 interact with MED25, the heterodimer then interacts with the FIT regulators EIN3/EIL1. MED16 has also been shown to directly interact with FIT to enhance the recruitment of FIT-bHLH complex to the promoters of *FRO2* and *IRT1* (Yang et al., 2014; Zhang et al., 2014). RNA POL II C-TERMINAL DOMAIN-LIKE PHOSPHATASE 1 (CPL1) which a subunit of RNA polymerase II complex has been shown to negatively regulate iron homeostasis by acting upstream of FIT (Aksoy et al., 2013). It has been reported that CPL1 interact with REGULATOR OF CBF GENE EXPRESSION 3 (RCF3) and affect the mRNA availability of FIT and Ib bHLHs (Aksoy et al., 2013; Jeong et al., 2013) (Fig. 1.3.).

The role of SHK1-BINDING PROTEIN1 (SKB1) has been shown in iron homeostasis. The SKB1 enzyme is involved in the symmetrical dimethylation of histone H4 arginine 3 (H4Rsme2). With chromatin immunoprecipitation, it has been shown that under sufficient iron supply H4Rsme2 binds to the promoters of all bHLH Ib genes which leads to their repression. *skb1* mutant plants showed increased tolerance to iron deficiency due to upregulation of bHLH Ib genes. This shows that epigenetic chromatin modifications also plays an essential role in the regulation of iron homeostasis (Fan et al., 2014) (Fig. 1.3.).

1.5.2 Post-transcriptional regulation of iron-uptake

In addition to transcriptional level control, genes that are involved in the uptake of iron are regulated at post-transcriptional level too. The central transcriptional regulator of iron uptake FIT and the principal iron importer IRT1 are subjected to post-transcriptional regulation to properly modulate iron homeostasis.

It is known that phytohormones such as auxin (IAA), ethylene (ET), gibberellic acid (GA) and the signal molecule nitric oxide (NO) are responsible to modulate certain environmental and developmental influences including iron homeostasis (García et al., 2010; Williams, 2010). The central regulator of iron uptake FIT, activity is affected by NO and ethylene (Fig. 1.3.). It is reported that treatment with NO and ethylene enhances the expression of many genes involved in iron homeostasis including *FIT* and its tomato homolog *FER* (Graziano and Lamattina, 2007; García et al., 2011; Meiser et al., 2011). NO is shown to help in the stability of the FIT protein by preventing its proteasome-mediated degradation (Meiser et al., 2011; Sivitz et al., 2011). Meiser et al (2011) showed that NO acts as a signal which promotes the activation of *FIT* and its protein stability. The active state of FIT could be obtained through the modification of FIT protein either by addition or removal of covalent modifications or due to the interaction with bHLH38 and bHLH39 which is induced at iron-starved condition (Yuan et al., 2008; Meiser et al., 2011). Additionally, NO also regulates the expression of *GENERAL REGULATORY FACTOR 11* (*GRF11*) which acts downstream of NO. *GRF11* encodes a 14-3-3 protein which is involved in the promotion of *FIT* transcription and in turn, FIT directly binds to the E-box motif of *GRF11* to regulate its transcription, so they work in a reciprocal manner (Yang et al., 2013). It has been shown that auxin affects iron deficiency responses positivity by acting upstream of NO and regulating its signaling. Exogenous application of auxin

to plants enhances the level of NO which in turns triggers the upregulation of *FRO2* as well as *FIT* (Chen et al., 2010) (Fig. 1.3.).

In addition to this, FIT also interacts with the ethylene-responsive genes ETHYLENE INSENSITIVE 3 (EIN3) and EIN3-LIKE1 (EIL1) (Fig. 1.3.). This interaction promotes iron uptake, because of this interaction degradation of FIT is reduced and FIT remains in its active state. Reduced FIT levels were observed when wild-type plants were treated with ethylene inhibitor AVG and also in the *ein3 eil1* double mutant (Lingam et al., 2011). NO and ethylene are interconnected with each other by feedforward mechanism meaning that both influences each other biosynthesis (García et al., 2011). Both NO and ethylene have a positive effect on *FIT* transcription, this may be needed because FIT is required for promoting its own gene transcription (Wang et al., 2007; García et al., 2010; Lingam et al., 2011).

Gene expression analysis of GA-deficient mutants showed that GA has a positive effect on the transcript abundance of iron uptake marker genes; *bHLH38*, *bHLH39*, *FRO2* and *IRT1* (Matsuoka et al., 2014). It has been shown that DELLA protein physically interacts with FIT, bHLH38, and bHLH39 to inhibit its transcriptional activity by not allowing them to bind with its target promoters. Limited iron availability and high content of GA antagonizes this situation by degradation of DELLA protein which allows the transcription of *FRO2* and *IRT1* (Wild et al., 2016) (Fig. 1.3.).

1.5.2.1 Post-transcriptional regulation of IRT1

For the maintenance of nutrient homeostasis in plants, it is important to tightly regulate the plasma membrane-localized transporters. IRT1, the principal importer of iron in the root is also strictly regulated for the homeostasis of iron (Zelazny et al., 2011). Transgenic plants, overexpressing *IRT1* showed a high level of transcript both in roots and shoots during iron sufficiency as well as during iron deficiency. Interestingly, IRT1 proteins accumulate in iron-starved roots only, suggesting that post-transcriptional regulation plays role in controlling the IRT1 protein abundance (Connolly et al., 2002). Different post-transcriptional events are required to regulate the prominent iron uptake genes activity, localization, and stability (Jakoby et al., 2004; Yuan et al., 2008). The subcellular localization of IRT1 plays a critical role in regulating its activity, Despite being a transmembrane protein, IRT1 was found to localize also to intracellular compartments (Early endosome; EE/Trans Golgi

network; TGN) (Barberon et al., 2011; Ivanov et al., 2014) suggesting that IRT1 cycles between EE/TGN and plasma membrane (Zelazny et al., 2011). Internalization of IRT1 from the plasma membrane to the cytoplasm is achieved through ubiquitin-dependent clathrin-mediated endocytosis (CME) (Barberon et al., 2011). Ubiquitination is a post-translational modification in which a small (8 kDa; 76 amino acids) conserved protein, Ubiquitin is attached to the lysine residue of the targeted protein for signal initiation of endocytosis (Mazzucotelli et al., 2006). It is a well-known process in yeast that helps to mediate the internalization and sorting into the endosomal compartments for the degradation of plasma membrane-localized proteins, like transporters and receptors (Bonifacino and Weissman, 1998). Two lysine residues (K154 and K179) in the variable region of IRT1 are monoubiquitinated. Replacing the two lysine residues in the variable region of IRT1 by arginine ($IRT1_{K154K179R}$) leads to the impairment in ubiquitination, which ultimately results in stabilization of IRT1 at the plasma membrane, this demonstrates the importance of ubiquitination for IRT1 dynamics in the cell (Kerkeb et al., 2008; Barberon et al., 2011). IRT1 DEGRADATION FACTOR 1 (IDF1) a RING-type E3 ligase has been shown to mediated IRT1 ubiquitination. *Idf1* mutant showed overaccumulation of IRT1 and was tolerant to iron-deficiency because of the delayed degradation of IRT1. Monoubiquitination is a prerequisite for CME-dependant endocytosis of IRT1 (Barberon et al., 2011; Shin et al., 2013). Once ubiquitinated IRT1 is then subjected to the endocytic pathway and it has been proposed that after endocytosis IRT1 has two possible fates: at EE/TGN, IRT1 is either sent to the vacuole for degradation or it is retrieved from the degradation pathway and sent back to the plasma membrane for another round of activity. The cargo protein (IRT1) can be retrieved from the late steps of endocytosis by the retromer complex. In the retromer complex, the protein is deubiquitinated and then is sorted for sending back to the plasma membrane. Along with Vacuolar Protein Sorting (VPS26, VPS29, and VPS35) proteins two other proteins are thus far known to play a critical role in the sorting step, a dimer of SORTING NEXINS (SNX) which is involved in stress response trafficking regulation and a plant-specific ESCRT complex sub-unit FYVE1 (Zelazny et al., 2013; Barberon et al., 2014; Zelazny and Vert, 2014; Brumbarova et al., 2015; Heucken and Ivanov, 2018). It has been shown that FYVE1 is involved in the recycling of IRT1 from the endosomal compartments back to the plasma

membrane (Barberon et al., 2014). Both, ubiquitination and endocytic cycling of IRT1 is important to calibrate the amount of IRT1 protein at the plasma membrane.
Although, iron concentration does not affect the plasma membrane localization of IRT1 (Barberon et al., 2011), the presence of non-iron metal substrates (Zn^{2+}, Mn^{2+}, and Co^{2+}) dynamically controls the localization of IRT1 between EE/TGN and the outer surface of the cell. To avoid non-iron metal toxicity IRT1 changes its localization from the plasma membrane to the cytoplasm (EE/TGN) while in the absence of these metals IRT1 is localized predominantly to the extra-cytoplasmic face of the plasma membrane (Barberon et al., 2014). Minimizing the pool of IRT1 at the plasma membrane seems to be a protective mechanism because IRT1 can also import the aforementioned non-iron available heavy metals (Zelazny et al., 2011; Barberon et al., 2014).

To maintain a balanced amount of iron in the plant it is important that plant responds to the ever-changing conditions. Thus, the regulation of principle iron-importer IRT1 is extremely important because as a fact that iron is essential for life, it is also toxic. Constitutive uncontrolled iron acquisition can lead to extensive oxidative damage (Reyt et al., 2015). Until now very limited information is available regarding the post-transcriptional regulation of iron homeostasis.

1.6 Peripheral membrane proteins

For many cellular functions like signaling and trafficking, an association of proteins with the surface of membranes is required (Lemmon, 2008). There are three types of membrane binding proteins, namely integral, anchored and peripheral. Most of the integral membrane proteins span the entire lipid bilayer and remain embedded in the bilayer. Proteins that are involved in signal transduction and those that serve as ion channels are integral membrane proteins. Those proteins which bind to the membrane surface through lipid molecules are called anchored proteins. They bind covalently to certain lipids like fatty acids (myristic acid and palmitic acid) and glycosylphosphatidylinositol (GPI). The third type, peripheral membrane proteins, are bound to the membrane surface reversibly via non-covalent bonds like hydrogen bonds and ionic bonds (Taiz and Zeiger, 2002). They can be dissociated from the membrane surface by mild treatments like increasing the ionic strength of the medium or by addition of a chelating agent. Furthermore, in the dissociated state

they tend to solubilize in neutral aqueous buffers (Singer and Nicolson, 1972; Fujiki et al., 1982).

During cell signaling and membrane trafficking events, many cytosolic proteins are transiently recruited to different membranes to exert their function in protein-protein or protein-lipid interactions (Cho and Stahelin, 2005; Lemmon, 2008). Many enzymes that are involved in the metabolism of phospholipids are cytosolic, for example, phospholipases are normally cytosolic or extracellular proteins but for their catalytic activity they are transiently docked to the membrane (Goñi, 2002).

The liquid crystallographic analysis showed that the structure of lipid bilayer is highly polarized consisting of the central hydrocarbon core region and the two flanking interfacial regions (Wiener and White, 1992). Based on where they bind to the membrane peripheral proteins can be divided into three categories; (1) S-type proteins, which interact predominantly with the polar head groups and are localized only at the membrane surface to the shallow interfacial region, (2) I-type proteins which penetrate into the interfacial region and reach to the level of phosphate and (3) H-type proteins can reach all the way to the hydrocarbon core region of the lipid bilayer (Cho and Stahelin, 2005). Peripheral protein goes through conformational change at the membrane interface in order to expose their buried hydrophobic residues. Conformational changes, the effective concentration of protein and the initial attachment to the membrane, all these factors contribute to facilitating the penetration of protein into the interfacial and hydrocarbon core region of the bilayer. Indeed, some proteins depend largely on partial membrane insertion to perform their biological activities (Ford et al., 2002; Stahelin et al., 2002; Stahelin et al., 2003).

Membrane-bound organelles inside the cell contain specific lipids in their membrane which serve as a recognition site for the intracellular trafficking machinery (Behnia and Munro, 2005). Ceramide-activated protein phosphatases 1 and 2A and some isozymes of protein kinase C are proposed to bind ceramides through their cysteine-rich domains (Zhang et al., 1997; van Blitterswijk, 1998; Chalfant et al., 2001). Other proteins are also reported that do not possess specific binding sites but are still able to bind the cell membrane. Examples include ADP-ribosylation factor and small G-protein Rho A which associate with the membrane in the presence of GTP (Brown et al., 1993; Kahn et al., 1993).

Many peripheral proteins contain one or more modular domains through which they bind with lipids. Membrane targeting domain is another term for these structural modules, some common domains are protein kinase C (PKC) conserved 1 (C1) (Cho et al., 2001; Brose and Rosenmund, 2002; Yang and Kazanietz, 2003), PKC conserved 2 (C2) (Nalefski and Falke, 1996; Rizo and Südhof, 1998; Cho et al., 2001), Pleckstrin homology (PH) (Ferguson et al., 2000; LEMMON and FERGUSON, 2000), FYVE (Stenmark et al., 2002) and Phox (PX) domain (Wishart et al., 2001; Yue et al., 2001). Because in this study we are investigating a C2 domain-containing protein (EHB1), the focus will only be on C2 domains.

1.6.1 C2 domain

1.6.1.1 Discovery and occurrence

C2 domain was originally identified as the Ca^{2+} binding site in protein kinases C (PKC) and it is named after the second homology region in conventional PKCs (Nishizuka, 1988; Kikkawa et al., 1989). Initially, C2 domain was considered to be Ca^{2+} ion sensor only but after its discovery in other proteins which also bind lipids, synaptotagmins and cytosolic phospholipase A2 (cPLA$_{2}\alpha$), it became clear that C2 domains are involved in lipid binding in a Ca^{2+}-dependent manner (Perin et al., 1990; Clark et al., 1991). The Ca^{2+}-dependent lipid binding ability of the C2 domain has been confirmed by isolating C2 domains of synaptotagmin 1, cPLA$_{2}\alpha$ and rabphilin-3A (Clark et al., 1991; Davletov and Südhof, 1993; Yamaguchi et al., 1993; Chapman and Jahn, 1994; Nalefski et al., 1994). However, it has been reported that some C2 domains bind the membrane independently of Ca^{2+} such as that of PTEN which is involved in tumor suppression and plays a critical role in cell signalling and regulation, whereas some others are known to be involved in protein-protein interactions, examples are C2 domains of phospholipases-C β1 and β2 (Lee et al., 1999; Wang et al., 1999; Das et al., 2003). It is now well established that C2 domains are independently folded modules of about 130 amino acid residues in length which are found in many eukaryotic proteins (Nalefski and Falke, 1996; Cho and Stahelin, 2006).

1.6.1.2 Structure and role of Ca^{2+} ions in lipid binding

Structurally, C2 domains are composed of eight antiparallel β-sandwich strands connected by surface loops which are also called variable loops, it has been known that all C2 domains share this common fold. Topologically, C2 domains are either

type I or type II based on slight differences in their *β*-strand connectivity (Sutton et al., 1995; Perisic et al., 1998; Sutton and Sprang, 1998). The surface loops have variable amino acid sequence and conformation and play critical roles in lipid binding specificity during membrane docking (Stahelin, 2009). The Ca^{2+} binding sites are formed by three Ca^{2+} binding loops (CBL1-3), which are located on one side of the domain. Amino acid side chains (mostly conserved Asp) and peptide backbone in the CBLs are involved in multiple Ca^{2+} ion coordination, most of the Ca^{2+}-dependent C2 domains bind two-three Ca^{2+} ions. In Ca^{2+}-independent C2 domains the amino acid side chains which coordinate with Ca^{2+} ions are absent (Sutton et al., 1995; Essen et al., 1997; Perisic et al., 1998; Sutton and Sprang, 1998). Mutation in the CBL region leads to the conversion of Ca^{2+}-dependent C2 domains to Ca^{2+}-independent ones (Medkova and Cho, 1998; Ananthanarayanan et al., 2002). Structural and functional studies reveal that both the integrity of CBLs and the presence of conserved aspartic acid (Asp) residues in the loops are required for the binding of C2 domains to membranes *in vitro* as well as to plasma membrane in cells (Edwards and Newton, 1997; Johnson et al., 2000; Kohout et al., 2002). It has been proposed that the presence of Ca^{2+} ions in these loops serves as an “electrostatic switch” which makes C2 domains able to bind anionic phospholipids. Mutation of the conserved Asp residues neutralizes the acidic binding pocket but it does not bypass the requirement of Ca^{2+} to promote membrane binding of C2 domains (Edwards and Newton, 1997).

In addition to the Ca^{2+} binding loop region, which is involved in membrane binding, a second basic patch, found in many C2 domains, is present in the concave face of *β*-sandwich (termed as cationic *β*-groove) it varies in size and electrostatics among different C2 domains (Cho and Stahelin, 2006). The *β*-groove has been shown to be involved in lipid (Ceramide-1-phosphate and phosphatidylinositols) binding, suggesting that some C2 domain-containing proteins may engage different membranes simultaneously by CBLs and cationic *β*-groove (Corbalán-García et al., 2003; Stahelin et al., 2007; Lemmon, 2008; Stahelin, 2009). Lipid selectivity is not specific in the large C2 domain family because it lacks a well-defined lipid binding pocket, that’s why it shows a weak lipid specificity. Some Ca^{2+}-dependent C2 domains like that of PKCs, bind phosphatidylserine preferentially while other C2 domains bind to all anionic phospholipids and still some others prefer to bind zwitterionic phospholipids (Cho and Stahelin, 2005; Lemmon, 2008). Concentration

of Ca^{2+} ion can also affect the lipid selectivity of C2 domains. The relative contribution of the two lipid binding sites in C2 domains (CBLs and *β*-groove) can be different at different Ca^{2+} concentration (Schiavo et al., 1996; Bai et al., 2004). Bound Ca^{2+} ions in the CBLs confer positive charge which switches the electrostatics of the binding site due to which it attracts the negatively charged membranes (Murray and Honig, 2002). The bound Ca^{2+} ions also induce conformational changes in the calcium binding regions and can also coordinate directly with lipids by forming calcium bridges (Shao et al., 1998; Bittova et al., 1999; Verdaguer et al., 1999; Kulkarni et al., 2002).

1.6.1.3 C2 domains in plants

There are numerous genes in higher plants encoding proteins with C2 domains. It has been reported that there are at least 123 proteins in *Arabidopsis thaliana* which contain C2 domains (Rodriguez et al., 2014). Like their animal counterparts, these proteins are most likely involved in signal transduction pathways. Plant proteins with C2 domains are classified into four groups and so far single C2 domain-containing proteins are identified only in plants (Kopka et al., 1998; Yang et al., 2008). The activity of phospholipase A_2 (PLA_2) has been demonstrated in plants, *PLA_2* is a homolog of cytosolic phospholipase A_2 (*$cPLA_2$*) which is reported to be an important component of certain signal transduction pathways in animal cells (Kopka et al., 1998; Valentín-Berríos et al., 2009). Phospholipase D (PLD), phosphatidylinositol 3-kinase, Phosphoinositide-specific phospholipase C (PI-PLC), OsERP3 and protein kinase C are among the other known plant proteins which contains C2 domains (Nanmori et al., 1994; Welters et al., 1994; Hirayama et al., 1995; Pical et al., 1997; Wang, 1997; Cooper et al., 2003). These proteins use their C2 domains to associate themselves with membranes, it has been shown for the rice protein OsPBP1 involved in pollen fertility in rice, that it binds membrane phospholipids in a calcium-dependent manner via its C2 domain. Similarly, another rice small C2 domain protein OsERG1a also bind lipids in a calcium-dependent manner (Yang et al., 2008; Kang et al., 2013). Very recently Liu et al, 2017, identified a 16-member family of multiple C2 domain and transmembrane region proteins (MCTPs) in Arabidopsis. QUIRKY (QKY, MCTP14) a membrane-anchored protein belongs to MCTPs family contains four C2 domains. QYK is localized to plasmodesmata and play an important role in tissue morphogenesis (Liu et al., 2017).

Recently, in their search for interacting partners of the PYR/PYL (intracellular plant hormone ABA receptors) Rodriguez and co-workers (2014) identified a small family of proteins which interact with PYR/PYL and regulate ABA activity in Arabidopsis. The identified small family of proteins consists of 10 members which possess a single C2 domain and hence named C2-DOMAIN ABSCISIC ACID-RELATED (CAR) proteins. Different CAR proteins interact with several PYR/PYLs and mediate the Ca^{2+}-dependent transient recruitment of PYR/PYL to the plasma membrane (Rodriguez et al., 2014). Members of this family are specific to plants and are characterized by their small sizes, simple structures and most importantly they contain only a single C2 domain. They are soluble proteins but can loosely associate with plasma membrane via reversible binding to phospholipids so they shuttle between the cytosol and plasma membrane (Rodriguez et al., 2014; Yung et al., 2015).

1.6.1.4 Signature domain of CAR proteins

To gain further molecular insights into the CAR proteins Rodriguez et al (2014) solved the x-ray structure of CAR4 in complex with Ca^{2+} ions. The overall structure of CAR4 looks identical to that reported for other C2 domains by having compact two four-stranded antiparallel *β*-sandwich with type II topology (Fig. 1.4 left.). Crystallographic analysis shows that in addition to C2 domain CAR4 contains a plant-specific CAR signature domain that is likely used for interaction with other proteins by the CAR family members. The signature domain is 43 amino acid in length and connects the two four-stranded *β*-sheets (*β*3*β*2*β*5*β*6 with *β*4*β*1*β*8*β*7) and fold itself as an *α*-helix which is followed by *β* hairpin (*α1β*A*β*B) (Fig. 1.4 right.). The signature domain is conserved among the CAR family of proteins and it is situated in the protein face opposite to the CBLs (L1 and L3) (Rodriguez et al., 2014). Furthermore, the crystallographic analysis also reveals a polybasic region in CAR4 which can bind phospholipids in Ca^{2+}-independent manner and stabilizes the protein in the plasma membrane (Diaz et al., 2016).

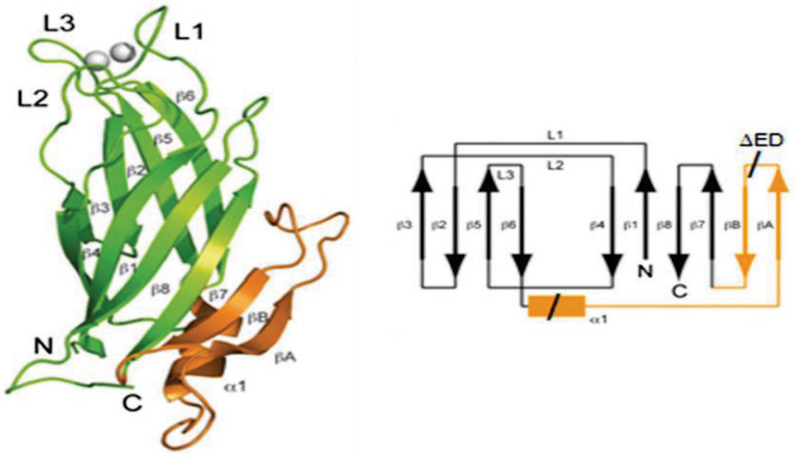

Figure 1.4. Crystal structure of CAR4. A ribbon representation (left), the green ribbons represents the *β*-sheets. The signature domain is represented by orange ribbons. L1, L2, and L3 represent the Ca^{2+} binding loops on the top. The right shows the same CAR4 structure but represented in lines. Adopted from Rodriguez et al (2014) (Rodriguez et al., 2014).

The signature domain of CAR4 was required for protein-protein interaction with PYR/PYL ABA receptor proteins. Rodriguez et al also characterized other members of the CAR family, knockout mutants of CAR1, CAR5, CAR4, and CAR9 showed reduced sensitivity to ABA-mediated inhibition of seedling establishment and root growth. This shows that CAR proteins are involved in protein-protein interaction for the recruitment of signaling protein complexes to the membrane (Knauer et al., 2011; Rodriguez et al., 2014).

EHB1/CAR6 which is also a member of the CAR family protein was previously investigated and was found as an interacting partner of NPH3, component of the phototropin-mediated blue light signal transduction pathway. Hypocotyl bending was enhanced in response to blue light in the T-DNA loss-of-function mutants *ehb1-1* and *ehb1-2* (hence the name ENHANCED BENDING 1 = EHB1) suggesting that EHB1/NPH3 complex might work as a negative regulator of tropism response in Arabidopsis (Knauer et al., 2011; Dümmer et al., 2016). *EHB1* gene is about 1 kb in length (1086 bp) having three exons and two introns, EHB1 protein (19.6 kDa) has a C2 domain at N-terminal and a signature domain at the C-terminal end (Knauer et al., 2011; Rodriguez et al., 2014). EHB1 has been reported to be present in phloem sap as well as it has been found to be specifically expressed in flowers (Giavalisco et al., 2006; Rehrauer et al., 2010).

The structure of rice GTPase-activating protein 1 (OsGAP1) which is a homolog of CAR4 in rice has also been solved, Structurally, CAR4 and OsGAP1 are identical (Yung et al., 2015).

1.7 Previous work

The main focus of our group is to investigate the iron uptake and its regulation in plants. The aim is to understand the regulatory process by characterizing novel gene functions and proteins which coordinate iron homeostasis responses. So to gain further insight into the factors responsible for the regulation of IRT1 trafficking and function, a yeast two-hybrid screen was carried out in our group to identify potential interacting partners of IRT1.

Because of its proposed importance in the regulation of IRT1 activity in response to iron, the large cytosolic loop of IRT1 (located between TMD III and IV, also called variable region, IRT1vr) was used as bait to screen a cDNA library from Arabidopsis roots grown on iron-deficient media. As a result, several potential candidates were identified which interacted with the large cytosolic loop of IRT1 (the interacting partners are termed as ‘‘IRT1 cytosolic loop interaction partners’’ = ICLIPS) (R. Ivanov, R. Gratz and P. Bauer, unpublished). The protein interactions have been reconfirmed in targeted yeast two-hybrid assay. Among the ICLIPS, EHB1 was identified as one of the potential interacting partners of IRT1vr.

To further characterize EHB1 an overexpression line was needed. Therefore, an HA_3-EHB1 fusion gene construct was created in our group, this construct was used to transform Arabidopsis plants to obtain a stable transgenic homozygous over-expression T3 lines (ox-lines) HA-EHB1. Along with two knock-out mutant *ehb1-1* and *ehb1-2,* the two overexpression lines HA-EHB1(2) and HA-EHB1(3) were used for further investigation during the course of the study.

Furthermore, some initial physiological analysis was performed which showed that *ehb1-2* mutants have an altered iron deficiency response regulation, they performed well under iron-starved conditions. The chlorophyll content of *ehb1-2* was significantly higher than in the wild type in iron sufficient condition. An increase in shoot iron content of *ehb1-2* plant grown under iron-limited condition was observed which was consistent with increased iron mobilization via root iron reductase activity performed by FRO2 (Ivanov, R. unpublished)

2. Working hypothesis and Aims

2.1 Working hypothesis

In preliminary studies performed in our group for the involvement of EHB1 in iron deficiency the transcriptional activity of *EHB1* in response to differential iron supply was investigated in wild-type (Col-0) and in *fit* knock-out mutant which is severely iron deficient. *EHB1* expression was down-regulated under iron-deficiency compared to normal iron supply in both genotypes, however, the expression in the *fit* mutant was generally stronger than in the wild type. On the contrary, *IRT1* expression was strongly induced under iron-deficiency in the wild-type, but only weakly in the *fit* mutant. This suggests that EHB1 is negatively affected by the presence of FIT and positively by the iron supply, thus showing principally opposite responses to these of *IRT1*.

Due to these initial results, it can be speculated that under Fe sufficient conditions IRT1 may bind to EHB1, and perhaps only a small part of the IRT1 population is actively transporting iron into the cell. Under iron-deficiency, the equilibrium is shifted towards the active IRT1. Both genes are oppositely regulated, suggesting that EHB1 might negatively regulate IRT1 by either affecting its transport activity or plasma membrane localization or stability. Therefore, it can be proposed that IRT1 may be inactivated by EHB1 (Fig. 2.). While during the iron-deficiency situation, it could be that less EHB1 is synthesized in the cell and the majority of IRT1 protein remains free (not in complex with EHB1) and is therefore actively transporting iron (Fig. 2.).

Therefore, we hypothesized that EHB1 might serve as a negative regulator of iron uptake machinery of Arabidopsis. To further elaborate the role of EHB1 in iron homeostasis I have set some aims for my doctoral study which are mentioned below.

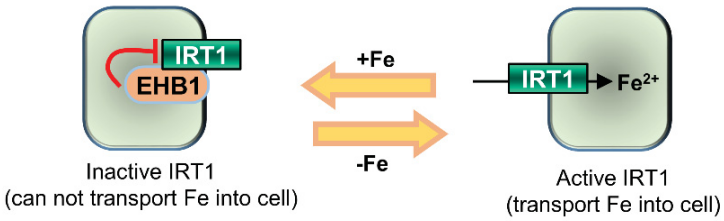

Figure 2. Hypothetical model for the role of EHB1 in IRT1 regulation. Under normal Fe situation, IRT1 expresses less and mostly present in a complex with EHB1 in inactive form so, cannot transport Fe into the cell. While during Fe deficient situation the scenario changes, EHB1 becomes less available to form a complex with IRT1, in that way IRT1 is set free to perform its activity (Fe transport into the cell) (modified from Ivanov, R. unpublished work).

2.2 Aims

1. Verification of interaction between EHB1 and IRT1vr

EHB1 was found in a yeast two-hybrid screen in our lab to interact with IRT1vr. This interaction should be confirmed *in planta*. *In planta* verification of interaction between EHB1 and IRT1 will be confirmed dually by using two different approaches, bimolecular fluorescence complementation (BiFC) and Co-immunoprecipitation (Co-IP). To show that the signature domain of EHB1 is responsible for interaction with IRT1vr, the signature domain of EHB1 will be deleted, creating EHB1-ΔSig, and then it will be subjected to BiFC. EHB1-ΔSig would no longer be able to interact with IRT1vr. Furthermore, to find out which part of the IRT1 variable region is involved in protein-protein interaction, different IRT1vr fragments should be generated and then should be tested for interaction with EHB1 using BiFC.

2. Investigation of the subcellular localization of EHB1

To identify the proper function of a protein it is important to find out its subcellular localization. Subcellular localization determines the environment around the protein, which in turn influences the function of the protein. So knowledge of the localization of proteins plays an important role to elucidate the cellular function of the protein (Scott et al., 2005).

Subcellular fractionation can be performed to find out if EHB1 protein is present in the microsomal or cytosolic fraction. Having the C2 domain it can be expected that EHB1 might be present in microsomal fraction (plasma membrane) as well as in the cytosolic fraction of the cell.

To know exactly, which compartment of the cell EHB1 is localized, live cell imaging can help to answer this question. Fluorescently labeled proteins (GFP-tagged) are widely used now to study protein localization, dynamics, and interaction. GFP tagged EHB1 would co-localized with plasma membrane markers.

3. Investigation of EHB1 binding to membrane phospholipids

It has been shown that C2 domain binds to membrane phospholipids (Davletov and Südhof, 1993) because EHB1 also harbors a C2 domain. It should be investigated to which specific membrane phospholipids EHB1 binds through its C2 domain.

Additionally, it should also be investigated weather EHB1-C2 domain binding with membrane phospholipids is Ca^{2+}-dependent.
This will be investigated through membrane lipid-binding assay and liposome-binding assay. Both the assays will be performed in the presence and absence of Ca^{2+}.

4. Reconfirmation and additional experiments for verification of EHB1 function as negative regulator

The aim is to test our initial hypothesis that EHB1 might act as a negative regulator of iron homeostasis in Arabidopsis. The molecular and physiological consequences of an *EHB1* loss-of-function *ehb1-1* mutant should be investigated. Using reverse transcription quantitative PCR (RT-qPCR), the expression of *EHB1* has to be examined under physiological conditions related to iron deficiency. According to the hypothesis, it is expected that the expression of *EHB1* would be up-regulated at iron sufficient situation, while that of *IRT1* would be down-regulated at iron sufficiency. And during iron-deficiency, the situation should reverse i.e. *EHB1* would be down-regulated and *IRT1* would be up-regulated.

Iron reductase activity of FRO2 in roots of plants grown in the presence (+Fe) and absence (-Fe) of iron should be investigated. The FRO2 activity (Fe reduction) is expected to be increased in *ehb1-1* mutant as compared to wild-type and HA-EHB1 lines. The chlorophyll and metal ion (Fe) content of mutant *ehb1-1* and HA-EHB1 lines should also be investigated. We expect that the chlorophyll content of young leaves in *ehb1-1* mutant would be higher than in the wild type and HA-EHB1. And also the seeds of mutant *ehb1-1* plants would have accumulated more iron in comparison with wild-type and HA-EHB1. Qualitative measurement of iron localization in plants root should also be performed. It is expected that from the apoplast mutant *ehb1-1* will take up more iron than HA-EHB1. Thus, we expect that more iron will be retained in the apoplast of HA-EHB1.

3. Materials and Methods

3.1 Materials

3.1.1 Plant materials

The plants listed below were used for physiological and molecular analysis in this study.

- *Arabidopsis thaliana* ecotype Columbia (Col-0) has been used as wild-type (WT).
- *Nicotiana benthamiana*

List of plants used in this study

Name/Abbreviation	Gene/Accession	Genotype/Phenotype	Source
ehb1-1	SALK_134720.56.00.x /AT1G70800.1	T-DNA insertion line; 274 bp in Exon 1	Knauer et al., 2011
ehb1-2	SAIL 385_C07.v1	T-DNA insertion line; Exon 3	Knauer et al., 2011
HA-EHB1	AT1G70800	pAlligator 2 , *2xCaMV35S:3xHA*-EHB1 over expression line in Col-0 background	Rumen Ivanov
fit-3	*FIT/* AT2G28160	T-DNA insertion 207 bp downstream of ATG/ Chlorotic	Jakoby et al., 2004
irt1-1	AT4G19690.1	T-DNA insertion in 3rd exon/ Chlorotic	Vert et al., 2002

3.1.2 Bacterial strains for molecular cloning

Strain	Genotype	Usage	Manufacturer
***Escherichia coli* (*E. coli*) DH5-alpha**	fhuA2 Δ(argF-lacZ)U169 phoA glnV44 Φ80 Δ(lacZ)M15 gyrA96 recA1 relA1 endA1 thi-1 hsdR17	Propagation/ multiplication	Invitrogen Cat. No. C2987I
***Escherichia coli* (*E. coli*) *ccd*B Survival™ 2 T1**	F- mcrA Δ(mrr-hsdRMS-mcrBC) Φ80lacZΔM15 ΔlacX74 recA1 araΔ139 Δ(ara-leu)7697 galU galK rpsL (StrR) endA1 nupG fhuA::IS2	Propagation/ multiplication	Invitrogen Cat. No. A10460
BL21(DE3) pLysS	F–, ompT, hsdSB (rB–, mB–), dcm, gal, l(DE3), pLysS, Cmr	Protein expression	Promega Cat. No. L1191
Agrobacterium tumefaciens	C58; GV2260/pGV2260; Rif^r, Cn^r	Plant transformation	

3.1.3 Plasmids

Basic Plasmids used in the study

Plasmid	Manufacturer	Structure	Selection
pDONR207	Invitrogen	Entry vector with Gateway cassette containing P1 and P2 attachment sites	*ccdb* suicidal gene as insertional control, Gm^r: for selection in bacteria
pDONR221 P1P4	Invitrogen	Entry vector with Gateway cassette containing P1 and P4 attachment sites	*ccdb* suicidal gene as insertional control, Km^r: for selection in bacteria
pDONR221 P3P2	Invitrogen	Entry vector with Gateway cassette containing P3 and P2 attachment sites	*ccdb* suicidal gene as insertional control, Km^r: for selection in bacteria
pBiFct-2in1 CC	Grefen, C. and M. R. Blatt (2012), Biotechniques	Expression vector Containing multiple expression cassettes within a single vector backbone	lacZ and *ccdb* suicidal gene as insertional control, Spec^r: for selection in bacteria
PMDC83	Invitrogen	Gateway compatible plant transformation vector containing a C-terminal GFP tag	*ccdb* suicidal gene as insertional control, Km^r: for selection in bacteria
pAlligator 2	Bensmihen, S., et	Gateway compatible plant transformation	Contains a gateway cassette

	al. (2004), FEBS letters	vector Containing an 3xHA tag at N-terminal	between aat1 and att2, Spec^r: for selection in bacteria
pETStrepII	Hashimoto et al., (2012), *J. Biol. Chem*	Expression vector containing an Strep tag at N-terminal	Contains AKT2-Ct between SpeI and XhoI restriction sites, Km^r: for selection in bacteria
pAUL 1	Lyska, D., et al., (2013), PloS one	Gateway compatible plant transformation vector containing an 3xHA tag at C-terminal	*ccdb* suicidal gene as insertional control, Km^r: for selection in bacteria

*r: resistance

Plasmids generated in this work for protein expression in plants

Plasmid name	Original plasmid	Insertion place in plasmid	Inserted fragment	Bacterial selection	Reference
EHB1ns-pDONR207	pDONR207	Inserted between P1 and P2 att sites replacing *ccdb*	EHB1: EHB1ns generated with 5`EHB1B1 & 3`EHB1cterB2 nonstop primers	Gm^r: transformation control in bacteria	This work
EHB1ΔSigns-pDONR207	pDONR207	Inserted between P1 and P2 att sites replacing *ccdb*	EHB1ΔSig: EHB1ΔSigns generated with 5`EHB1B1 & 3`EHB1cterB2 nonstop primers	Gm^r: transformation control in bacteria	This work
EHB-4x ns-pDONR207	pDONR207	Inserted between P1 and P2 att sites replacing *ccdb*	EHB1-4x: EHB1-4x ns generated with 5`EHB1B1 & 3`EHB1cterB2 nonstop primers	Gm^r: transformation control in bacteria	This work
EHB1-PMDC83	PMDC83	Inserted between R1 and R2 att sites replacing *ccdb*	EHB1ns: generated from EHB1ns-pDONR207	Km^r: transformation control in bacteria	This work
EHB1ΔSig-PMDC83	PMDC83	Inserted between R1 and R2 att sites replacing *ccdb*	EHB1ΔSigns: generated from EHB1ΔSigns-pDONR207	Km^r: transformation control in bacteria	This work
EHB1-4x-PMDC83	PMDC83	Inserted between R1 and R2 att sites replacing *ccdb*	EHB1-4x ns: generated from EHB1-4x ns-pDONR207	Km^r: transformation control in bacteria	This work
EHB1-pAUL1	pAUL1	Inserted between R1 and R2 att sites replacing *ccdb*	EHB1ns: generated from EHB1ns-pDONR207	Km^r: transformation control in bacteria	This work
EHB1-pDONR207	pDONR207	Inserted between P1 and P2 att sites replacing *ccdb*	EHB1: generated with 5`EHBnter1B1 & 3`EHB1B2 primers	Gm^r: transformation control in bacteria	This work
EHB1-4x-pDONR207	pDONR207	Inserted between P1 and P2 att sites replacing *ccdb*	EHB1-4x: generated with 5`EHBnter1B1 & 3`EHB1B2 primers	Gm^r: transformation control in bacteria	This work
EHB1-pAlligator 2	pAlligator 2	Inserted between R1 and R2 att sites replacing *ccdb*	EHB1: generated from EHB1-pDONR207	Spec^r: transformation control in bacteria	This work
EHB1-4x-pAlligator 2	pAlligator 2	Inserted between R1 and R2 att sites replacing *ccdb*	EHB1-4x: generated from EHB1-pDONR207	Spec^r: transformation control in bacteria	This work
EHB1 c-ter pDONR221-P1P4	pDONR221 P1P4	Inserted between P1 and P2 att sites replacing *ccdb*	EHB1 c-ter P1P4 generated with 5`EHB1B1 & 3`EHB1cterB4 primers	Km^r: transformation control in bacteria	This work
EHB1 c-ter pDONR221-P3P2	pDONR221 P3P2	Inserted between P1 and P2 att sites replacing *ccdb*	EHB1 c-ter P3P2 generated with 5`EHB1B3 & 3`EHB1cterB2 primers	Km^r: transformation control in bacteria	This work
EHB1ΔSig c-ter - pDONR221-P1P4	pDONR221 P1P4	Inserted between P1 and P2 att sites replacing *ccdb*	EHB1ΔSig-P1P4 generated with 5`EHB1B1 & 3`EHB1cterB4 primers	Km^r: transformation control in bacteria	This work
EHB1ΔSig c-ter - pDONR221-P3P2	pDONR221 P3P2	Inserted between P1 and P2 att sites replacing *ccdb*	EHB1ΔSig-P3P2 generated with 5`EHB1B3 & 3`EHB1cterB2 primers	Km^r: transformation control in bacteria	This work
EHB1-4x c-ter-pDONR221-P1P4	pDONR221 P1P4	Inserted between P1 and P2 att sites replacing *ccdb*	EHB1-4x-P1P4 generated with 5`EHB1B1 & 3`EHB1cterB4 primers	Km^r: transformation control in bacteria	This work
EHB1-4x c-ter-pDONR221-P3P2	pDONR221 P3P2	Inserted between P1 and P2 att sites replacing *ccdb*	EHB1-4x-P3P2 generated with 5`EHB1B3 & 3`EHB1cterB2 primers	Km^r: transformation control in bacteria	This work
IRT1-loop c-ter-pDONR221-P1P4	pDONR221 P1P4	Inserted between P1 and P2 att sites replacing *ccdb*	IRT1-loop-P1P4 generated with 5`I1LatgB1 & 3`I1LB4 primers	Km^r: transformation control in bacteria	This work
IRT1-loop c-ter-pDONR221-P3P2	pDONR221 P3P2	Inserted between P1 and P2 att sites replacing *ccdb*	IRT1-loop-P3P2 generated with 5`I1LB3 & 3`I1LB2 primers	Km^r: transformation control in bacteria	This work

SNX1 c-ter-pDONR221-P1P4	pDONR221 P1P4	Inserted between P1 and P2 att sites replacing *ccdb*	SNX1-P1P4 generated with 5`SNX1B1 & 3`SNX1cterB4 primers	Km^r: transformation control in bacteria	This work
SNX1 c-ter-pDONR221-P3P2	pDONR221 P3P2	Inserted between P1 and P2 att sites replacing *ccdb*	SNX1-P3P2 generated with 5`SNX1B3 & 3`SNX1cterB2 primers	Km^r: transformation control in bacteria	This work
EHB1-nYFP+IRT1loop-cYFP- pBiFct-2in1 CC	pBiFct-2in1 CC	Inserted between R1-R4 att sites replacing *ccdb* and between R3-R2 replacing lacZ	EHB1 c-ter-P3P2+IRT1loop c-ter-P1P4: generated from EHB1 c-ter P2P2 and IRT1-loop c-ter-P1P4	$Spec^r$: transformation control in bacteria	This work
EHB1-4x-nYFP+IRT1loop-cYFP- pBiFct-2in1 CC	pBiFct-2in1 CC	Inserted between R1-R4 att sites replacing *ccdb* and between R3-R2 replacing lacZ	EHB1-4x c-ter-P3P2+IRT1loop c-ter-P1P4: generated from EHB1-4x c-ter P2P2 and IRT1-loop c-ter-P1P4	$Spec^r$: transformation control in bacteria	This work
EHB1 ΔSig -nYFP+IRT1loop-cYFP- pBiFct-2in1 CC	pBiFct-2in1 CC	Inserted between R1-R4 att sites replacing *ccdb* and between R3-R2 replacing lacZ	EHB1 ΔSig c-ter-P3P2+IRT1loop c-ter-P1P4: generated from EHB1 ΔSig c-ter P2P2 and IRT1-loop c-ter-P1P4	$Spec^r$: transformation control in bacteria	This work
EHB1-nYFP+SNX1-cYFP- pBiFct-2in1 CC	pBiFct-2in1 CC	Inserted between R1-R4 att sites replacing *ccdb* and between R3-R2 replacing lacZ	EHB1 c-ter-P3P2+SNX1 c-ter-P1P4: generated from EHB1 c-ter P2P2 and SNX1 c-ter-P1P4	$Spec^r$: transformation control in bacteria	This work
IRT1loop-nYFP+SNX1-cYFP- pBiFct-2in1 CC	pBiFct-2in1 CC	Inserted between R1-R4 att sites replacing *ccdb* and between R3-R2 replacing lacZ	IRT1loop c-ter-P3P2+SNX1 c-ter-P1P4: generated from IRT1loop; c-ter P2P2 and SNX1 c-ter-P1P4	$Spec^r$: transformation control in bacteria	This work
SNX1-nYFP+SNX1-cYFP- pBiFct-2in1 CC	pBiFct-2in1 CC	Inserted between R1-R4 att sites replacing *ccdb* and between R3-R2 replacing lacZ	SNX1 c-ter-P3P2+SNX1 c-ter-P1P4: generated from SNX1 c-ter P2P2 and SNX1 c-ter-P1P4	$Spec^r$: transformation control in bacteria	This work

*ns: nonstop: r: resistance

Plasmids generated in this work for protein expression *E. coli (BL21)*

Plasmid name	Original plasmid	Insertion place in plasmid	Inserted fragment	Bacterial selection	Reference
EHB1- pETStrepII	pET StrepII	Inserted between SpeI and XhoI restriction site at multiple cloning region of vector	EHB1-StrepII: generated with 5`E1Strepii SpeI & 3`E1Strepii XhoI primers	Km^r: transformation control in bacteria	This work
EHB1-4x-pETStrepII	pET StrepII	Inserted between SpeI and XhoI restriction site at multiple cloning region of vector	EHB1-4x-StrepII: generated with 5`E1Strepii SpeI & 3`E1Strepii XhoI primers	Km^r: transformation control in bacteria	This work
EHB1ΔSig-pETStrepII	pET StrepII	Inserted between SpeI and XhoI restriction site at multiple cloning region of vector	EHB1ΔSig-StrepII: generated with 5`E1Strepii SpeI & 3`E1Strepii XhoI primers	Km^r: transformation control in bacteria	This work

*r: resistance

3.1.4 Antibiotics used during the course of studies

Antibiotic	Dissolve in	Stock concentration	Dilution for the use
Gentamycin	H_2O	50 mg/ml	1:2000
Kanamycin	H_2O	50 mg/ml	1:1000
Spectinomycin	H_2O	70 mg/ml	1:1000
Carbenicillin	H_2O	60 mg/ml	1:1000
Rifampicin	DMSO	50 mg/ml	1:1000

3.1.5 Antibodies

- Mouse monoclonal anti-HA tag antibody (diagenode-Cat. Nr. C15200190) Used for detection of HA tagged proteins.
- Mouse IgG1 (clones 7.1) anti-GFP antibody used to detect GFP tagged proteins.
- Strep-Tactin horseradish peroxidase anti-Strep tag antibody (iba-Cat.no: 2-1502-001) Used for detection of Strep tagged proteins.
- Rabbit polyclonal anti-H^+ATPase antibody (Agrisera- AS07 260) used to detect plasma membrane H^+ATPase.
- Rabbit polyclonal anti-UGPase antibody (Agrisera- AS05 086) used to detect UDP-glucose pyrophosphorylase (cytoplasm marker).
- Rabbit polyclonal anti-BiP2 antibody (Agrisera- AS09 481) used to detect BiP lumenal-binding protein.
- Anti-mouse horseradish peroxidase secondary antibody raised in goat for detection of GFP antibodies (Promega-Cat.no: W4021).
- Polyclonal goat anti-Rabbit horseradish peroxidase secondary antibody (Sigma Aldrich) to detect H^+ATPase, UGPase and BiP2 antibodies.

3.1.6 Oligonucleotides

Primers for RT PCR

Gene	Primer name	Primer Sequence
EHB1	EHB1 5‘ RT1	5‘ GCTTGTCTGAAGATAGCATA 3'
	At1g70800 3‘ Std r	5‘ CTGTTGAAGAATGTCGAATGCG 3'
Efc	EFc-5'	5‘ TATGGGATCAAGAAACTCACAAT 3'
	EFc-3'	5‘ CTGGATGTACTCGTTGTTAGGC 3'
bHLH39	RT 5'bHLH39	5‘ GACGGTTTCTCGAAGCTTG 3'
	RT 3'bHLH39	5‘ GGTGGCTGCTTAACGTAACAT 3'
Efg	AtEF-gen-5' (2522)	5‘ TCCGAACAATACCAGAACTACG 3'
	AtEF-gen-3' (2726)	5‘ CCGGGACATATGGAGGTAAG 3'
FER1	FER1 5'	5‘ ACGCACTCTCGTCTTTCACC 3'
	FER1 3'	5‘ GAAAGGCTGGAACACGACTC 3'
FRO2	AtFRO2-c-5' (1806)	5‘ CTTGGTCATCTCCGTGAGC 3'
	FRO2-c3-RT3'	5‘ AAGATGTTGGAGATGGACGG 3'
IRT1	IRT1 5‘ RT extended	5‘ AAGCTTTGATCACGGTTGGACTTCTAAATGC 3'
	IRT1 3' RT extended	5‘ TTAGGTCCCATGAACTCCGCAGCTAG 3'
FIT	FIT 5'(166-187) RT	5‘ CCCTGTTTCATAGACGAGAAC 3‘
	FIT-RT 3' MN	5‘ ATCCTTCATACGCCCTCTCC 3‘

All primers were ordered in 100 uM concentration

Primers for *EHB1* genotyping

Gene/T-DNA	Primer name	Primer Sequence
EHB1	EHB1B1	5’ATGGAGAAAACAGAGGAAGAG 3’
	EHB1B2	5’TCAGAGTCCACTACCACCTGGAT 3’
	LBSALK	5’ACCGAGCTCGAATTTCCCCG 3’

Primers for standard-PCR reactions

Gene	Primer name	Primer Sequence
EHB1	EHB1B1	5' GGGGACAAGTTTGTACAAAAAAGCAGGCTATGGAGAAAACAGAGGAAGAG 3'
	EHB1B2	5' GGGGACCACTTTGTACAAGAAAGCTGGGTTCAGAGTCCACTACCACCTGGAT 3'
	EHB1f	5' ATGGAGAAAACAGAGGAAGAG 3'
	EHB1r	5' TCAGAGTCCACTACCACCTG 3'

Primers for molecular cloning

Gene	Primer name	Primer sequence
EHB1	E1Strepii SpeI fwd	5' TTTTACTAGTATGGAGAAAACAGAGGAAGAG 3'
	E1Strepii XhoI Rev	5' TTTTCTCGAGTCAGAGTCCACTACCACCTG 3'
	EHB1B1	5' GGGGACAAGTTTGTACAAAAAAGCAGGCTATGGAGAAAACAGAGGAAGAG 3'
	EHB1B2	5' GGGGACCACTTTGTACAAGAAAGCTGGGTTCAGAGTCCACTACCACCTGGAT 3'
	EHBnter1B1	5'GGGGACAAGTTTGTACAAAAAAGCAGGCTTTATGGAGAAAACAGAGGAAGA 3'
	EHB1B4	5'GGGGACAACTTTGTATAGAAAAGTTGGGTTCAGAGTCCACTACCACCTGGAT 3'
	EHBnterB3	5'GGGGACAACTTTGTATAATAAAGTTGTAATGGAGAAAACAGAGGAAGA 3'
	EHB1B2	5'GGGGACCACTTTGTACAAGAAAGCTGGGTTCAGAGTCCACTACCACCTGGAT 3'
	EHB1B1	5'GGGGACAAGTTTGTACAAAAAAGCAGGCTATGGAGAAAACAGAGGAAGA 3'
	EHB1cterB4	5'GGGGACAACTTTGTATAGAAAAGTTGGGGGAGTCCACTACCACCTGGAT 3'
	EHB1B3	5'GGGGACAACTTTGTATAATAAAGTTGATGGAGAAAACAGAGGAAGA 3'
	EHB1cterB2	5'GGGGACCACTTTGTACAAGAAAGCTGGGTTGAGTCCACTACCACCTGGAT 3'
IRT1-loop	I1LatgB1	5'GGGGACAAGTTTGTACAAAAAAGCAGGCTATGTCCATGGCCACGAGCCTATA 3'
	I1LnsB4	5'GGGGACAACTTTGTATAGAAAAGTTGGGTGTCGGTATCGCAAGAGCTGTG 3'
	I1LatgB3	5'GGGGACAACTTTGTATAATAAAGTTGATGTCCATGGCCACGAGCCTATA 3'
	I1LnsB2	5'GGGGACCACTTTGTACAAGAAAGCTGGGTTTCGGTATCGCAAGAGCTGTG 3'
	I1LB1	5'GGGGACAAGTTTGTACAAAAAAGCAGGCTTTTCCATGGCCACGAGCCTATA 3'
	I1LB4	5'GGGGACAACTTTGTATAGAAAAGTTGGGTTTATCGGTATCGCAAGAGCTGTG 3'
	I1LB3	5'GGGGACAACTTTGTATAATAAAGTTGTATCCATGGCCACGAGCCTATA 3'
	I1LB2	5'GGGGACCACTTTGTACAAGAAAGCTGGGTTTATCGGTATCGCAAGAGCTGTG 3'
SNX1	SNX1B1	5'GGGGACAAGTTTGTACAAAAAAGCAGGCTATGGAGAGCACGGAGCAGC 3'
	SNX1cterB2	5'GGGGACCACTTTGTACAAGAAAGCTGGGTTGACAGAATAAGAAGCTT 3'
	SNX1B3	5'GGGGACAACTTTGTATAAAGTTGATGGAGAGCACGGAGCAGC 3'
	SNX1cterB4	5'GGGGACAACTTTGTATAGAAAAGTTGGGTTGACAGAATAAGAAGCTT 3'

Primers for cloning different fragments of *IRT1vr*

Gene	Primer name	Primer sequence
Full loop	I1LatgB1	5’ GGGGACAAGTTTGTACAAAAAAGCAGGCTATGTCCATGGCCACGAGCCTATA 3’
	I1LnsB4	5’ GGGGACAACTTTGTATAGAAAAGTTGGGTGTCGGTATCGCAAGAGCTGTG 3’
	I1LatgB3	5’ GGGGACAACTTTGTATAATAAAGTTGATGTCCATGGCCACGAGCCTATA 3’
	I1LnsB2	5’ GGGGACCACTTTGTACAAGAAAGCTGGGTTTCGGTATCGCAAGAGCTGTG 3’
Δ2	I1LatgB1	5’ GGGGACAAGTTTGTACAAAAAAGCAGGCTATGTCCATGGCCACGAGCCTATA 3’
	2cternsB4	5’ GGGGACAACTTTGTATAGAAAAGTTGGGTGGGGGCCGTGACCATGACCATG 3’
	I1LB3	5’ GGGGACAACTTTGTATAATAAAGTTGATGTCCATGGCCACGAGCCTATA 3’
	2cternsB2	5’ GGGGACCACTTTGTACAAGAAAGCTGGGTTGGGGCCGTGACCATGACCATG 3’
Δ3	3cterB1	5’ GGGGACAAGTTTGTACAAAAAAGCAGGCTATGCCCCATGGTCATGGTCATGGT 3’
	3cternsB4	5’ GGGGACAACTTTGTATAGAAAAGTTGGGTGTCGGTATCGCAAGAGCTGTG 3’
	3cterB3	5’ GGGGACAACTTTGTATAATAAAGTTGATGCCCCATGGTCATGGTCATGGT 3’
	3cternsB2	5’ GGGGACCACTTTGTACAAGAAAGCTGGGTTTCGGTATCGCAAGAGCTGTG 3’
Δ4	4cterB1	5’ GGGGACAAGTTTGTACAAAAAAGCAGGCTATGCCCCATGGTCATGGTCATGGT 3’
	4cternsB4	5’ GGGGACAACTTTGTATAGAAAAGTTGGGTGCGAATCATCTTCTTTTATTGG 3’
	4cterB3	5’GGGGACAAGTTTGTACAAAAAAGCAGGCTATGGAGAAAACAGAGGAAGA 3’
	4cterB3	5’ GGGGACAACTTTGTATAATAAAGTTGATGCCCCATGGTCATGGTCATGGT 3’
	4cternsB2	5’ GGGGACCACTTTGTACAAGAAAGCTGGGTTCGAATCATCTTCTTTTATTGG 3’

Primers for Signature domain deletion

Gene	Primer name	Primer sequence
EHB1-ΔSig	EHB1B1	5’ GGGGACAAGTTTGTACAAAAAAGCAGGCTATGGAGAAAACAGAGGAAGAG 3’
	E1deltaSig1	5’ AGATGGGAGATGCGCAGATAGGCAAGATCGTTCAGGACAT 3’
	E1deltaSig2	5’ ATGTCCTGAACGATCTTGCCTATCTGCGCATCTCCCATCT 3’
	EHB1B2	5’ GGGGACCACTTTGTACAAGAAAGCTGGGTTCAGAGTCCACTACCACCTGGAT 3’

Primers for EHB1 C2 domain mutation

Gene	Primer name	Primer sequence
EHB1- 4x	EHB1 D31/36A1	5’ GCTCGTCGAGCTGCTCTAAGCAGCGCTCCTTTTGTC 3’
	EHB1 D31/36A2	5’ GACAAAAGGAGCGCTGCTTAGAGCAGCTCGACGAGC 3’
	EHB1 D82/84A1	5’ ATGGTGTATGCTAAAGCTACATTTACA 3’
	EHB1 D82/84A2	5’ TGTAAATGTAGCTTTAGCATACACCAT 3’

Primers for His-domain deletion from large cytosolic loop of *IRT1*

Gene	Primer name	Primer sequence
IRT1-ΔHis	I1LB1	5' GGGGACAAGTTTGTACAAAAAAGCAGGCTTTTCCATGGCCACGAGCCTATA 3'
	5AM1	5' AAGGTAACATCATTTGCGGGGGGCATGATACCAACTGCGT 3'
	5BM2	5' ACGCAGTTGGTATCATGCCCCCCGCAAATGATGTTACCTT 3'
	I1LB4	5' GGGGACAACTTTGTATAGAAAAGTTGGGTTTATCGGTATCGCAAGAGCTGTG 3'

Primers for sequencing

Gene/ Plasmid	Primer name	Primer sequence
pDONR207	pDSeq 1	5` GCAGTTCCCTACTCTCGG 3`
	pDSeq 2	5`CATCAGAGATTTTGAGACAC 3`
pDONR221	pDONR-5	5` TAACGCTAGCATGGATCTC 3`
	pDONR-3	5` GCAATGTAACATCAGAGAT 3`
PMDC83	M13-F'	5` TGTAAAACGACGGCCAG 3`
	M13-R'	5` CAGGAAACAGCTATGAC 3`
pAlligator 2	HA-F'	5` GATGTTCCTGACTATGCGGGC 3`
P3P2-CC	RB fwd	5` GGCGGGAAACGACAATCTGATCC 3`
	nYFP rev	5` ATGGGCACCACCCCGGTGAA 3`
P1P4-CC	RFP fwd	5` AGGGCCGCCACTCCACCG 3`
	cYFP rev	5` CTCGTTGGGGTCTTTGCTCAGG 3`

3.1.7 Enzymes and Kits

Enzymes

Enzyme	Company
RED Taq Ready Mix (0.06 U/µL)	Sigma-Aldrich
***Q5* high fidelity DNA polymerase (2 U/µL)**	New England BioLabs
BcuI (SpeI) (10 U/µL)	Thermo Scientific
XhoI (20 U/µL)	New England BioLabs
DpnI (10 U/µL)	Thermo Scientific
BP Clonase II Enzyme mix	Thermo Scientific
LR Clonase II Enzyme mix	Thermo Scientific
T4 DNA Ligase (20 U/µL)	New England BioLabs

Kits

Name	Company	Usage
GeneJET Plasmid Miniprep kit	Thermo Scientific	Plasmid isolation
GeneJET Gel Extraction kit	Thermo Scientific	Band purification
Peq GOLD Plant RNA kit	Peqlab	RNA extraction
Quick Ligation kit	New England BioLabs	DNA ligation
GFP-Trap®	Chromotek	Anti GFP beads

3.1.8 Markers

Description	Usage	Manufacturer
Gene Ruler 1 kb Plus DNA Ladder	Agarose gel-Electrophorese	Thermo Scientific (SM1331)
Gene Ruler 1 kb DNA Ladder	Agarose gel-Electrophorese	Thermo Scientific (SM0311)
Page Ruler Prestained Protein Ladder	SDS page Gel-Electrophorese	Thermo Scientific (26616)

3.1.9 Chemicals

Name	Concentration	Stored at
IPTG	1M	-20 °C
$CaCl_2$	0.5 M	RT
EDTA (pH 8.0)	0.5 M	RT
NaCl	1 M	RT
PMSF	100 mM	4 °C
FeNa-EDTA	50 µM	4 °C
Tris-HCl (pH 8.0)	1 M	RT
SDS	10 %	RT
BSA	10 mg/ml	-20 °C
dNTP	10 mM each	-20 °C
Triton-X	0.2 %	RT
NaH $2PO_4$ (pH7.2)	100 mM	RT
Na $2HPO_4$ (pH7.2)	100 mM	RT
Protease Inhibitor Cocktail	7x	-20 °C
Lysozyme	0.35 mg/ml	-20 °C
DTT	100 mM	-20 °C
Brij-35	1 mM	RT
Urea	8M	RT
Strep-Tactin® Macro Prep	50 %	8°C
α-Desthiobiotin	2.5 mM	8°C

3.1.10 Buffers and Media

A. Buffers for western blotting

a. SDS-Page

Buffers	Ingredients	Concentration	pH
10x Running buffer	Tris base	250 mM	8.3
	Glycine	2.5 M	
	SDS	10 %	
For 1x 1L buffer take 100 ml 10x buffer and add 900 ml ddH_2O			
Transfer buffer (1 L Ready to use)	100 ml Running buffer (10x)	1x	8.3
	200 ml Ethanol (technical)		
	700 ml dd-H_2O		
10x TBS	NaCl	80 g/L	7.6
	Tris base	24.2 g/L	
For 1x TBS-T take 100 ml 10x TBS add 900 ml ddH_2O and 1 ml Tween20			
Blocking solution	Milk powder	5 %	
	1x TBS-T	100 ml	
Ponceau S	Ponceau S (Sigma)	2 g/L	
	Trichloraceticacid (TCA)	30 g/L	
	S-Sulfosalicylicacid	30 g/L	
2x Laemmli buffer (10 ml)	Tris-HCl	120 mM	6.8
	DTT	200 mM	

	SDS	4 %
	glycerol	20 %
	Bromophenol blue	0.2 %
	ddH_2O	600 µL
ECL-Solution (Amersham)	Luminol Solution A	50%
	Peroxid Solution B	50%

b. Other solutions

Buffer for Agarose gel electrophoresis

1 L 50x TAE
40 mM Tris
20 mM acetic acid
1 mM EDTA pH 8

Buffers for liquid Iron reductase assay

Wash solution
100 mM $Ca(NO_2)_3$

Fe reductase solution
300 µM Ferrozine
100 µM FeNaEDTA

1x Tobacco infiltration solution pH 5.6
50 mM MES
2mM NaH2PO4
5% Glucose
100µM Acetosyringon

Solution for Perl staining for 10 ml

Fixing solution
6 ml Methanol
3 ml Chloroform (End concentration is 6:3:1)
1 ml Glacial acetic acid

Staining solution
4% $K_4Fe(Cn)_6$
4% HCl (37%)

Buffers for Co-Immunoprecipitation
50 mM Tris HCl pH8
150 mM NaCl
1mM EDTA
1% Triton-X 100
Protease inhibitor (1 tablet for 10 ml)

Buffers for cell Fractionation

Buffers for Homogenization medium
0.3 M sucrose
50 mM MOPS-KOH
5 mM EDTA-KOH pH 7.5
5 mM PVPP
5 mM DTT
5 mM ascorbic acid
0.2% (w/v) casein
100 mM PMSF
Protease inhibitor 25x

Buffers for Resuspension medium
0.3 M sucrose
5 mM potassium phosphate pH 7.8
0.1 mM EDTA–KOH, pH 7.8
1 mM DTT
Protease inhibitor 25x

Buffers for protein purification

Lysis Buffer
100 mM Tris-HCl, pH 8.0
150 mM NaCl
5 mM DTT
0.35 mg/ml Lysozyme
1x PIC
1 mM Brij-35

Wash Buffer-I
100 mM Tris-HCl, pH 8.0
150 mM NaCl
1 mM Brij-35
8 M Urea

Wash Buffer-II
100 mM Tris-HCl, pH 8.0
1 mM Brij-35
1 mM Brij-35

Wash Buffer-II
100 mM Tris-HCl, pH 8.0
150 mM NaCl

Elution Buffer
100 mM Tris-HCl, pH 8.0
150 mM NaCl
1 mM Brij-35
2.5 mM α-Desthiobiotin

B. Media

a. Medium for bacterial growth

LB-Media (pH 7)

1% Bacto Tryptone
0.5% Yeast Extract
0.17 M NaCl

LB-Agar
1.6% LB agar

YEP media 1 L (pH 7)

1 g Yeast extract
5 g Beef extract
5 g Sucrose
5 g Bacto peptone
0.5 g $MgSO_4$ $7H_2O$
Add 15 g/L agar for plate

b. Medium for plant growth

Hoagland Medium for 1 L (pH 6)

Micronutrients	Macronutrients	others components
50 mM KCl	0.75 mM $MgSO_4$ $7H_2O$	1 % Sucrose
50 µM H_3BO_3	0.5 mM KH_2PO_4	0.8 % Plant agar
10 µM $MnSO_4$ H_2O	1.25 mM KNO_3	50 µM FeNaEDTA (+Fe)
2 µM $ZnSO_4$ $7H_2O$	1.5 mM $Ca(NO_3)_2$	0 µM FeNaEDTA (-Fe)
1.5 µM $CuSO_4$ $5H_2O$		
0,075 µM $(NH_4)_6Mo_7O_{24}$ $4H_2O$		

3.1.11 Gels

a. Agarose Gel for DNA

1 g Agarose for 1% gel in 100 ml 1x TAE

Run for 45 minutes at 100 mV.

b. Gels for protein separation (SDS-PAGE)

Precast gels from Bio-Rad was used during the study the details can be found here,

http://www.bio-rad.com/en-do/product/mini-protean-precast-gels/mini-protean-tgx precast-gels
For making the gels manually in the lab the following recipe was used

	Running gel 12%	Stacking gel 5%
H_2O	3.5 ml	3 ml
Buffer	2.5 ml	1.25 ml
AA-BAA	4 ml	0.67 ml
APS	50 µL	50 µL
Temed	5 µL	5 µL

3.1.12 other materials

Material	Company	Usage
Petri dish (Round)	Sarstedt	Bacterial growth
Petri dish (Square)	Greiner	Plant growth
50 ml tubes	Greiner	miscellaneous
15 ml tubes	Greiner	miscellaneous
12 ml tubes	Greiner	miscellaneous
2 ml tubes	Sarstedt	miscellaneous
1.5 ml tubes	Sarstedt	miscellaneous
PCR strips (colored)	Sarstedt	miscellaneous
96 well PCR plate full skirt	Sarstedt	qPCR
GRE96ft half area multi well	Greiner	Iron reductase assay
Nitrocellulose Membranes	GE Healthcare	Western blotting

3.1.13 Devices

Name	Company
CFX96 Touch Real-Time PCR Detection System	Bio-Rad
FluoChem Q system	Proteinsimple
Lipid mini extruder	Avanti lipids
Infinite 200 PRO series	TECAN
Confocal Microscopy	Zeiss LSM 780 Laser Scanning Microscope
PROTEAN Electrophoresis Chambers	Bio-Rad
FAS-V Gel imager	Nippon genetics
Branson digital Sonifier 250	Branson Ultrasonics
Thermocycler	PeqLab
PRECELLYS 24	Precellys
Growth Chambers	Percival
DNA Gel system	PeqLab
Vacuum pump	Vacuubrand
Centrifuges and cool centrifuges	Thermo
Ultracentrifuge L-80 XP	Beckman
S20 – Seven-Easy pH meter	Mettler toledo

3.1.14 Software and online tools

Name	URL
ApE- A plasmid Editor	http://biologylabs.utah.edu/jorgensen/wayned/ape/
Snapgene	http://www.snapgene.com/
LSM software	www.zeiss.de/micro
AlphaView	http://www.proteinsimple.com/software_alphaview.html
Bio-Rad CFX Manager	http://www.bio-rad.com/en-us/product/cfx manager-software
JMicro Vision	http://www.jmicrovision.com/
TAIR	https://www.arabidopsis.org/
ImageJ	https://imagej.nih.gov/ij/download.html
Origin 9 pro	http://www.originlab.com/

3.2 Methods

3.2.1 Physiological iron response assays

3.2.1.1 Seed sterilization

Before plating on the media Arabidopsis seeds were surface sterilized with 6% Sodium hypochlorite, 1% Triton X-100 for 8 minutes and then washed 5 times with distilled water, the seeds were then stratified for 2-3 days in the dark at 4°C in 0.1% plant agar.

3.2.1.2 Arabidopsis plant growth

After sterilization, the seeds were plated on Hoagland agar medium containing 50 µM FeNa-EDTA (+Fe) or 0 µM FeNa-EDTA (-Fe) and were grown vertically in the square plates placed in Percival growth chamber at 21°C/24°C and 16 h light, 8 h dark cycles (long-day condition) with a 110-150 µmol $m^{-2}s^{-1}$ light intensity. The plant growth time is described in the respective experiment.

3.2.1.3 Iron reductase activity assay

The transparent Ferrozine makes a complex with Fe(II) and changes its color to purple. This color changing ability of Ferrozine is used to quantify the activity of root-associated ferric-chelate reductase (FRO2). To perform a liquid Fe reductase assay plants were grown on Hoagland agar medium in square Petri plates for 14 days under sufficient iron condition (+Fe) and then were split into -Fe (iron deficient) or fresh +Fe plates for further 3 days growth. The assay solution for measuring Fe(III) reductase activity consisted of 0.1 mM FeNa-EDTA and 0.5 mM Ferrozine in distilled water.

Five plants were pooled as a group and the seedlings were washed with 2 ml 100 mM $Ca_2(NO_3)_2$ wash solution. Afterwards, the entire roots of the plants were submerged in 1ml of iron reductase solution and were kept in the dark at room temperature. After 1 hour the reductase activity was measured spectrophotometrically. The absorbance of assay solution was determined at 562 nm using Infinite 200 PRO (TECAN). The assay was performed in three biological replicates and two technical replicates. Using a molar extinction coefficient of 28.6 mM^{-1} cm^{-1} the concentration of Fe(II)-Ferrozine complex (reductase activity normalized against seedlings weight) was calculated.

3.2.1.4 Metal measurement

To determine metal content in seeds, seeds were collected in bulk from the soil grown plants. The seeds were dried at room temperature and again were kept at

120°C overnight in the oven. The seeds were then shifted to 70°C, where the seeds were kept for further 3 days. The completely dried 30 mg seeds were then powdered and finally, metal content was determined with inductively coupled plasma optical emission spectrometry (ICP-OES) at the Leibniz Institute für Neue Materialien (INM, Saarbrücken) by Dr. Claudia Fink-Straube.

3.2.1.5 Measurements of Photosynthetic pigments

To determine different photosynthetic pigments (chlorophyll a, b and carotenoid) of the plants grown for 14 days on Hoagland agar medium under +Fe and then were shifted to -Fe or fresh +Fe plates to grow them 3 days more. Chlorophyll was extracted from young leaves (100 mg), the leaves were powdered with liquid nitrogen and pigments were extracted by adding 100% (v/v) acetone. The absorbance of samples was measured at 470, 645 and 662 nm. The following formula was used to calculate different pigments: Chlorophyll a: (µg/ml) = 11.24 A_{662} -2.04 A_{645}: Chlorophyll b: (µg/ml) = 20.13 A_{645} -4.19 A_{662}: Carotenoids: (µg/ml) = (1000 A_{470} -1.90 Chl-a – 63.14 Chl b)/214.

3.2.1.6 Root length measurement

Root length was measured from the frontal images of plants roots grown on agar plates by using JMicroVision software, version 1.2.7 (http://www.jmicrovision.com). Spatial calibration was performed by converting pixel values into centimeters. To measure the root length lines were drawn on roots images using the freehand tool. Average and SD were calculated from the line length. A minimum of 15 plants was used for measurement. The experiment was performed on independently grown sets of plants.

3.2.1.7 Perls staining for iron visualization

To further enhance the understanding of iron (Fe) homeostasis, it is important to visualize the localization and distribution of apoplastic iron in roots of different plants lines. For this purpose, Perls Fe staining assay was performed. The assay solution consisted of ferrocyanide which upon reaction with Fe(III) is converted to insoluble crystals of Prussian blue. The insoluble crystals cannot diffuse from the tissues and thus reflect the amount of iron in the living tissue quantitatively. 8 days old plant materials were fixed in 1 ml fixation solution under vacuum (500 mbar) for 2 hours. The fixation solution was removed and the seedlings were washed 3 times for 1-2 minutes each with distilled H_2O. One ml pre-warmed (37°C) staining solution was then added to the seedlings and were incubated for 30 minutes under vacuum (500

mbar). The staining solution was removed and the seedlings were washed 3 times with distilled H_2O. The seedlings were stored in distilled H_2O and were imaged.

3.2.2 Gene Expression analysis

To investigate gene expression of certain Fe uptake related genes, we performed Reverse transcription real-time quantitative PCR (RT-qPCR). The gene expression analysis was performed as described by Abdallah and Bauer (2016) (Abdallah and Bauer, 2016).

mRNA isolation and cDNA synthesis

Roots of plants grown for two weeks in +Fe and –Fe condition were used to isolate mRNA. About 100 mg materials were deeply frozen and powdered/homogenized under liquid nitrogen. The total mRNA was then isolated with the help of Peq GOLD Plant RNA kit (Peqlab) according to manufacturer's protocol. After extraction the total RNA was DNase-treated and the cDNA was synthesized as described by Abdallah and Bauer (2016) (Abdallah and Bauer, 2016).

Quantitative Real-Time PCR

After cDNA was synthesized it was diluted 1:10 to perform qPCR. The qPCR was performed with Real-time PCR cycler CFX96 touch (Bio-Rad) by using 2x DyNAmo Flash SYBR Green qPCR Kits. The gene expression was quantified by absolute quantification, which is based on standard curve. The absolute quantity of initial transcript was determined through standard curve for each gene. The data were normalized against the averaged expression values of the constitutive control housekeeping gene *EFBALPHA2* (EF) primer sequences for EF is described by Wang et al (2007) (Wang et al., 2007). Serial dilution of standards (1.0 kb fragment, 10^7, 10^6, 10^5, 10^4, 10^3 and 10^2) was amplified in parallel as a template in each PCR run for quantification of gene expression and to determine PCR efficiency. The qPCR reaction was performed in a 96 well qPCR plate, three biological and two technical replicates were used for amplification of each sample.

qPCR reaction mix

cDNA or standard	10 µl
2x SYBR Green mix	9.6 µl
Primer (15 µM)	0.2 µl
Primer (15 µM)	0.2 µl
Total volume	20 µl

PCR thermal profile

Initial denaturation: 95°C for 3 m
Denaturation: 95°C for 10 s
Annealing: 60°C for 15 s } 40x
Elongation: 72°C for 20 s
Melting curve analysis: 65°C - 95°C

Data analysis

Before evolving the data, the quality and integrity of each PCR reaction have to be verified by considering, the threshold cycles (Ct value) to check the reproducibility of technical replicates. To exclude the pipetting mistake, the curves for the technical replicates were analysed for consistency. For validation of PCR specificity melt curve was checked, melt curve analysis indicates both the specificity of primers and purity of the cDNA sample.

Data analysis was performed by using CFX Manager (version 3.1) software from Bio-Rad. The expression data were exported to Microsoft Excel. For each sample, absolute expression values (SQ mean values) were subtracted from water control and expression values obtained from genomic DNA control gene (Efg; intron region) and then was normalized against the cDNA constitutively expressing housekeeping gene (EFC; exon region). Finally, the average and standard deviation were calculated from three biological replicates and the bar diagrams were generated in Microsoft Excel showing the absolute normalized gene expression.

3.2.3 Cell fractionation

Cytosolic and microsomal fraction of HA-tagged EHB1 proteins were performed as described previously by Alexandersson et al (2008) (Alexandersson et al., 2008). Briefly, 300 mg seedlings of 35S:HA_3-EHB1 plants grown on Hoagland agar medium were grounded in liquid nitrogen and homogenized in homogenization medium (material section 3.1.10). To remove insoluble plant debris the lysate was centrifuged at 10,000 *g* for 10 min at 4°C. High-speed ultra-centrifugation was performed in Beckman L-80 XP with an SW40Ti swinging rotor at 100,000 *g* for 45 min at 4°C to pellet microsomal membranes and to obtain the cytosolic soluble fraction. After the final centrifugation, the pellet was resuspended in the resuspension medium. Both homogenization and resuspension mediums were supplemented with 100 µM $CaCl_2$. Western blotting was performed to detect HA-EHB1 protein.

3.2.3.1 Western Immunoblot analysis

Western blot analysis was performed as described by Sambrook et al (1989) (Sambrook et al., 1989). Shortly, the transiently expressed protein in tobacco leaves was extracted. Total protein extract containing HA-EHB1 protein was separated in 12% SDS-polyacrylamide gel. Electrophoresis was performed in Tris-Gly buffer (Running buffer) using mini gel equipment from Bio-Rad. After electrophoresis, the proteins were transferred in transfer buffer to Protran Nitrocellulose membrane (GE

Healthcare). For loading control, the membranes were stained with Ponceau S (Sigma-Aldrich). To inhibit nonspecific binding of antibody, the nitrocellulose membrane was blocked for 45 min with 5% milk solution dissolved in TBST followed by 1-hour incubation of a dilution of anti HA antibody (1:1000) in 2.5% milk-TBST. Afterwards, the membrane was washed 4 times (10 min each) in TBST. ECL system (GE Health Care) was used to detect.

Protein band signal quantification

Protein band intensity signal was quantified with the AlphaView software. To measure the signal intensity, the region of interest (ROI) was drawn with the help of a rectangle around the protein band. Every signal was caught with the same size of ROI. The background was subtracted with the help of regional background subtraction tool to ensure that the background intensity did not influence the protein band intensity. The data for the intensity is listed in a table in the software and was then exported to Microsoft excel for further calculation.

3.2.3.2 Fluorescence microscopy and Quantification of colocalization

An LSM Axio imager M2 (Zeiss) microscope with a Plan-Apochromat 40x/1.4 oil DIC (UV) VIS-IR M27 objective was employed to detect the GFP/mRFP signal in the leaves of tobacco epidermal cells. For GFP, excitation at 488 nm and for detection 500-550 nm filter were used. For mRFP/mCherry Excitation at 563 nm and for detection 570-640 nm filter was used. Images were recorded in 1936 x 1460 pixel format, resulting in pixel sizes (xy resolution) between 1.60 and 24.11 mm.

For colocalization, 8-bit grayscale image pairs, which represents the two channels (green and red) were used. Images were loaded in ImageJ software (https://imagej.nih.gov/ij/download) and were analyzed in ImageJ plugin for colocalization JACoP (https://imagej.nih.gov/ij/plugins/track/jacop). JACoP is a compilation of general colocalization indicators and the recently published methods. To prevent low-level image acquisition noise from distorting the statistics, the threshold level was adjusted manually for each image ranging from 21 to 40. Then, the Pearson's coefficient correlation (PCC) was calculated. PCC it is a linear correlation coefficient which provides an estimate of the goodness or badness of colocalization. PCC is a well-defined and widely accepted for defining the extent of overlap among image pair. It is used to describe the correlation of intensity distributions between channels.

The valves of PCC ranges from -1 to 1 with values from 0.5 - 1 indicate colocalization and values from -1 - 0.5 indicates no colocalization. 1 means complete positive correlation (complete colocalization), -1 means negative correlation (no colocalization) and zero stands for no correlation (Bolte and Cordelieres, 2006; Dunn et al., 2011; Jalewa et al., 2014).

3.2.4 DNA and RNA techniques

3.2.4.1 PCR based Site-directed mutagenesis

Site-directed mutagenesis (SDM) was used to mutagenize specific amino acid in the C2 domain of EHB1. pDONR207 plasmid containing cDNA of EHB1 was used as template to introduce mutation at different positions through primers EHB1D31/36A1 and EHB1D31/36A2 or EHB1D82/84A1 and EHB1D82/84A2. The 25 µL PCR reaction was performed as follow,

PCR mixture	**PCR thermal profile**
5-20 ng of template DNA	initial denaturation: 95°C for 30 s
5 µL of 5x *Q5* buffer	Denaturation: 95°C for 30
1 µL of each primers	annealing: 55°C for 1 m (18x)
1 µL of dNTPs mix	Elongation: 72°C for 10 m
1 U (0.5 µL) of *Q5* DNA polymerase	Final elongation: 72°C for 7 m
H_2O as the residual volume	

After PCR the mixture was further treated for 1 h at 37°C with 1µl Dpn1 (restriction enzyme) which digest the methylated DNA (non-mutagenized). Afterwards, the plasmid (pDONR207 with mutagenized *EHB1*) was used to transform *E. coli* for multiplication. Gentamycin was used to select the transformed bacteria. Four randomly selected colonies were grown in liquid LB medium overnight and the plasmid was isolated from them. The correctly mutated *EHB1* was verified by sequencing. Subsequently, mutated *EHB1* was transferred from pDONR207 to different binary destination vectors (PMDC83 / pAlligator 2).

3.2.4.2 PCR-driven overlap extension signature domain deletion

Overlap extension PCR is extensively used in molecular biology both for site-directed mutagenesis and the cloning of spliced segments. Special chimeric primers are used to splice segments, each primer contains a 5' overhang of the segment which has to be joined.

To delete the signature domain from *EHB1* two set of special chimeric primers were designed (material section 3.1.6. oligonucleotides), in the first primary PCR one set of primers (A+B) were used to amplify 1st part of *EHB1* and the other set of primers

(C+D) were used to amplify 2nd part of *EHB1*. Next, in the ligation PCR the two amplified fragments generated during the primary PCR were joined using only primers for far ends (A+D) resulting in the deletion of Signature domain from *EHB1* (Fig. 3.1.).

The PCR mixture and thermal conditions are listed here,

PCR mixture

2 µL of template DNA
5 µL of 5x *Q5* buffer
1 µL of each primers
1 µL of dNTPs mix
1 U (0.5 µL) of *Q5* DNA polymerase
H_2O as the residual volume

PCR thermal profile

initial denaturation: 98°C for 30 s
Denaturation: 98°C for 20 s
annealing: 58°C for 30 s
Elongation: 72°C for 30 s
} 35x
Final elongation: 72°C for 2 m

After the primary PCR the gel electrophoresis was performed and the correct sized bands were purified from the gel through GeneJET Gel Extraction kit. The purified products were then used as template for the ligation PCR.

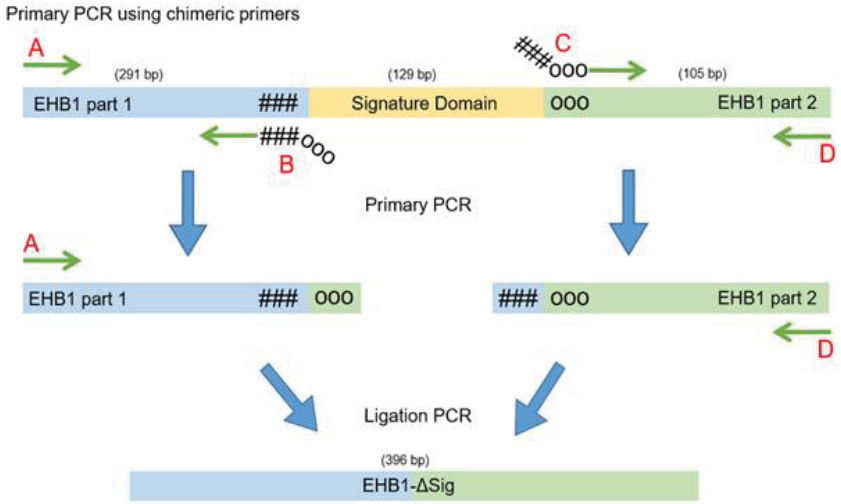

Figure 3.1. Deletion of Signature domain via overlap extension PCR. The signature domain has been deleted by two PCRs using internal primers (B and C) and flanking primers (A and B). In the first PCR (Primary PCR), combination of (A+B) and (C+D) primers was used to generate intermediate PCR product which do not contain the signature domain. Primers B and C adds the overlapping sequence to each fragment that is generated during the first PCR. During the second PCR (Ligation PCR) the two fragments are then combined by using the flanking primers (A+D).

3.2.4.3 PCR-driven overlap extension His-domain deletion

The same procedure which was used to delete the signature domain from *EHB1* was performed to delete the His-domain from the large cytosolic loop of *IRT1*. Except that the primers were designed for deleting the His-domain.

3.2.4.4 Molecular cloning

a. Cloning for protein expression in *E. coli BL21 (DE3)*

We use pETStrep-II system (Novagen) for protein expression in *E. coli*. Strep-tag was attached to *EHB1* at the 5' end (for EHB1 protein purification). Classical cloning method was performed to clone *EHB1* in pET plasmid (Fig. 3.2 left.).

Restriction digestion

For this purpose, first restriction sites (SpeI and XhoI1) were added to *EHB1* (amplified from cDNA of *Arabidopsis thaliana*) through PCR by using E1StrepiiSpeI-fwd and E1StrepiiXhoI-rev primers. After extracting and purifying the *EHB1* band from agarose gel it was subjected to SpeI and XhoI1 restriction enzymes for digestion. The pET vector was also digested with the same set of enzymes (Fig. 3.2 right.). The digestion reaction mixture (total 20 µL) was prepared as follow:

Enzymatic restriction of insert	enzymatic restriction of plasmid
100 ng-1µg of DNA	2 µg of plasmid (pETStrepII)
2 µL of 10x reaction buffer	2 µL of 10x reaction buffer
2 µL BSA	2 µL BSA
1 µL of each restriction enzyme	1 µL of each restriction enzyme
H_2O as the residual volume	H_2O as the residual volume

After mixing the components the reaction mix was incubated at 37°C for 1-2 hours. The enzyme in the reaction was inactivated thermally by incubating at 80°C for 10 minutes. The digested DNA and plasmid were then inspected by agarose gel electrophoresis.

Ligation

The digested fragment and plasmid has to be ligated now, the ligation enzyme T4 DNA ligase will be used for this purpose (Fig. 3.2 right.). The concentrations of both the digested fragment and plasmid were determined spectrophotometrically because the ratio of the vector and the inserted fragment is an important factor to be considered for the ligation reaction. We used 1:3 concentration for vector and the inserted DNA fragment respectively, about 50 ng of vector with 3 fold molar excess of fragment.

The ligation reaction mixture was comprised of the following components.

Quick T4 DNA Ligation mixture
10 µL of 2x quick ligation buffer
50 ng of vector DNA (3 µL)
3x ng of insert DNA (5 µL)
1 µl of T4 DNA ligase (5 U/µl)
H_2O as the residual volume (total 20 µL)

After mixing the components the reaction mix was incubated at 25°C for 5 minutes. After the incubation time, the reaction mixture was chilled on ice for short time.

Afterwards, the ligation mixture was applied in the *E. coli BL21 (DE3)* cells transformation (Fig. 3.2 right.).

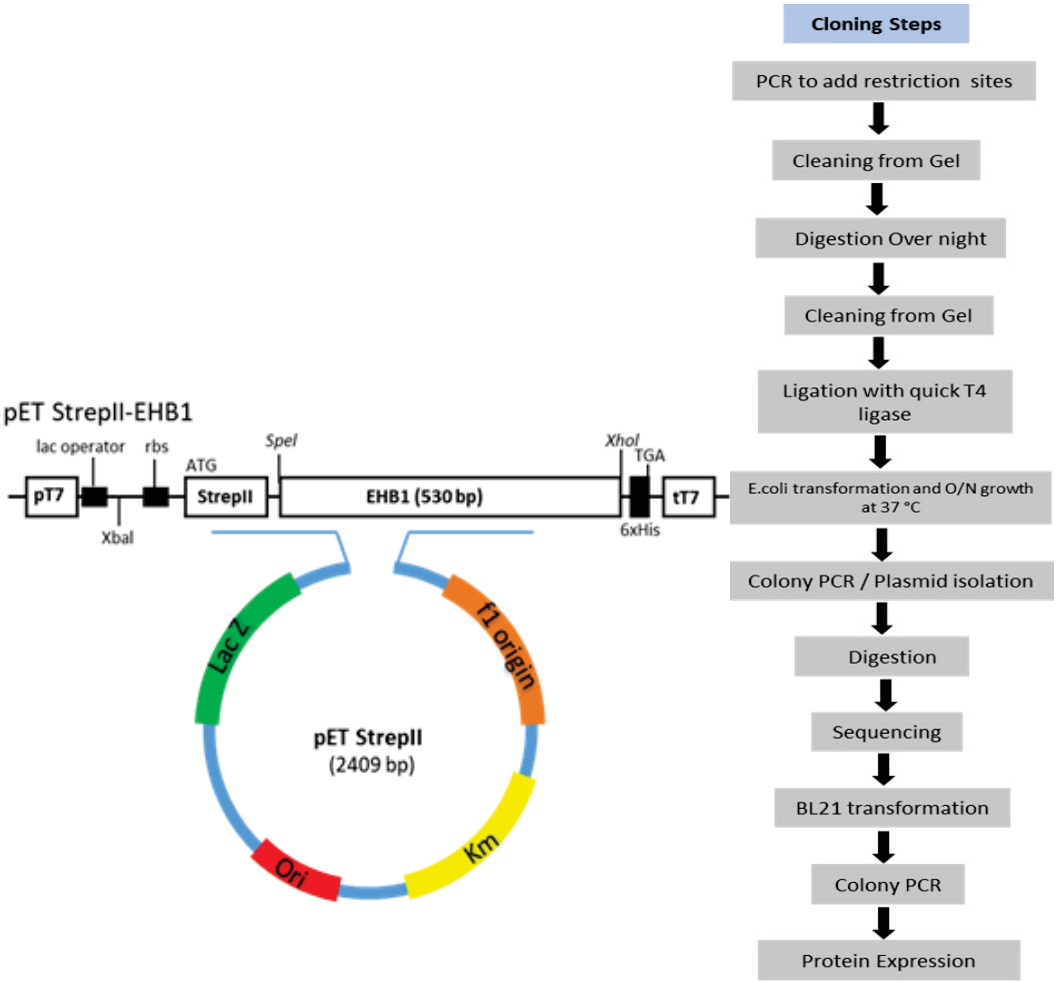

Figure 3.2 Schematic illustration of pET destination plasmid showing expression cassette on the top (left). The plasmid is about 2409 bp in length and it has a StrepII tag and a kanamycin resistance gene for selection. The expression is driven by strong bacteriophage T7 promoter. Restriction sites SpeI and XhoI was used for restriction digestion. On the right is the complete procedure for cloning *EHB1* in the plasmid.

Transformation of competent *E. coli*

First, 0.5 µg (5 µL) of recombinant vector DNA was mixed with 10 µL of competent *E. coli* cells. The mixture was incubated for 30 minutes on ice, after incubation the mixture was heat shocked at 42°C for 30 seconds. The bacteria were incubated for another 2 minutes on ice. Then 1 ml of LB medium without antibiotics was added and the samples were shaken at 200 rpm at 37°C for 40 minutes. Then the transformed bacteria were centrifuged 30 seconds at 13000 rpm, the supernatant was discarded the pellet was resuspended in 100 µL of LB medium and was plated on agar LB plates containing the corresponding antibiotics.

b. Gateway cloning for rBiFC experiment

For in vivo protein-protein interaction studies, bimolecular fluorescence complementation (BiFC) has been successfully applied over the years. The technique is based on interaction of two non-fluorescent fragments of yellow fluorescent protein (YFP) which in turns combine and forms fluorescent complex (Zamyatnin et al., 2006). We used a modified version of conventional BiFC which is known as ratiometric bimolecular fluorescence complementation (rBiFC). In rBiFC two independent and functional expression, cassettes are present at the same vector backbone. In addition, there is a third expression cassette which contains a fluorescent cytosolic marker (RFP) which act as transformation control marker by identifying cells that express the transgenes (Grefen and Blatt, 2012). A special cloning strategy 2in1 as named by the manufacturers (Grefen and Blatt, 2012) that uses the recombination system of the λ-phage is used to simultaneously clone two genes into two different independent expression cassettes on the same vector backbone (pBiFCt-2in1-CC).

To investigate the interaction between EHB1 and IRT1 cytosolic loop in planta rBiFC has been performed. For this purpose, *EHB1* has been cloned in different combination and orientation with other genes (Table.1.).

For cloning the genes into the entry clone plasmid (pDONR221), a PCR was performed with primer combination EHB1cterB3 and EHB1B2 for EHB1 and I1LatgB1 and I1LnsB4 for IRT1 cytosolic loop to attach the attachment site (*att*-sites). The bands were cleaned from the gel and the BP reaction was performed.

BP-Reaction

The BP reaction was performed to insert the amplified PCR fragment (gene with *att* site) into entry clone. Recombination occurs between *att*B of PCR fragment and *att*P of donor vector (pDONR221) resulting in *att*L (entry clone) and *att*R (By-product). The BP reaction is catalyzed by BP clonase enzyme mix, the enzyme mix is consists of bacteriophage λ Integrase (Int) and *E. coli* Integration Host Factor (IHF) which is synthesized during λ lysogenic pathway.

The reaction mixture setup was as follow:

PCR fragment: 3 µl (10 ng)
Donor vector: 1 µl (100 ng)
BP Clonase: 1 µl (1 U)

The reaction was incubated overnight at 25°C, then the competent *E. coli* cells were transformed with the entry clone for further multiplication of the generated entry

clone. The successful generation of the entry clone was confirmed by sequencing. Two entry clones were generated EHB1c-ter-DONR221-P3P2 and IRT1-loopc-ter-DONR221-P1P4. A generalized view of BP reaction is depicted in figure 3.3.

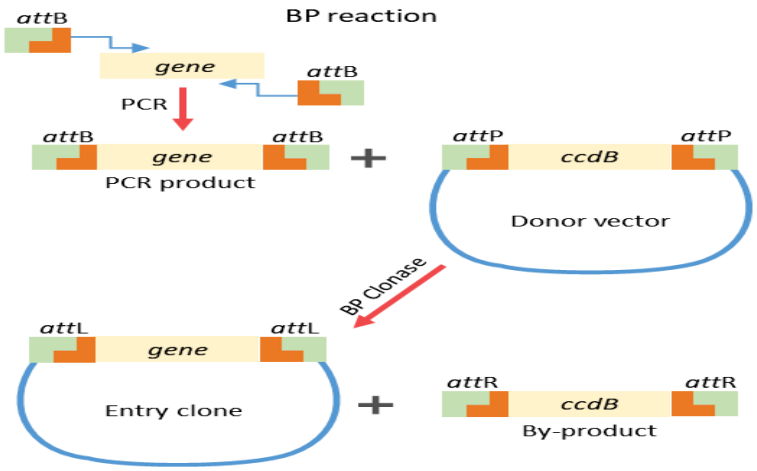

Figure 3.3 Schematic illustration of the BP reaction of the gateway cloning system. The system is based on homologous recombination. In the PCR specific primers, B1 and B2 were used to amplify and add the flanking attachment (*att*B) sites to the gene of interest (*EHB1*). The PCR product was then transferred in a BP reaction (first reaction) to a gateway compatible entry vector (pDONR221). The BP reaction is catalyzed by BP clonase enzyme mix. The gateway vectors contain a suicidal gene (*ccdb*) between the attachment sites (*att*P). In case of successful recombination, the gene of interest will replace the suicidal gene and the suicidal gene will go out as by-product. The attachment sites of the gene of interest (*EHB1*) changes from *att*B to *att*L during the BP reaction.

LR-Reaction

After the successful generation of entry clone, the LR reaction was performed to transfer the cloned gene from entry clone to the destination vector for obtaining the final expression clone (Fig. 3.4.).

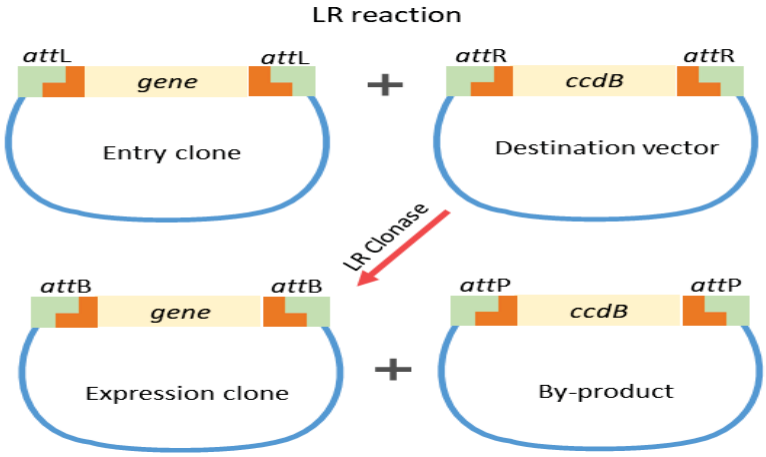

Figure 3.4 Schematic illustration of the LR reaction of the gateway cloning system. After successful generation of the entry clone. The second reaction (LR reaction) was performed. During the LR reaction which is catalysed by the LR clonase enzyme mix the gene of interest (*EHB1*) can be

transferred from the entry clone to the final expression clone (pBiFCt-2in1-CC). In the LR reaction recombination occurs between *att*L of entry clone and *att*B of the expression vector.

During the LR reaction recombination occur between *att*L of entry clone and *att*R of destination vector (pBiFCt-2in1-CC) resulting in *att*B (expression clone) and *att*P (By-product) (Fig. 3.4.). The two generated entry clones were used in the LR reaction to transfer the genes from two separate entry clones to a single destination vector which contains multiple expression cassettes in the single vector backbone. The LR reaction is catalyzed by LR clonase enzyme mix, the enzyme mix is consists of λ Int and Excisionase (Xis) proteins and *E. coli* Integration Host Factor (IHF) proteins which is synthesized during λ lytic pathway.

The reaction mixture setup was as follow:

Entry clone 1:	1 µl (10 ng)
Entry clone 2:	1 µl (10 ng)
Destination vector:	2 µl (200 ng)
LR Clonase:	1 µl (1 U)

After mixing all the components of LR reaction together, the same procedure as with the BP reaction has been followed. The reaction was incubated for 1 hour at 25°C, then the competent *E. coli* cells were transformed with the expression clone for multiplication of expression clone. The correctness of the expression clone was confirmed by sequencing. The same procedure was adopted to clone the other genes for BiFC namely *EHB1-4x*, *EHB1-ΔSig,* and *SNX1*. For different combination and orientation of genes (Table 1.).

Agrobacterium strain C58 (pGV2260) cells were transformed with different plasmids. The transformed bacteria were used for the infiltration of *Nicotiana benthamiana* leaves as described by Hötzer et al (2012) (Hötzer et al., 2012).

Table 1. Different combination of genes for rBiFC

No	Combination	Orientation	P3P2-nYFP	P1P4-cYFP	Interaction
1	*EHB1 + IRT1vr*	CC	*EHB1*	*IRT1vr*	Yes
2	*EHB1-Δsig + IRT1vr*	CC	*EHB1-Δsig*	*IRT1vr*	No
3	*EHB1 + SNX1*	CC	*EHB1*	*SNX1*	No
4	*IRT1vr + SNX1*	CC	*IRT1vr*	*SNX1*	No
5	*SNX1 + SNX1*	CC	*SNX1*	*SNX1*	Yes
6	*EHB1-4x + IRT1vr*	CC	*EHB1-4x*	*IRT1vr*	Yes
7	*EHB1-Sig + IRT1vr*	CC	*EHB1-Sig*	*IRT1vr*	Yes

Confocal Laser Scanning Microscopy

48-72 h of *Nicotiana benthamiana* after transformation, YFP signals were detected in the leaves epidermal cells by using LSM 510 Meta confocal laser-scanning microscope (Zeiss) with a Plan-Neofluar 40x/1.3 oil immersion objective located at

Centre for Advanced Imaging (CAi) HHU Düsseldorf or with an LSM Axio imager M2 (Zeiss) microscope with a Plan-Apochromat 40x/1.4 oil DIC (UV) VIS-IR M27 objective located at the department of botany HHU Düsseldorf. The fluorophore YFP was excited at 488 nm excitation wavelength by using detection filter 505-550 nm and mRFP was excited at 561 nm excitation wavelength and detection filter was 575-615 nm. The pixel size for images was 0.23 µm x 0.23 µm x 3.0 µm. After image acquisition the post-processing was performed using Zeiss LSM image browser version 4.2.0.121. To get a separate image for each channel, the acquired confocal image was split into green channel (YFP) and red channel (mRFP) by clicking the split image option in the software. The software-default optimal brightness and contrast values were used in each image.

3.2.5 Co-Immunoprecipitation (Co-IP) of EHB1 and IRT1

Co-IP was performed to confirm the interaction between EHB1 and IRT1. For this purpose, *Nicotiana benthamiana* (tobacco) were transformed with the help of Agrobacterium containing HA-EHB1/IRT1-GFP constructs for transient expression of proteins. The leaves were harvested and grounded into powder in liquid nitrogen. 1.5 ml IP-buffer was added to the powder material and was incubated for 10 minutes at room temperature. After incubation, the samples were centrifuged at max speed for 10 min, the supernatant was transferred to new tubes. 30 µL was collected from the samples at this point as input control. Input control is important for the successful transformation of plants (Fig. 3.5.). After this 25 µL of GFP-trap beads (Chromotek) aka anti-GFP nanobody coupled with magnetic beads, were added to the sample and were incubated on revolving wheel overnight at 4°C. This allows the binding of anti-GFP magnetic beads to protein complexes that possess the GFP tag. The beads can be easily collected with a magnet. The samples were centrifuged for 1 min at 5000 rpm, the supernatant was collected as flow-through. The beads were washed 3x with IP-buffer and finally, the beads were resuspended in 50 µL of 2x Laemmli buffer (IP fraction). Both input and IP fractions were boiled at 95°C for 5 min, this step allows the elution of protein-complexes from the magnetic beads. And to analyze the results, SDS-Page protein gel (western blot) was performed (Fig. 3.5.).

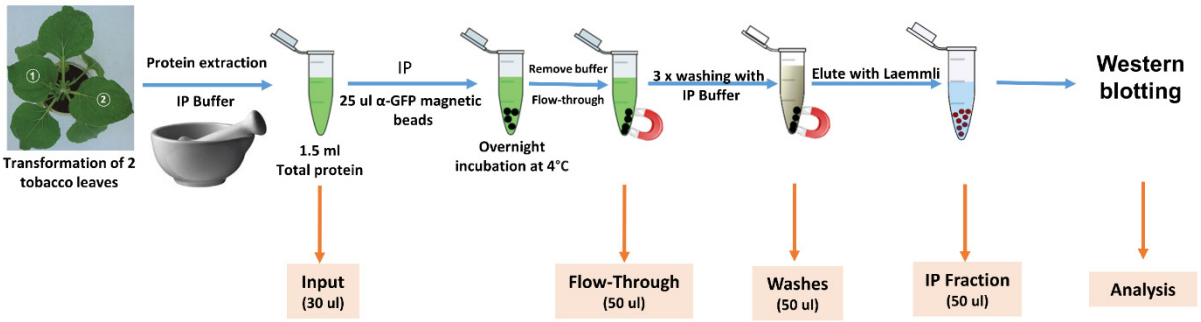

Figure 3.5. Illustration of Coimmunoprecipitation (Co-IP). Tobacco leaves were transformed with HA-EHB1/IRT1-GFP constructs for transient protein expression. The total proteins were extracted from tobacco leaves in the presence of 1.5 ml IP-buffer. The samples were centrifuged at mix speed for 10 minutes. 30 µL was collected at this point as input. The rest were incubated overnight at 4°C with 25 µL of GFP-trap beads. After centrifugation, the supernatant was collected as flow through and the beads were washed three times with IP-buffer the washes were also collected. The magnetic beads were removed with the help of a magnet. The beads were boiled at 95°C for 5 minutes in 50 µL of 2x Laemmli buffer (IP fraction). Afterwards western blots were performed.

3.2.6 Heterologous protein expression in *E. coli BL21 (DE3)*

After cloning, EHB1 strep tagged protein was expressed in *E. coli BL21 (DE3)*. For this purpose first, a small culture (4 ml) of *BL21* containing pETStrep-II-EHB1 (*IPTG* inducible) construct was prepared in liquid LB medium, the culture was incubated at 37°C overnight. Next day the overnight small culture was diluted in fresh 200 ml (big culture) of LB medium containing 1 µL/ml Kanamycin. The cells were grown at 37°C to mid-log phase (A600 = 0.6 to 1.0) at constant shaking at 200 rpm, after reaching to desired OD (0.5 - 0.6) the expression of *EHB1Strep-II* was induced by adding *IPTG* 0.1 mM final concentration and allowing the cells to grow for additional 1 hour at 28°C.The culture was then centrifuged and the pellet was stored at -20°C.

3.2.6.1 Protein purification using Strep-tag®/Strep-Tactin® system

The expressed protein was then purified from the crude protein through affinity purification Strep tactin system (https://www.iba-lifesciences.com/strep-tag.html). Shortly, the pellet which was stored at -20°C from the expressed protein was resuspended in 1.5 ml of lysis buffer in 2 ml Eppendorf tube and were incubated on ice for 30 min, after that 0.1% of Triton X-100 was added to the tube and the sample was sonicated 3 times 30 sec each (Amplitude 20%, Cycle 0.5) to lyse the cells. The samples were then centrifuged at 14000 rpm for 30 mins at 4°C. At this point, 100 µl was taken from the sample as an unpurified sample. The supernatant was stored and the purification was continued with the pellet.

Next, the pellet was resuspended in 1.2 ml wash buffer-I containing 8M urea and was incubated overnight in the cold room at rotary shaker at 4°C. Next morning the samples were centrifuged at 14000 rpm for 15 mins at 4°C, the supernatant was transferred to new tubes (1.2 ml). 12.5 µl avidin (100 µg/ml) was added to the sample and were incubated 30 min rotating in the cold room. Avidin, a protein related to streptavidin, binds the free biotin that is produced by the *E. coli* and likely biotinylated proteins that would be co-purified because they would also bind to the Strep-Tactin beads (IBA manual). Although, α-Desthiobiotin (modified biotin) is used for later on for the elution of tagged protein from the beads.

The samples were then diluted 1:10 with wash buffer-II in 50 ml falcon tube to bring the final volume to 20 ml. the sample was centrifuged shortly (5 mins) at 5000 g to remove any aggregates. After that, 400 µl (3 times washed) 50% suspension Strep-Tactin Macro-Prep (IBA) were added to the diluted protein extracts. The mixture was incubated for one hour at room temperature constantly shaking.

After the incubation the mixture was loaded into Econo-Pac disposable Chromatography columns (Bio-Rad), the bottom cap was removed and the mixture was collected as a flow through. Then, four wash steps with 400 µl Wash Buffer-III was performed the washes was also collected. After the washing step, the proteins were eluted by five times 150 µl Elution Buffer, the final volume after elution was 750 µl. the concentration of proteins was determined by Bradford assay and western blot was performed for both the purified and un-purified samples. These purified proteins were then used in further in vitro assays.

3.2.6.2 Membrane binding assay

The Membrane Lipid Strip™ (Echelon) membrane was blocked with 3% Fatty Acid-free BSA (blocking buffer) for about 3 hours at room temperature. After blocking the membrane was incubated with the purified protein (Strep-EHB1, 2 µg/ml) in 2 ml blocking solution in a sealed plastic bag shaken overnight in the cold room at 4°C. The experiment was performed in the presence of different concentration of $CaCl_2$ (0 µM, 100 µM).

Next day, the solution containing proteins was removed and the membrane was washed five times for 10 min with TBST shaking on a vertical shaker in a Petri plate. After washing the membrane was incubated in a sealed plastic bag with 1:1000 diluted *α-Strep-tag* antibody in blocking buffer and incubated for 1 h at room

temperature on an orbital shaker. After antibody incubation, the membrane was washed four times for 10 min with TBST shaking on a horizontal shaker in a Petri plate. After washing ECL system (GE Health Care) was used to detect.

3.2.6.3 Preparation of Liposome

A 75:25 (w/w) mixture of Phosphatidylcholine: Phosphatidylinositol or Phosphatidylcholine: Phosphatidylinositol 4-phosphate (Sigma-Aldrich) was prepared by a freeze-thaw-sonication procedure as described by Linka et al (2008) (Linka et al., 2008). Briefly, the phospholipids were sonicated (2 min on ice Branson digital Sonifier 250, Amplitude 20%) to a final concentration of 2% (w/v) in 50 mM HEPES, pH 6.8, 100 mM NaCl. the phospholipids were then aliquoted in Eppendorf tube, the tubes were freeze chilled in liquid nitrogen. After several freeze-thaw cycles, the liposomes were pulsed 10 times to yield unilamellar vesicles. Finally, the liposomes were extruded by using mini-lipid extruder (Avanti lipids) with 0.2-µm pore size polycarbonate membrane to obtain the equal sized liposomes the liposomes were passed several times through the membrane.

Liposome binding Assay

The generated liposomes were used to perform protein-lipid binding assay. 5 µg of purified recombinant Strep tagged EHB1 protein were incubated with 50 µL of liposomes for 30 min at 30°C. The solution was then centrifuged at 100,000 *g* for 30 min in an SW40Ti swinging rotor (Beckman) to separate supernatant and pellet fractions. The protein should be present in the pellet fraction if it is binding with liposomes (Phospholipids). The experiment was performed in the presence of different concentration of $CaCl_2$ (0 µM, 100 µM). In the end, western blotting was performed and the protein was detected by a dilution of anti-Strep antibody (1:1000).

4. Results

4.1 EHB1 interacts via its signature domain with the large IRT1vr

In a yeast two-hybrid screen EHB1 was found as one of the potential interacting partners of IRT1vr. To test whether this interaction takes place also *in planta* bimolecular fluorescence complementation (BiFC) was performed. BiFC was used because the technique is established in our lab and was successfully used to detect the protein-protein interaction *in vivo* directly in the plant cell. Other advantages of BiFC include low background signal and the stability and specificity of the reconstituted fluorophore complex (Hu et al., 2002; Hu and Kerppola, 2003). The technique is based on the interaction of two non-fluorescent segments of yellow fluorescent protein (YFP), the non-fluorescent segments are fused to two different proteins. When the proteins come close enough the split YFP is reconstituted and gives the fluorescence signal. It is important to use proper negative controls to rule out the possibility of a false positive signal (Kodama and Hu, 2012; Xing et al., 2016).

For the purpose to perform BiFC assay both *EHB1* and *IRT1vr* were cloned into the expression vector pBiFCt-2in1-CC (Grefen and Blatt, 2012). The vector pBiFCt-2in1-CC contains two independent functional expression cassettes in the same vector backbone and along with this it also contains a third expression cassette which expresses a fluorescent cytosolic marker (mRFP) that can be used as a transformation control (Grefen and Blatt, 2012). Tag orientation of the interacting proteins is an important factor to be considered (Xing et al., 2016). Based on the assumption, that EHB1 interacts with other proteins through its signature domain which is located at its C-terminal end, both *EHB1* and *IRT1vr* were cloned in CC orientation (C-terminally tagged) to nYFP and cYFP, respectively, so that the tags are in closer proximity than in the NN orientation. The final vector was introduced into tobacco through Agrobacterium-mediated transformation and the fluorescence was investigated under microscope. Two leaves per plant were transformed and the images of the BiFC signals were obtained from many individual transformed leaf epidermal cells.

A positive BiFC signal in figure 4.1 A indicated that EHB1 and IRT1vr interact in this system. The mRFP signal in figure 4.1 C shows that the transformation was successful.

As a negative control in BiFC Sorting Nexin-1(SNX1) was tested against both EHB1 and IRT1vr. All the constructs were obtained by the same way as described above for EHB1 and IRT1vr interaction. SNX1 is a member of the retromer complex and its role has been shown in protein sorting during protein endocytosis in the model plant *Arabidopsis thaliana* (Brumbarova et al., 2015; Robinson and Neuhaus, 2016). It has been shown that SNX1 localized to TGN or developing MVBs (Stierhof et al., 2013; Heard et al., 2015). No fluorescence was seen in the negative control which suggests that neither EHB1 nor IRT1vr interacted with SNX1 (Fig. 4.1 M-R and supplemental-Fig. S1. A-F.). As a positive control, the fluorescent signal was seen in figure 4.1.S and Supplemental Fig. S1.G-I which shows that SNX1 interacted with SNX1 and formed a homodimer, which has already been shown (Pourcher et al., 2010).

To investigate the binding domain of EHB1, we deleted a 43-amino acid long signature domain which is located at the C-terminal end of EHB1 (Fig. 4.1. i.). To get the truncated version of EHB1 (EHB1-ΔSig) the signature domain from EHB1 was deleted via PCR-driven overlap extension PCR (Fig. 3.2 and Fig. 4.1. ii.). Primer sequences used to delete the signature domain from EHB1 are listed in materials section 3.1.6. The truncated EHB1-ΔSig was then tested against IRT1vr in BiFC, No BiFC signal was detected indicating that EHB1-ΔSig could not interact with IRT1vr (Fig. 4.1. D-F.).

To further verify the interacting domain of EHB1 for interaction with other proteins. We cloned only the signature domain of EHB1 and tested for interaction with IRT1vr in BiFC. A positive BiFC signal was detected in figure 4.1. G suggesting that the signature domain alone was able to interact with IRT1vr. With these results, we could show that EHB1 needed the signature domain to interact with IRT1vr, because in the absence of the signature domain (EHB1-ΔSig) EHB1 was not able to interact with IRT1vr in the BiFC system. The involvement of the signature domain in protein-protein interaction is consistent with previous reports (Rodriguez et al., 2014). As a perspective, these findings can be further verified with other protein-protein interaction methods like Y2H, Co-immunoprecipitation or FRET.

We also investigated the interaction of the C2 domain quadruple mutant EHB1 (EHB1-4X) with IRT1vr. EHB1-4X was generated by replacing four aspartic acids (D31/D36, D82/D84) in the C2 domain with alanines (A) via site-directed

mutagenesis (Fig. 4.1.iv.). These aspartic acid residues are reported to play a role in Ca^{2+} ion coordination in CAR-family proteins which in turn helps in Ca^{2+}-dependent phospholipid binding of CAR4 protein (Rodriguez et al., 2014). To check whether this mutation has any effect on the protein interacting ability of EHB1 we subjected EHB1-4x to BiFC against IRT1vr. EHB1-4x and IRT1vr constructs were generated in the same way as described above. We observed that EHB1-4x did not lose the ability to interact with IRT1vr (Fig. 4.1 J.). As mentioned earlier, an explanation could be that the C2 domain is not needed for protein-protein interaction but rather required for protein-lipid binding. That's why EHB1-4x was still able to interact with IRT1vr suggesting that EHB1 uses another domain or motif to interact with other proteins.

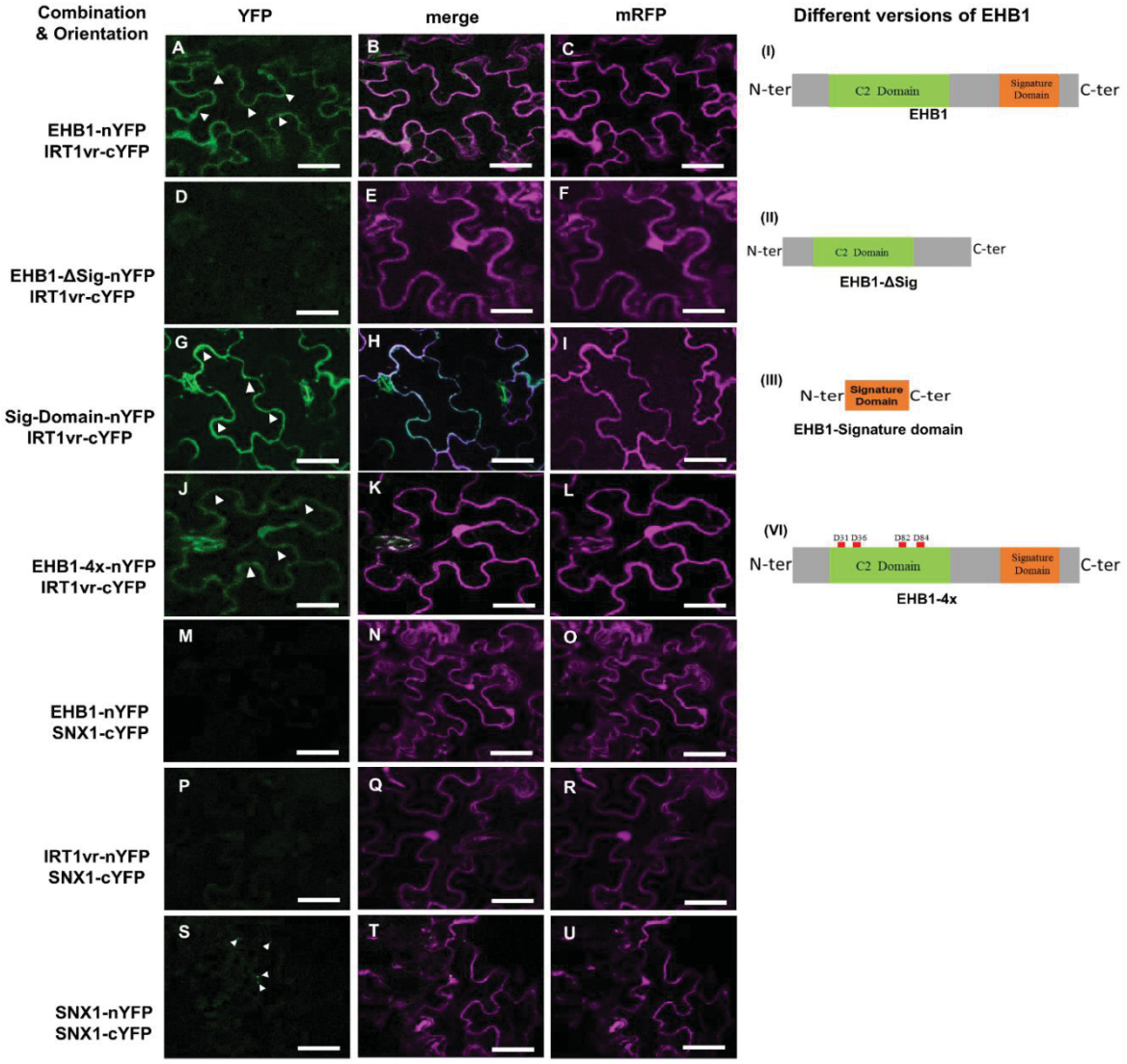

Figure 4.1.Targeted BiFC: EHB1 physically interacts with IRT1vr via its Signature domain. CLSM images of leaf epidermal cells of *Nicotiana benthamiana* two days after transformation with

Agrobacterium containing pBIFCt-2in1-CC. (A-C) The signal in the YFP channel can be seen due to the reconstitutions of functional YFP protein as a result of interaction between EHB1 and IRT1vr. The fluorescence signal is indicated by white arrowheads. (i) Schematic representation of the EHB1 protein, the position of C2 domain and signature domain is indicated. (D-F) No YFP signal is present in the YFP channel because EHB1-ΔSig did not interact with IRT1vr due the absence of Signature domain in EHB1. (ii) Schematic representation of EHB1-ΔSig protein the position of the C2 domain is indicated. (G-I) YFP signal can be seen in the YFP channel due to the interaction between Signature domain and IRT1vr. The white arrowhead indicates the YFP signal. (iii) Schematic representation of EHB1-Sig protein. (J-L) The interaction between EHB1-4x and IRT1vr, The fluorescence signal is indicated with white arrowheads. (iv) Schematic representation of the EHB1-4X protein, mutated aspartic acid are shown in red in the C2 domain. (M-R) Negative control: No YFP signal can be seen because Sorting Nexin-1(SNX1) did not interact with EHB1 and IRT1vr. (S-U) SNX1 interact with SNX1. The figure shows representative images derived from three independent experiments. Bars, 20 µm.

4.1.1 Identification of the specific interacting part of IRT1vr with EHB1

After confirming the interaction between EHB1 and IRT1vr, we were interested to find out which specific part of the IRT1vr is interacting with EHB1. For this purpose, we have cloned different parts of the IRT1vr (Fig. 4.2.) and subjected them to BiFC against EHB1. Analysis of the predicted structure of IRT1 shows that the loop consists of three helices and two disordered regions (DR1 and DR2) (Fig. 4.2 A.). Two of the three helices are bordering the transmembrane domains. The histidine motif is located in DR2 (Ivanov and Bauer, 2016). Considering these structural characteristics, the whole variable region was fragmented into four different regions namely; IRT1vrΔ1, IRTvrΔ2, IRT1vrΔ3 and IRT1vrΔ4 (Fig. 4.2 C-F.). IRT1vrΔ1 covers the first part of the loop having two helices, one of which borders the transmembrane domains, the entire DR1 and part of DR2 having the Histidine motif (Fig. 4.2 C.). IRTvrΔ2 covers the last part of the loop having one transmembrane domain bordering helices and the entire DR2 with the histidine motif (Fig. 4.2 D.). IRT1vrΔ3 lacks both the first and last part of the variable region i.e. it does not contain the two helices which border the transmembrane domains (III and IV). It covers only the middle part of the variable region (DR2 with the histidine motif) (Fig. 4.2 E.). The 4th fragment IRT1vrΔHis covers the first and last part of the loop (two helices bordering the transmembrane domains, the whole DR1 and part of DR2) but it lacks the entire histidine motif (Fig. 4.2 F.).

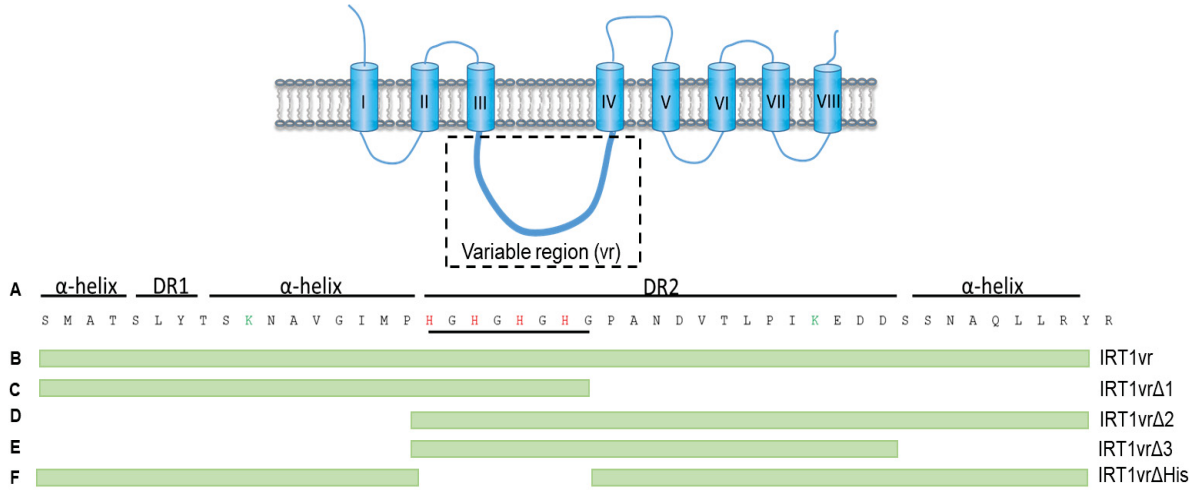

Figure 4.2. Schematic representation of the generated deletion fragments of IRT1vr as defined in Ivanov and Bauer (2017). The cartoon on the tops shows the predicted structure of IRT1. It has 8 predicted transmembrane domains and a large cytoplasmic loop also known as variable region (vr) between transmembrane domain III and IV. Vr is highlighted in the dotted rectangle. (A) Amino acid sequence and the important structural features of IRT1vr. (B) Full-length IRT1vr. (C) IRT1vrΔ1 contains the first part of the vr and the middle part (His-rich region) but missing the whole last part. (D) IRT1vrΔ2, contains the last part of the vr and the middle part (His-rich region) but missing the whole first part (E) Contains the His-rich region and small stretch of the last part but lacks the whole first part and the little piece of the last part. (D) IRT1vrΔHis, Full-length IRT1vr, except the His-rich region. DR: disordered region.

For BiFC analysis, EHB1 was always fused c-terminally with nYFP (EHB1-nYFP) and the fragment(s) were fused c-terminally with cYFP. For transient expression of proteins, tobacco leaves were transformed with the help of Agrobacterium and after 48-72 h CLSM was performed. The fluorescent signal in figure 4.3.A shows that IRT1vrΔ1-cYFP interact with EHB1-nYFP. The same can be seen for IRT1vrΔ2-cYFP and IRT1vrΔHis-cYFP (Fig. 4.3.D and J.). No fluorescent signal can be seen with IRT1vrΔ3-cYFP (Fig. 4.3. G), suggesting that IRT1vrΔ3-cYFP did not interact with EHB1-nYFP. To exclude the possibility that one of the proteins might not have been expressed, western blot analysis can be performed.

To summarize these results, it can be concluded that fragments IRT1vrΔ1, IRT1vrΔ2 and IRT1vrΔHis interact with EHB1 (Fig. 4.3.A, D, and J.) while fragment IRT1vrΔ3 did not interact with EHB1 (Fig. 4.3. G.) in this system.

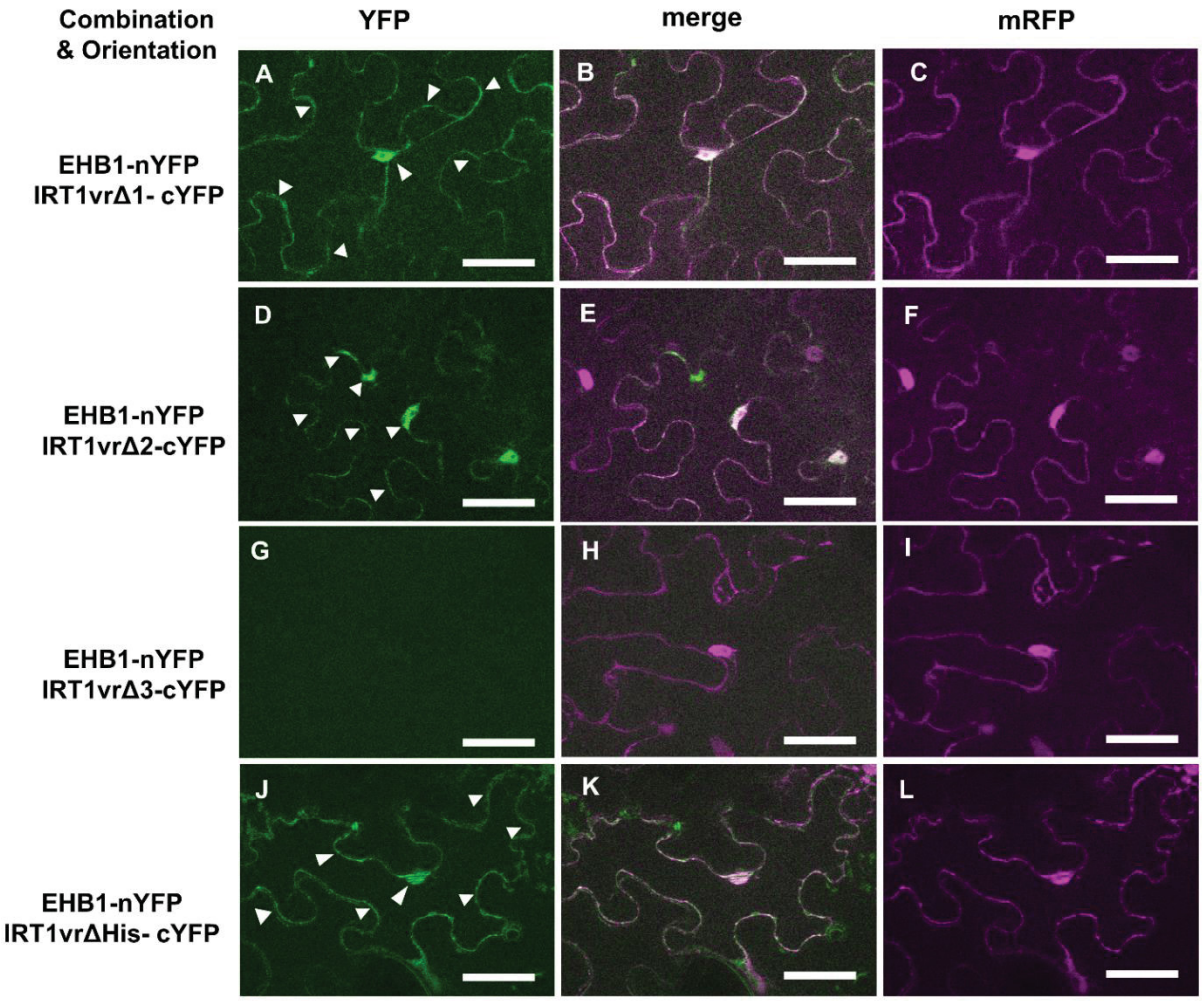

Figure 4.3.Targeted BiFC: Interaction between different deletion fragments of IRT1vr and EHB1. CLSM images of leaf epidermal cells of *Nicotiana benthamiana* two day after transformation with *Agrobacterium* containing pBIFCt-2in1-CC. (A-C) YFP signal in YFP channel can be seen due to the interaction between EHB1 and IRT1vrΔ1. The fluorescence signal is indicated by white arrowheads. (D-F) The interaction between EHB1 and IRT1vrΔ2. (G-I) No YFP signal can be seen because IRT1vrΔ3 did not interact with EHB1. (J-L) The interaction between EHB1 and IRT1vrΔHis. Bars, 20 µm.

4.1.2 Co-immunoprecipitation to verify the EHB1-IRT1 protein-protein interaction

In parallel to BiFC, Co-immunoprecipitation (Co-IP) was performed to confirm the interaction between EHB1 and full-length IRT1. Co-IP of EHB1, conjugated with HA tag and IRT1, conjugated with GFP tag was performed using anti-GFP magnetic beads followed by immunoblotting with anti-HA and anti-GFP antibodies (Fig. 4.4.).

In the first attempt when Co-IP was performed the specific bands for HA-EHB1 and IRT1-GFP was clearly visible following anti-GFP immunoprecipitation (Fig. 4.4. II and IV.). The band for HA-EHB1 in the IP fraction was very faint (Fig. 4.4. II.). to enrich EHB1 protein in the IP fraction, the Co-IP was performed in the presence of calcium

(Ca^{2+}) after reviewing the literature (Rodriguez et al., 2014; Diaz et al., 2016; Dümmer et al., 2016). Ca^{2+} might play a role in stabilizing EHB1 at the membrane and in this way EHB1-IRT1 interaction might become more stable. So, we repeated the Co-IP in the presence of 100 µM Ca^{2+} and we were able to enrich HA-EHB1 protein after Co-IP (Fig. 4.4. IV.).

After the Co-IP, first immunoblot was performed by using anti-HA antibodies to detect HA-EHB1 in the extracts. Two HA-EHB1 bands were observed in both, the crude extract (input) and the IP fraction. The double bands suggest that EHB1 might be present in different forms, one of which could be a post-translationally modified form. The possibly post-translationally modified EHB1 form (higher band) could still be able to interact with IRT1. The HA-EHB1 bands (expected size 25 kDa) in lane 3 and 4, which contained extract from leaves transformed with an HA-EHB1 construct (input fraction) were the positive controls for the anti-HA antibody (Fig. 4.4 A-B. III.). No bands could be seen in negative controls for anti-HA antibody in lane 1 which contains extract from non-transformed leaves and lane 2 which contains extract from the leaves transformed with IRT1-GFP (Fig. 4.4 A-B. III.). Analysing the positive and negative controls it can be concluded that no contamination occurred in crude extracts and IP fraction. Additionally, it confirms the successful transformation of plants with the HA-EHB1 construct. The HA-EHB1 band can also be seen in lane 8 of the membrane loaded with extract from the IP fraction (Fig. 4.4 A-B. IV.). A very weak band in lane 7 for HA-EHB1 can be seen which could be due contamination from the crude extract (input) or might be due to some leaking from the lane 8, but in comparison there is a very strong band in lane 8 for HA-EHB1 (Fig. 4.4 B. IV.) suggesting that HA-EHB1 has been co-precipitated with IRT1-GFP as Co-IP was performed with anti-GFP beads.

To verify the transformation and expression efficiency and to check whether IRT1 was pulled down during the Co-IP or not, the membrane was also probed with anti-GFP antibody. Bands in lanes 2 and 4 in the membrane loaded with crude extracts of the leaves transformed with IRT1-GFP (Fig. 4.4 A-B. I.) suggest that the transformation was successful. No bands can be seen in lanes 1 and 3 which were negative controls for the anti-GFP antibody because these lanes did not contain the extracts which have the GFP tag. The correctly sized IRT1-GFP bands (63 kDa; IRT1= 27 and GFP= 36 kDa) can be seen in lanes 6 and 8 (Fig. 4.4 A-B. II.), on the

membrane loaded with the IP fraction suggesting that IRT1-GFP was precipitated and that Co-IP worked successfully. Full-size images of the data shown in figure 4.4 are available in Supplemental Fig. S2.

After the above analysis, it can be concluded that the Co-IP experiments worked successfully and HA-EHB1 was co-immunoprecipitated with full-length IRT1-GFP. These results confirmed that the two-full length protein EHB1 and IRT1 interact with each other *in planta* and the presence of Ca^{2+} enhances the interaction of EHB1 with IRT1 suggesting that, in the plant cell environment Ca^{2+} might stabilize EHB1 at the membrane which can then interact with IRT1 more stably.

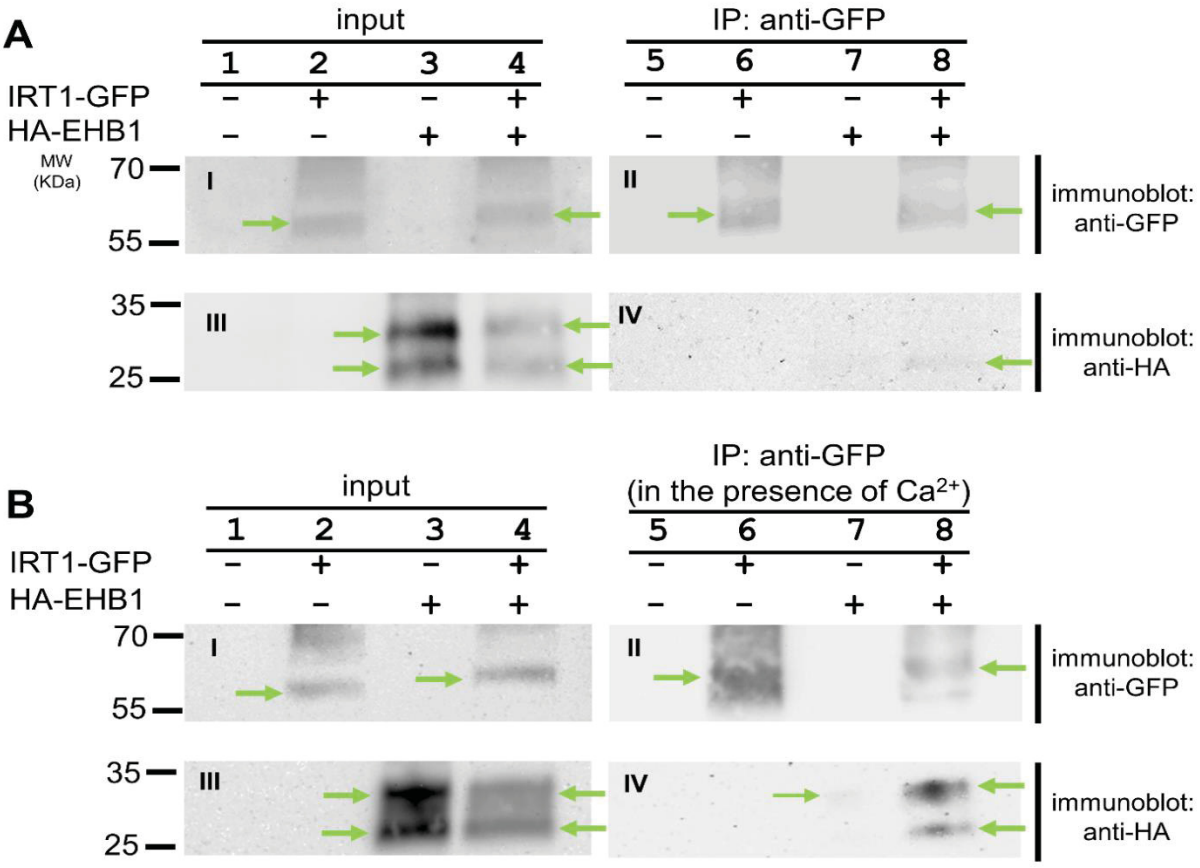

Figure 4.4. Co-immunoprecipitation of Full-length IRT1-GFP and HA-EHB1.GFP trap assay. The presence of IRT1 and EHB1 proteins is detected both in input fractions (total protein extracts) and IP fraction. The indicated proteins IRT1-GFP (band at, 63 kDa) and HA-EHB1 (band at, 25 kDa) were transiently expressed in *Nicotiana benthamiana* and detected in an immunoblot with anti-GFP and anti-HA antibodies. The experiment was performed in the absence (0 µM) or presence (100 µM) calcium. (A) IP: anti-GFP in the absence of calcium, a weak band can be seen in the IP fraction of anti-HA immunoblot, meaning that EHB1 was co-precipitated with IRT1. (B) IP: anti-GFP in the presence of calcium, a strong HA-EHB1 band can be seen in the IP fraction suggesting that HA-EHB1 was co-precipitated with IRT1-GFP. For full-size images see supplemental figure S2. The experiment was performed twice and the represented blots are from two independent assays. MW: molecular weight. KDa: kiloDaltons.

4.2 Subcellular localization of EHB1

For the proper function of a protein, it is important to find out its subcellular localization. Investigation of subcellular localization of a protein is a step forward in understanding its function. IRT1 is required for iron-uptake and it has been shown that it is localized in the cell at the plasma membrane as well as in trans-Golgi network (TGN/EE) (Vert et al., 2002; Barberon et al., 2011; Ivanov et al., 2014). So for EHB1, to have an effect on the activity of IRT1 it is required that it colocalizes with IRT1. EHB1 is a member of CAR family of plant proteins and members of this family are reported to be peripheral membrane proteins, meaning that they are present in the cell in two pools, cytoplasmic and membrane-associated (Rodriguez et al., 2014; Diaz et al., 2016). To analyze EHB1 localization in the cell we used two different approaches i.e. fluorescently labeled protein colocalization and cell fractionation.

4.2.1 Fluorescently labeled protein colocalization

Fluorescently labeled proteins (GFP tagged) are widely used now to study protein localization, dynamics, and interaction. In our studies, GFP tagged EHB1 was used for colocalization with IRT1-mCherry and plasma membrane marker AHA1-mRFP (Fig. 4.5.). We also investigated the localization of GFP tagged EHB1-ΔSig and EHB1-4x (Fig. 4.5.).

Translational fusion of EHB1 with GFP and IRT1 with mCherry were transiently co-expressed in *N. benthamiana* leaves by using Agrobacterium infiltration method to analyze their colocalization. After 48-72 h of tobacco transformation, fluorescence microscopy and colocalization analysis were performed as described in methods section 3.2.2.4. EHB1-GFP fusion expressed in tobacco epidermis cells showed a broad localization pattern with signals also visible in the nucleus (Fig. 4.5 A.). We performed a colocalization analysis between EHB1-GFP and IRT1-mCherry. Both proteins were co-expressed in the same cell and yellow signals indicated overlaps between the localization of EHB1-GFP and IRT1-mCherry (Fig. 4.5 B.). The two proteins colocalized in the cell periphery however not fully. EHB1-GFP signal was present in the cell periphery and nucleus but, being a membrane-bound protein, IRT1-mCherry signal was absent from the nucleus (Fig. 4.5 A-C.).

We also tested the colocalization of EHB1-GFP with plasma membrane proteins AHA1-mRFP and Lti6b-mRFP (Kurup et al., 2005; Caesar et al., 2011). The two

fusions displayed colocalization in the cell periphery (Fig. 4.5 D-F and G. Supplemental Fig. S3. A-C.). The resolution is not sufficient to claim that it is at the plasma membrane but EHB1 colocalized with these marker proteins.

These findings are consistent with published data where it has been reported that CAR-family proteins are partially localized at the plasma membrane (Cheung et al., 2010; Demir et al., 2013; Rodriguez et al., 2014).

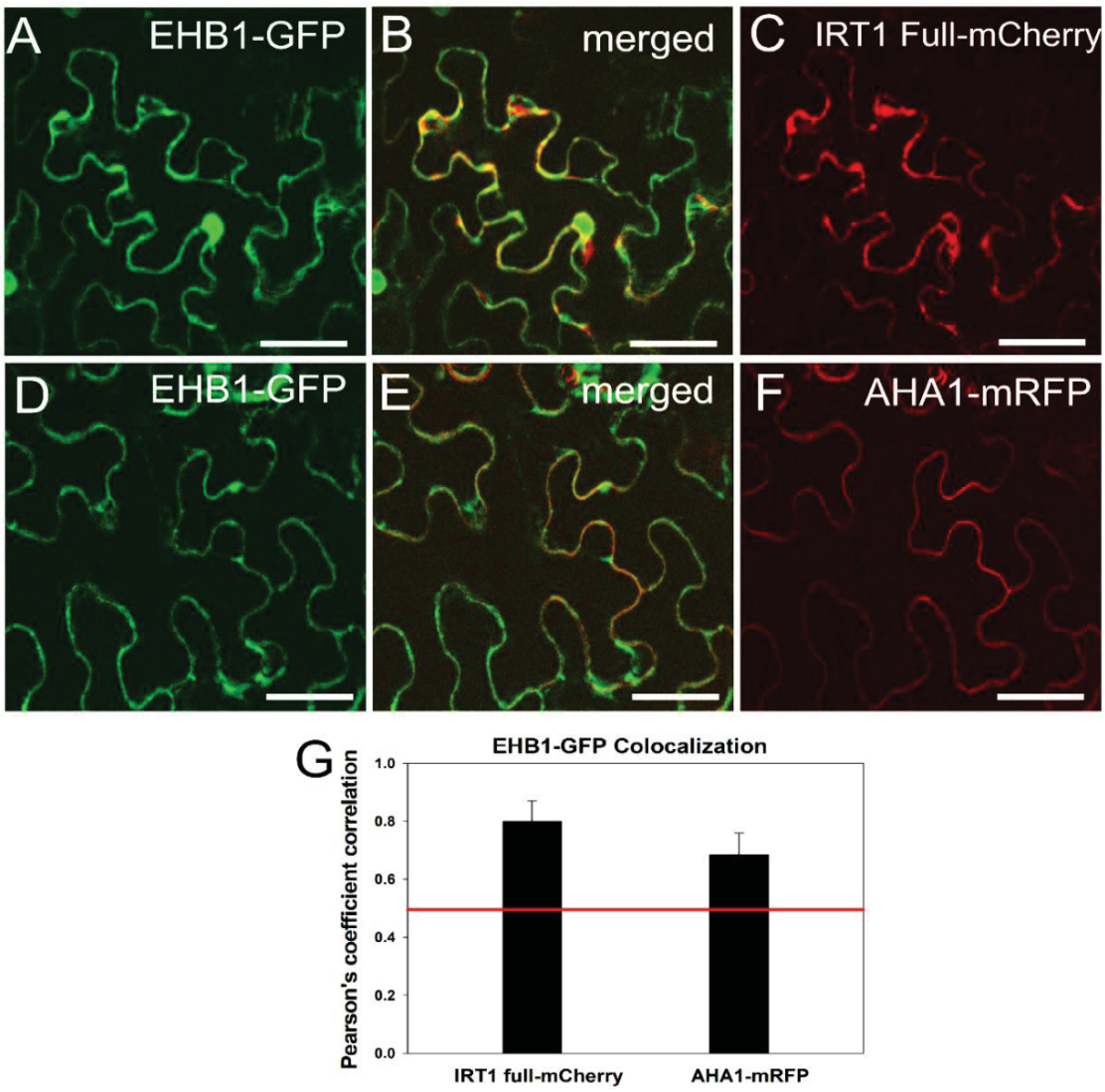

Figure 4.5. Subcellular localization of EHB1. (A-C) Colocalization between EHB1-GFP (A) and IRT1-mCherry (C).
(B) Yellow fluorescence signal indicates colocalization due to the merger of A and C.
(D-F) Colocalization between EHB1-GFP (D) and AHA1-mRFP (F) [Plasma membrane marker].
(E) Yellow fluorescence signal indicates colocalization due to the merger of D and F.
(G) Pearson's correlation coefficient (PCC) was calculated to estimate the degree of colocalization of EHB1-GFP with IRT1-mCherry and AHA1-mRFP. Red line shows the minimum correlation required for colocalization of two fluorophores. PCC for EHB1-GFP and IRT1-mCherry = 0.81± 0.074, n=10. And PCC for EHB1-GFP and AHA1-mRFP = 0.71± 0.070, n=10. Bars = 20 µm
At least 10 images for each combination was analyzed.

4.2.2 Deletion of signature domain or mutation in the C2 domain does not alter EHB1 subcellular localization

We were interested to investigate whether the deletion of signature domain or mutation in the C2 domain affected the colocalization of EHB1 with these marker proteins. To address this question we tested the GFP tagged EHB1-ΔSig and EHB1-4X for colocalization with IRT1-mCherry, AHA1-mRFP, and Lti6b-mRFP. Figure 4.6 A-C shows that both proteins were co-expressed in the same cell and yellow signals indicated the overlap between the localization of EHB1-ΔSig-GFP and IRT1-mCherry. Here again, the two proteins colocalized in the cell periphery but not fully. The same pattern can be seen for EHB1-ΔSig-GFP colocalization with AHA1-mRFP (Fig. 4.6 D-F and M) and Lti6b-mRFP (Supplemental Fig. S3. D-F.)

Likewise, figure 4.6 G-I show that EHB1-4X colocalized with IRT1-mCherry, figure 4.6 J-L show colocalization of EHB1-4X with AHA1-mRFP and supplemental figure. S3. G-I show colocalization of EHB1-4X with Lti6b-mRFP. These results suggest that the deletion of signature domain or mutation in the C2 domain does not affect EHB1 localization.

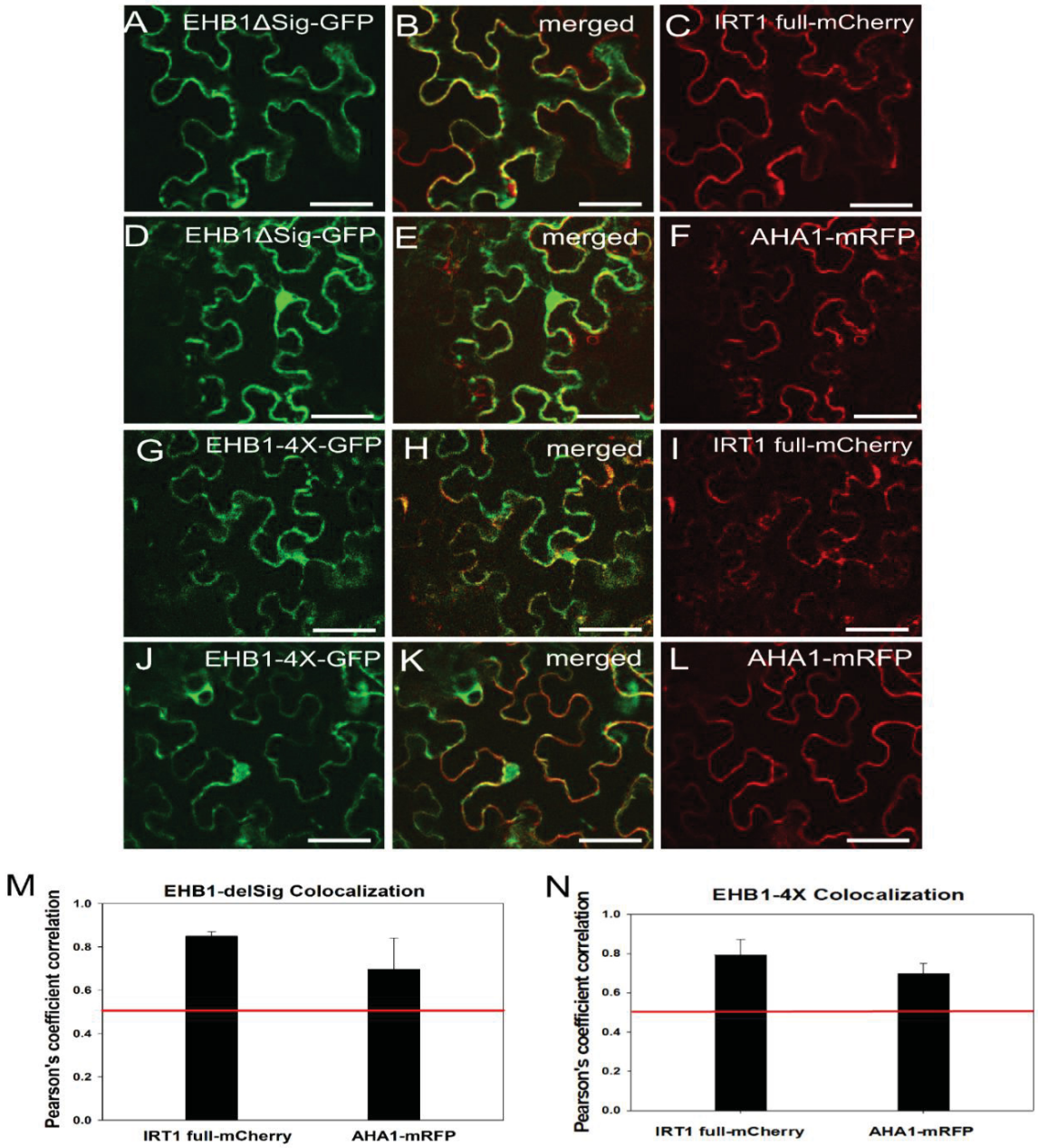

Figure 4.6.Subcellular localization of EHB1-ΔSig and EHB1-4x. (A-C) Colocalization between EHB1ΔSig-GFP (A) and IRT1-mCherry (C).
(B) Yellow fluorescence signal shows colocalization due to the merger of A and C.
(D-F) Colocalization between EHB1ΔSig-GFP (D) and AHA1-mRFP (F)
(E) Yellow fluorescence signal shows colocalization due to the merger of D and F.
(G-I) Colocalization between EHB1-4X-GFP (G) and IRT1-mCherry (I).
(H) Yellow fluorescence signal shows colocalization due to the merger of G and I.
(J-L) Colocalization between EHB1-4X-GFP (J) and AHA1-mRFP (L).
(K) Yellow fluorescence signal shows colocalization due to the merger of J and L.
(M-N) Pearson's correlation coefficient (PCC) was calculated to estimate the degree of colocalization of EHB1ΔSig-GFP with IRT1-mCherry, PCC = 0.84± 0.021, n=10 and with AHA1-mRFP, PCC = 0.69± 0.144, n=10. And for EHB1-4X with IRT1-mCherry PCC = 0.79± 0.079, n=10 and with AHA1-mRFP PCC = 0.69± 0.054, n=10. Red line shows the minimum correlation required for colocalization of two fluorophores.
At least 10 images for each combination was analyzed. Bars = 20 µm

4.2.3 Calcium enhances the interaction of EHB1 with plant membranes

In order to further evaluate the subcellular localization of EHB1, we performed cell fractionation coupled with immunodetection. For this purpose, transgenic plants expressing N-terminal HA epitope-tagged EHB1(HA-EHB1) were grown on Hoagland agar medium supplemented either with 50 µM iron (+Fe) or without iron (0 µM –Fe) for 8 days and then the cell fractionation experiment was performed as described previously (Alexandersson et al., 2008) (Method section 3.2.3). Antibodies against UDP-glucose pyrophosphorylase (UGPase) a soluble enzyme (Martz et al., 2002) and H^+-ATPase (plasma membrane marker) (Morsomme et al., 1998) were used as controls in the experiment. UGPase protein (52 kDa) was predominantly present in the soluble cytosolic fraction when the membrane was probed with an anti-UGPase antibody (Fig. 4.7 A and C.). For H^+-ATPase, a significant amount of protein (95 kDa) was present in the microsomal fraction and a very slight band could also be seen in the cytosolic fraction. H^+-ATPase was detected by an antibody against H^+-ATPase (Fig. 4.7 A and D.).

Because EHB1 contains the C2 domain, through which it can bind to membrane phospholipids, we were interested to find out whether Ca^{2+} affect this binding. Therefore, we performed cell fractionation in the presence (100 µM) or absence (0 µM) of calcium ($CaCl_2$ was added to the extraction buffer). The results show that in the absence of calcium, no significant presence of the HA-EHB1 fusion could be observed in the microsomal fraction. The presence of calcium, however, resulted in a marked increase of membrane-associated HA-EHB1 (Fig. 4.7 A-B.). The effect could be observed and was comparable both in standard-grown (+Fe) and iron-deficient (-Fe) grown plants (Fig. 4.7 A-B.). This shows that in the presence of calcium a substantial amount of EHB1 was present in the membrane-enriched microsomal fraction.

The experiment was repeated three times and the results were reproducible (Supplemental Fig S4 and Supplemental Fig S5). To estimate EHB1 abundance in the cytosolic soluble fraction and the microsomal fractions, we calculated the EHB1 signal intensities in these fractions. The quantification data showed that about 20% of the EHB1 protein was present in membrane-enriched microsomal fraction in the presence of Ca^{2+} and 80% in the cytosolic soluble fraction (Fig. 4.7 B.). While in case of absence of calcium most of the EHB1 protein was present in the soluble fraction and very little in the microsomal fraction (Fig. 4.7 B.). The quantification of

UGPase showed that more than 90% of the UGPase was present in the cytosolic soluble fraction and less than 10% in the microsomal fraction both in the presence and absence of calcium (Fig. 4.7 C.). For PM-ATPase the quantification showed that more than 90% of ATPase was present in the microsomal fraction and less than 10% in the cytosolic soluble fraction both in the presence and absence of calcium (Fig. 4.7 D.). Full-size images of the data shown in figure 4.7 A are available in Supplemental Fig. S4.A.

Taken together, this result showed that EHB1 is a peripheral membrane protein which could bind to membrane phospholipids and that calcium is important for this interaction *in planta*. At the same time, the data show that iron deficiency likely does not affect the availability of EHB1 binding sites in plant membranes.

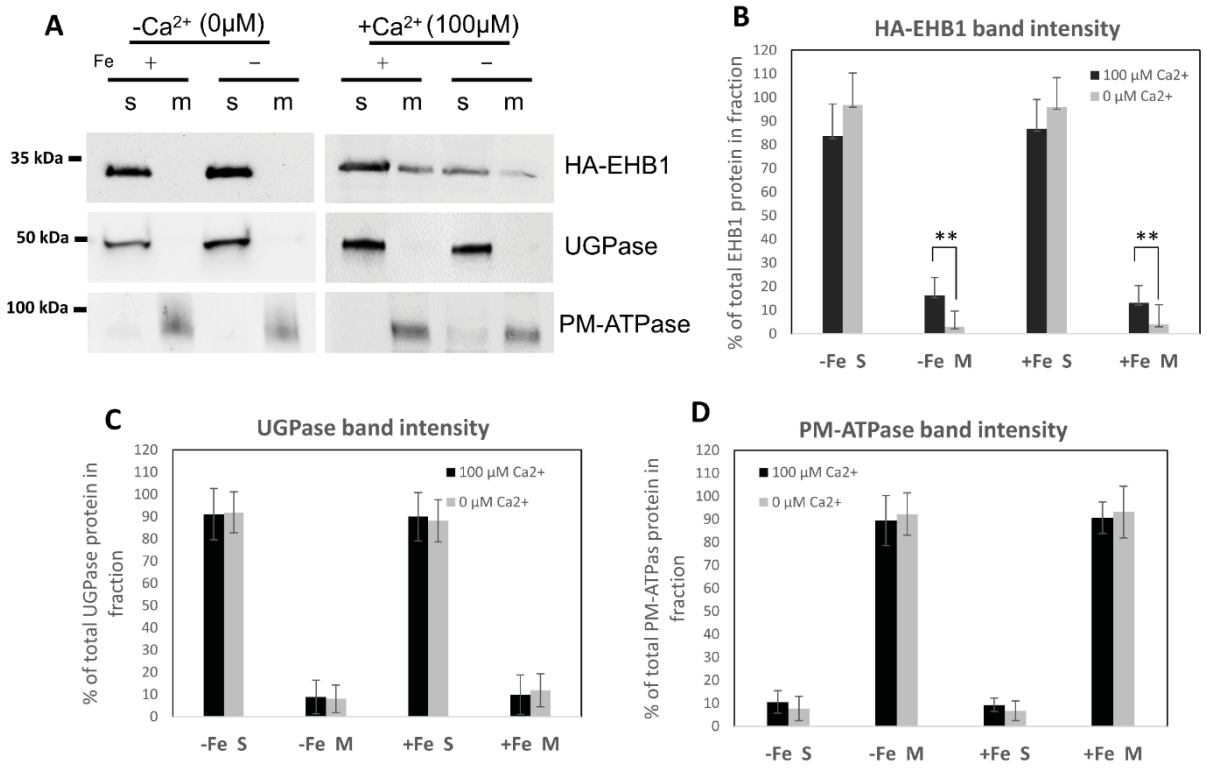

Figure 4.7. EHB1 membrane-association. (A) Protein immunoblot showing the presence of EHB1 in soluble (s) and microsomal fraction (m) of the protein extract from 8 days old seedling expressing HA-EHB1. The experiment was performed in the absence (0 µM) and presence (100 µM) of calcium in the extraction buffer. The samples were probed with antibodies against cytoplasmic marker UGPase (52 kDa), plasma membrane marker H^+ATPase (95 kDa) and to detect HA-EHB1 (25 kDa) antibody against HA tag was used. In the absence of calcium, significant amount of EHB1 is present in the cytosolic soluble fraction, while the presence of calcium enhanced the amount of EHB1 in microsomal fraction. (B-D) signal intensity quantification in fractions of HA-EHB1, UGPase, and PM-ATPase respectively, were calculated as percentage of the total luminescence of both cytosolic and microsomal fraction. Error bars represent SD of the mean (three replicates). Asterisks indicate statistically significant difference in 100 µM calcium microsomal fraction in comparison to 0 µM calcium microsomal fraction ($P < 0.01$). + And – represent +Fe and –Fe, s: soluble. m: microsomal fraction. KDa: kiloDalton

4.3 *In vitro* EHB1 interact with membrane phospholipids in a calcium-independent manner

The localization experiment showed that the EHB1 protein colocalized with plasma membrane marker proteins and cell fractionation also showed that a substantial amount of EHB1 was present in the membrane-rich microsomal fraction. We were then interested to establish an *in vitro* lipid-binding assay to further explore the lipid-binding characteristics of EHB1 e.g. to find out which specific membrane phospholipids it can bind.

4.3.1 Recombinant protein expression and purification

For *in vitro* protein-lipid binding assay we needed recombinant purified EHB1 protein. For this, *N*-terminal *Strep*-tag II constructs were generated by sub-cloning the cDNA for both mutated (EHB1-4x and EHB1-ΔSig) and non-mutated EHB1 into the pET-Strep-II vector. The *Strep*-tag II (*Strep*-tag from now on) is an eight amino acids long peptide and it has high affinity to binds with *Strep*-Tactin (an engineered streptavidin derivative) (Schmidt and Skerra, 2007). the pET-Strep-II plasmid was used to express the protein in *E. coli (BL21)*. To optimize conditions for protein expression, different time intervals, temperature, and concentration of *IPTG* were tested and the best condition was then chosen which was, to express the protein for 1 h at 28 °C and induce with 0.1 mM final *IPTG* concentration.

After expression, EHB1, EHB1-4x, and EHB1-ΔSig proteins were purified via the affinity purification strep tactin system (Fig. 4.8 A.), which has been described in detail in the methods section 3.2.6.1. These purified proteins were then used in further experiments.

4.3.2 Protein-lipid overlay assay of strep tagged proteins using membrane lipid strips™

To find out the association of EHB1 with membrane phospholipids, we used the purified recombinant full-length EHB1 or the C2 domain quadruple mutant EHB1-4X protein to test for direct lipid binding. Membrane strips with 100 pmol of 15 different hydrophobic membrane lipids (Fig. 4.8 D.) were incubated with Strep-tagged EHB1 or EHB1-4X protein followed by anti-strep tag antibody detection. The experiment was performed in the presence of (100 µM) or absence of calcium (0 µM). Two phospholipids showed a strong binding with EHB1 both in presence or absence of calcium. The same lipids also bound to EHB1-4X (Fig. 4.8 B & C.). It was expected

that the C2 domain quadruple-mutated EHB1 may lose the phospholipid binding ability, but it was not the case. The two lipids to which the proteins bound were, phosphatidylinositol (PI) and phosphatidylinositol-4-phosphate (PI(4)P). Interestingly, both the proteins bind to phospholipids also in the absence of calcium, although the presence of calcium (100 µM) enhanced the binding of the proteins with phospholipids but still in the absence of calcium proteins were able to bind with lipids (Compare fig. 4.8 B with 4.8 C.). This was somewhat surprising, but it could mean that EHB1 might need calcium to bind to membrane phospholipids in a plant cell environment but not *in vitro*.

The specificity of EHB1 for these lipids was further verified with liposome binding assay.

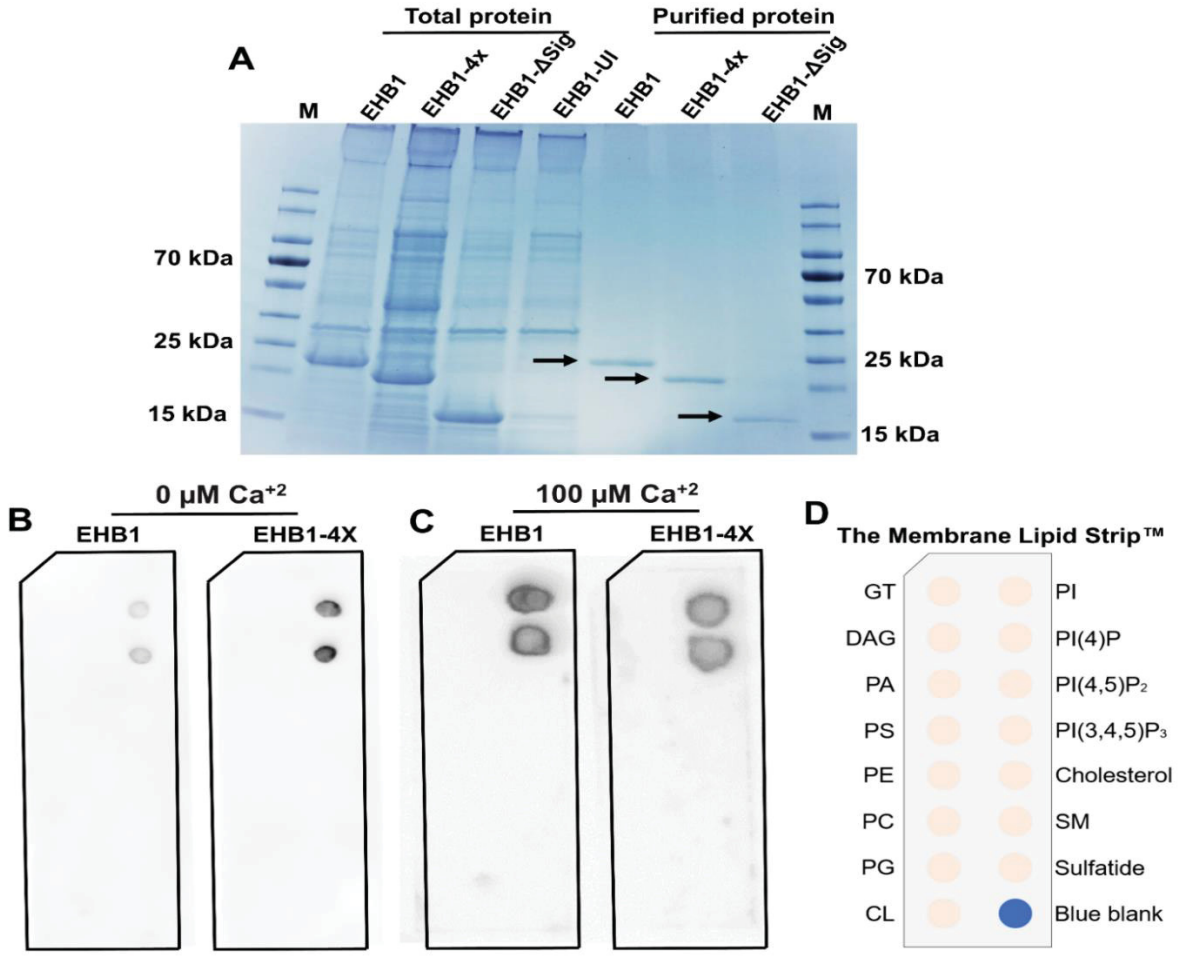

Figure 4.8. Phospholipid binding of purified recombinant Strep-EHB1/ Strep-EHB1-4X protein using membrane lipid Strips (Echelon, P-6002). (A) Strep-tactin purification of recombinant EHB1, EHB1-4x, and EHB1-ΔSig protein expressed in *E. coli* (BL21). Coomassie-stained SDS gel of the total protein (left) and purified protein (right) after elution from the strep-tactin column, bands for the purified proteins are indicated by black arrows. (B) Binding of EHB1 and EHB1-4X with PI and PI(4)P in the absence of calcium (0 µM). (C) Binding of EHB1 and EHB1-4X with PI and PI(4)P in the presence of calcium (100 µM). The proteins were detected with an antibody against Strep-tag. (D) A

sample of Echelon membrane strip spotted with different lipids, each spot contains 100 pmol of each lipid. M: Marker, UI: Un-induced.

4.3.3 Liposome binding assay

The liposome binding assay is a method of choice to examine protein-lipid binding because it is a simple and inexpensive method. With this technique, one can determine affinity and specificity of the protein-lipid binding. Another reason to use liposome is that it closely resembles the biological membranes. So, to ensure EHB1-lipid binding further we generated liposome and performed EHB1 liposome binding assay.

Based on the results of the membrane lipid binding assay, where EHB1 was able to bind preferentially to PI and PI(4)P. We decided to use the same phospholipids in the liposome binding assay as well. The liposomes prepared from phosphatidylcholine (PC), phosphatidylinositol 4, 5-bisphosphate ($PI(4,5)P_2$) and phosphatidylinositol-3,4,5-trisphosphate ($PI(3,4,5)P_3$) were used as controls in the experiment.

Three different versions of EHB1 proteins, namely full-length non-mutated EHB1, EHB1-4X, and EHB1-ΔSig were used in the assay to investigate its lipid binding ability. The liposome were prepared as described in the methods section 3.2.6.3. The assay was performed by incubating 5 µg of purified recombinant Strep-tagged proteins with 50 µl of liposome for 30 min at 30°C and then were processed further. To determine the dependency of EHB1 protein-lipid binding on calcium, the experiment was performed in the presence (100 µM) or absence (0 µM) of calcium. For the evaluation of protein binding profiles, SDS-PAGE was performed followed by immunodetection with an anti-Strep antibody. For negative controls, the same amount of proteins was mixed with 50 µl buffer without liposomes and also Strep-tagged FIT-c (12.2 kDa) purified protein was used. FIT is a known transcription factor and a central regulator of the iron uptake machinery of the model plant *Arabidopsis thaliana* and does not bind phospholipids (Fig. 4.9 B).

The results shown in figure 4.9.C confirm the binding of EHB1 with PI (Fig. 4.9 C. IV and 4.9. D.) and PI(4)P (Fig. 4.9 C. V and 4.9. D.). The bands in the pellet fraction (P) means that EHB1 proteins were co-pelleted with liposome due to its binding with phospholipids present in these liposomes. And if the proteins are not binding with the liposome they will be present in the soluble fraction. Figure 4.9 C. I-III shows that EHB1 did not bind to the liposome prepared from PC, $PI(4,5)P_2$ and $PI(3,4,5)P_3$

phospholipids because the bands can be seen in the soluble (S) fraction of the mixture, not in the pellet fraction. It was expected because in the results of the protein-lipid membrane strips binding assay EHB1 did not bind to PC, PI(4,5)P_2 and PI(3,4,5)P_3. That's why we decided to use these lipids as a negative control in this experiment.

The bands in the soluble fraction (S) in figure 4.9 C. IV and V can be explained. It is possible that the amount of protein present in the mixture exceeded the amount of liposome and at some point, during the binding assay, no more free liposome were available for further protein binding and instead to be present in the pellet fraction together with liposome some unbound protein remained in the soluble fraction.

Like the protein-lipid binding membrane strips assay, this experiment was also performed in the presence (100 µM) or absence (0 µM) of calcium (Fig. 4.9 C.). The presence of calcium enhanced the binding of EHB1 with PI (Fig. 4.9 C. IV and 4.9 D.), but overall, the protein was able to bind to phospholipids both in the presence and absence of calcium. Full-size images of the data shown in figure 4.9. C are available in Supplemental Fig. S6. This result confirms that EHB1 did not require calcium for binding to phospholipids in *in vitro* situation. The experiment was performed three times yielding comparable results (Supplemental Fig. S6).

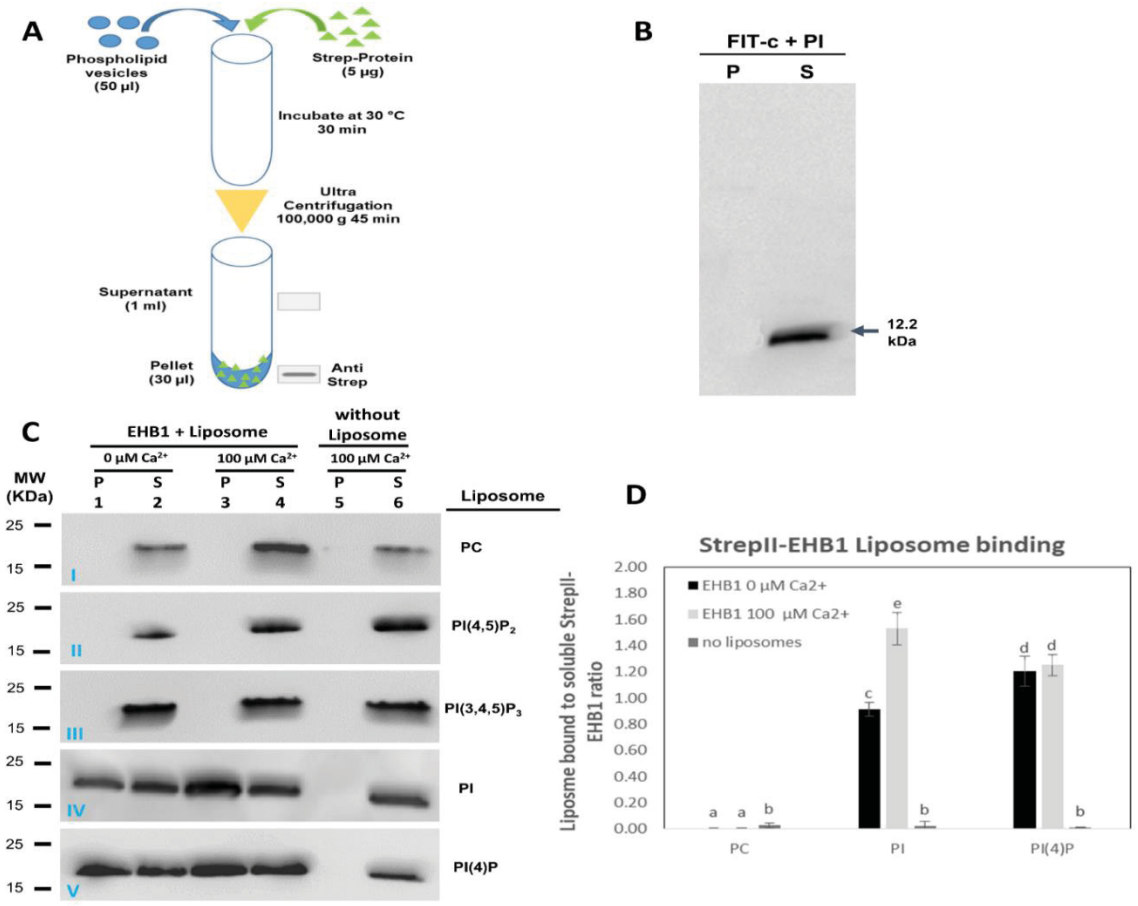

Figure 4.9. Liposome binding assay for EHB1 binding to PI and PI(4)P. (A) Scheme of the liposome binding assay to detect protein-phospholipid interaction. The protein-phospholipid vesicles were pelleted by ultracentrifugation and were analyzed with immunoblotting. (B) FIT-c protein showed no binding with liposome, used a negative control. (C) 5 µg of the indicated protein was incubated with liposome at 30°C for 30 min before ultracentrifugation, 15 µl was loaded on the gel for each sample. EHB1 bind to PI (IV) and PI(4)P (V) both in the presence (100 µM) and absence (0 µM) of calcium. While it did not bind to PC (I), PI(4,5)P_2 (II) and PI(3,4,5)P_3 (III). Quantification of the data presented in (C) represents the means of ratios of luminescence signal in soluble (S) fraction versus pellet (P) fraction in PC, PI, and PI(4)P. The ratio was calculated using the Taylor expansion method (Livak, 1997). Error bars represent SD of the mean (three replicates) Letters indicates statistical significance difference obtained with one way ANOVA-Tukey's $P < 0.05$. MW: molecular weight, P: pellet, S, soluble, PC: phosphatidylcholine, PI(4,5)P_2: phosphatidylinositol 4, 5-bisphosphate, PI(3,4,5)P3: phosphatidylinositol 3, 4, 5, trisphosphate, PI: phosphatidylinositol, PI(4)P: phosphatidylinositol 4 phosphate,

Like the non-mutated EHB1 protein, we also tested the phospholipid binding ability of mutated EHB1-4X the C2 domain quadruple mutant (4 aspartic acid residues were replaced with 4 alanine) and EHB1-ΔSig in the liposome binding assay (Fig. 4.10.). We did not observe any change in lipid binding and specificity of both the mutant EHB1-4X (Fig. 4.10 A-B.) and EHB1-ΔSig (Fig. 4.10 C-D.). They showed the same binding like EHB1 i.e. to PI and PI(4)P. Here again, the presence of calcium enhanced the binding of EHB1-4X (Fig. 4.10 B.) and EHB1-ΔSig (Fig. 4.10 D) to

phospholipids but the proteins were also able to bind with liposome in the absence of calcium. Full-size images of the data shown in figure 4.10.A and C are available in Supplemental Fig. S7 and S8. The experiment was performed three times yielding comparable results (Supplemental Fig. S7 and Supplemental Fig. S8). For EHB1-ΔSig it was expected that it will retain the phospholipid binding ability because it contained the whole intact C2 domain which is required for lipid interaction. The only deleted part was the signature domain which it uses to interact with other proteins.

To sum up the protein-phospholipid binding, it can be concluded from the results of both the *in vitro* protein-lipid membrane binding assay and liposome binding assay that EHB1, EHB1-4X, and EHB1-ΔSig preferentially bind to PI and PI(4)P and the presence of calcium enhanced the binding of EHB1 with phospholipids, suggesting that the capacity of EHB1 to bind lipids might be enhanced in the presence of calcium.

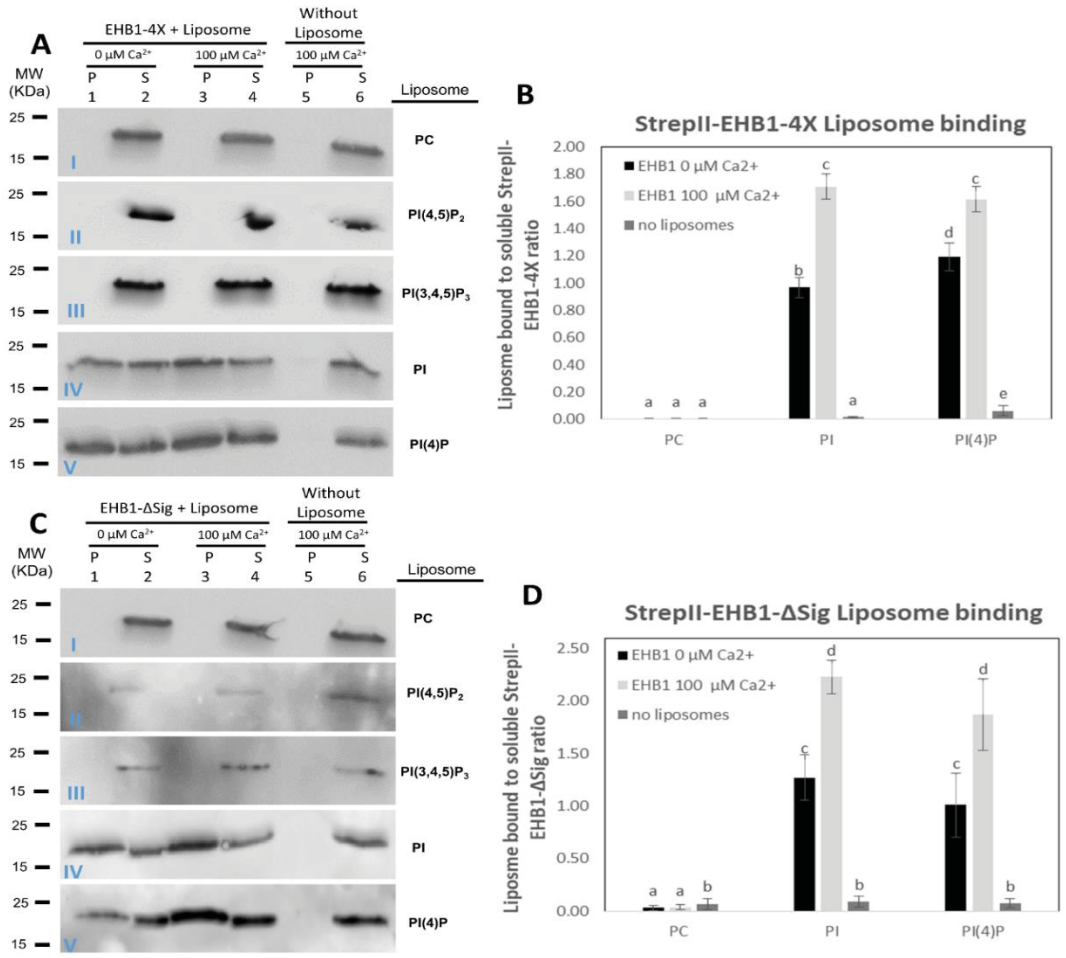

Figure 4.10. Liposome binding assay for EHB1-4X and EHB1-ΔSig binding to PI and PI(4)P. (A and C) 5 µg of the indicated protein was incubated with liposome at 30°C for 30 min before ultracentrifugation, 15 µl was loaded on the gel for each sample. EHB1-4X / EHB1-ΔSig bind to PI (IV) and PI(4)P (V) both in the presence (100 µM) and absence (0 µM) of calcium. While they did not

bind to PC (I), PI(4,5)P_2 (II) and PI(3,4,5)P_3 (III). (B and D) Quantification of band intensity of EHB1-4X / EHB1-ΔSi in PC, PI, and PI(4)P presented in (A and C) represents the means of ratios of luminescence signal in soluble (S) fraction versus pellet (P) fraction in PC, PI, and PI(4)P. The ratio was calculated using the Taylor expansion method (Livak, 1997). Error bars represent SD of the mean (n = 3). Letters indicates statistical significance difference obtained with one way ANOVA-Tukey's $P < 0.05$. MW: molecular weight, P: pellet, S, soluble.

4.4 Verification of EHB1 function as a negative regulator of iron uptake

4.4.1 EHB1 affects plant responses to iron deficiency

During the early investigations it was noted that, unlike wild-type (WT) Columbia plants (Col-0), the iron deficiency responses were elevated in *ehb1* mutant plants grown on –Fe conditions (0 µM FeNaEDTA). The mutant plants performed better in –Fe conditions compared to WT and overexpression EHB1 lines (2xCAMV35S: HA_3-EHB1). During our study, we analyzed two EHB1 loss-of-function alleles, *ehb1-1* and *ehb1-2*, for which we confirmed the absence of full-length EHB1 transcript (Fig. 4.11 A-B.)

We were interested to understand how the interaction between EHB1 and IRT1 affects the plant capacity to acquire iron. To estimate the role of EHB1 in iron acquisition, we first performed root Fe reductase assay to check the Fe reductase activity of FRO2, which indirectly indicates the efficiency of iron uptake. For this, plants were grown on media containing 50 µM iron (+Fe) for two weeks and then, the plants were transferred to either fresh +Fe or -Fe plates for 3 days (two-week growth system). Afterwards, Fe reductase activity was measured. The assay was performed with WT, *ehb1* mutant and HA-EHB1 plants. As expected, the FRO2 activity was strongly increased under iron-deficiency in all tested genotypes. At –Fe conditions the root FeIII-reductase activity of mutant *ehb1* plants (*ehb1-1* and *ehb1-2*) was found significantly higher compared to that of WT (Col-0) and overexpressing EHB1 plants [HA-EHB1(2) and HA-EHB1(3)] (Fig. 4.11 C and supplemental Fig. S9. A.). It could be that EHB1 might directly affect the activity of FRO2. This result demonstrates that in the absence of EHB1 the plant iron acquisition system is more active suggesting that EHB1 might function as a negative regulator of iron uptake.

To explore further the negative effect of EHB1 on the iron uptake ability of IRT1, the total chlorophyll content was measured. Chlorophyll content of the leaves is an important parameter which indicates the development of leaf chloroplasts, the photosynthetic ability and general health of the plant (Wu et al., 2008; Pavlovic et al., 2015). Plants respond to Fe deficiency by a marked decrease in photosynthetic

activity due to compromised chlorophyll synthesis which leads to interveinal chlorosis in developing young leaves (Rodríguez-Celma et al., 2013b). For chlorophyll content measurement plants were grown under two-week growth system. It sufficient iron condition (+Fe) the chlorophyll content of young developing leaves was significantly higher in *ehb1-1* mutant plants as compared to HA-EHB1(2), the total chlorophyll content of *ehb1-1* and WT was comparable (Fig. 4.11 D.). To summarize this, EHB1 affects Fe mobilization and Fe deficiency responses which in turn has an effect on chlorophyll content in the young developing leaves.

In addition, alterations were noted in the primary root growth (Fig. 4.11 E. and supplemental Fig. S9. B.). Therefore, the plants were grown on +Fe and –Fe conditions for 8 days. Under standard iron conditions (+Fe) there was no obvious change in root length, but under limited iron situation (-Fe) roots of *ehb1* mutants, lines grew longer as compared to WT and HA-EHB1 (Fig. 4.11 E.). The compensatory root growth was more prominent in *ehb1* mutant line as compared to WT and HA-EHB1 plants.

It can be concluded from these results that, EHB1 serves as a negative regulator of iron uptake responses in the model plant *Arabidopsis thaliana*.

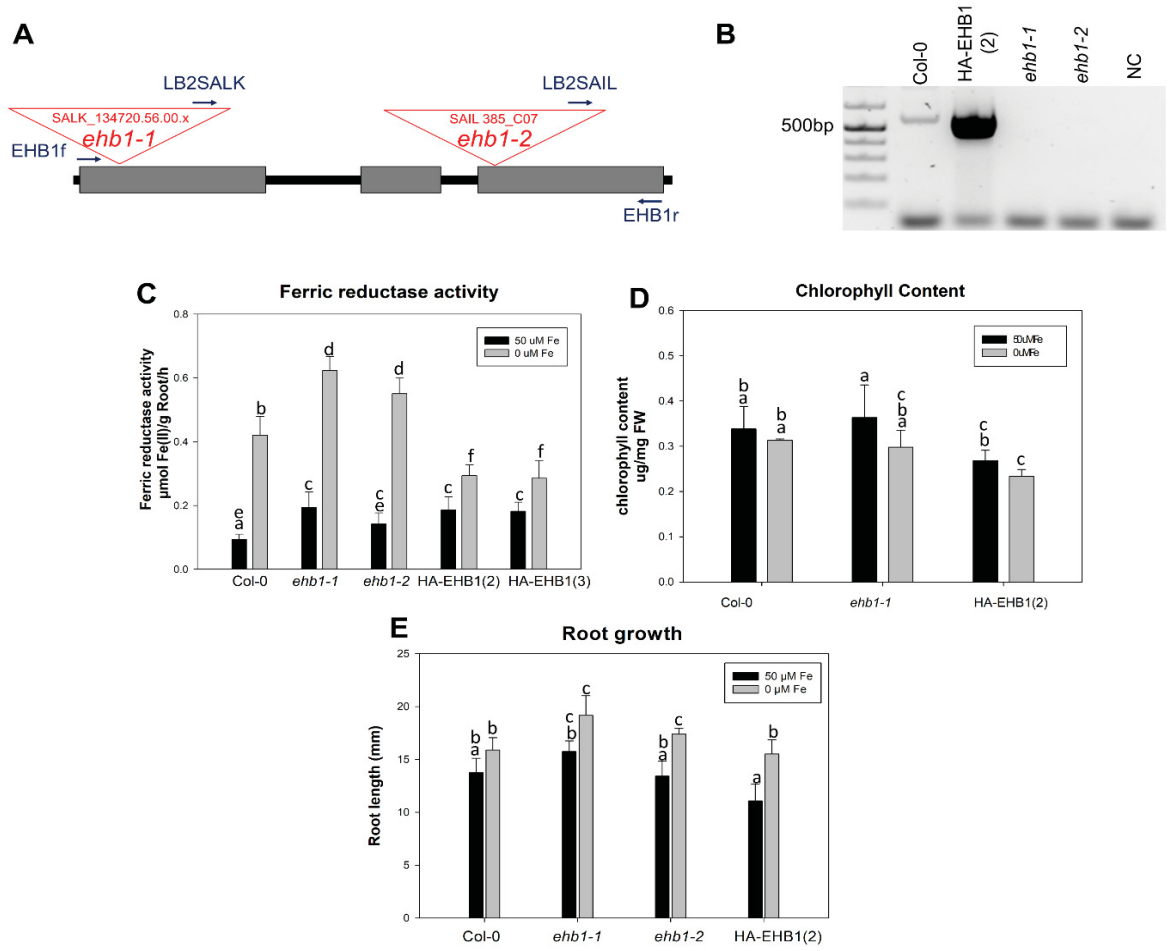

Figure 4.11. Physiological data showing the negative effect of EHB1 on the iron uptake. (A) Schematic representation of the EHB1 gene and the two alleles used in the study. The primers used for genotyping the two alleles are indicated.(B) Presence of full-length EHB1 transcript. cDNA from wild-type, EHB1-overexpressing, and two independent homozygous T-DNA insertion plants was tested using primers EHB1f and EHB1r, to amplify the full-length coding EHB1 sequence. The expected product size was 525 base pairs. As expected, the HA-EHB1 line contained large amounts of EHB1 transcript, while amplification was not possible in the two ehb1 mutant alleles.(C) Iron reductase activity of 17 d old seedlings grown on ± Fe medium (14 d +Fe and 3 d ± Fe). Note that the reductase activity of *ehb1-1* and *ehb1-2* is significantly higher than WT, HA-EHB1(2), and HA-EHB1(3) at –Fe condition. Error bars represent standard deviation (SD) of the mean (n = 5). (D) Total chlorophyll content quantified in the extract of young developing leaves of the plants grown on ± Fe medium (14 d +Fe and 3 d ± Fe). The chlorophyll content of *ehb1-1* is significantly higher than HA-EHB1 at +Fe. Error bars represent standard deviation (SD) of the mean (n = 5). (E) Root lengths of Col-0, *ehb1-1*, *ehb1-2* and HA-EHB1 plants grown for 8 d under +Fe or –Fe conditions. Error bars represent SD of the mean (n = 15), root length was calculated using Jmicrovision-1.2.7. Roots of the EHB1 mutant *ehb1-1* and *ehb1-2* grows longer at –Fe condition. Letters indicate statistical significance obtained with one way ANOVA-Tukey's $P < 0.05$. The results were obtained from three biological replicates. FW: fresh weight, NC: negative control.

4.4.2 EHB1 suppresses the import of apoplastic iron and seed iron content

To understand cellular Fe homeostasis it is needed to have both quantitative and qualitative information about the subcellular pools of iron in plant tissues (Roschzttardtz et al., 2013). To dig in more into the negative effect of EHB1 on iron

homeostasis, we investigated the role of EHB1 in apoplastic iron import. Perls/DAB staining was performed to visualize the apoplastic iron in the roots of different genotypes (WT, *ehb1-1*, HA-EHB1(2), and *fit*) grown for 8 days under standard iron supply. The outer epidermal cell walls were stained in the tested genotypes which suggests the accumulation of iron in the apoplast (Fig. 4.12 A-O.). Roots of Col-0 showed moderate staining at the base of the root (Fig. 4.12 A-B.), which decreased in the early differentiation zone (Fig. 4.12 A-C.). On the other hand, the roots of *fit-3* mutant, which did not express *IRT1*, were stained much stronger than WT (Fig. 4.12 M-O.), as shown previously for *IRT1* loss-of-function plants (Ivanov et al., 2014). In comparison to Col-0, the roots of *ehb1* mutant plants showed strongly decreased iron staining (Fig. 4.12 D-I.), while roots of HA-EHB1 plants showed enhanced staining in the early differentiation zone in comparison to Col-0 (Fig. 4.12 J-L.). These results are consistent with the observation on the physiological data of EHB1 loss- and gain-of-function plants and showed that EHB1 affects the import of apoplastic iron which is mediated by IRT1.

After the qualitative measurement of iron localization in plant roots, we were interested to analyze the effect of EHB1 quantitatively on stored iron content in the sink tissues. Studies involving many crops shows that seed iron concentration is a useful indicator which helps in identifying the genotypes which possess high resistance to iron deficiency (Wiersma, 2012). For plants, seeds are an important sink and the end point of the long-distance transported nutrients (Wiersma, 2012; Grillet et al., 2014). To further elaborate the effect of EHB1 on iron homeostasis, we then examined the iron content in seeds of soil grown plants (Fig. 4.12 P.). In addition to the Fe content, Zn and Mn contents of seeds were also determined (Fig. 4.12 Q-R.) because IRT1 can also transport these divalent metals. The concentrations of these metals also serve as a fingerprint for iron deficiency (Eide et al., 1996; Palmer et al., 2013a). Figure 4.12 P shows that seed iron content of EHB1 loss of function (*ehb1-1*) and WT are significantly higher as compare to HA-EHB1. The iron content of the seeds of *ehb1-1* was as high as of WT (Fig. 4.12 P.).

As mentioned, in addition to Fe, IRT1 is also capable of taking up Zn as well. The Zn content of seeds is shown in figure 4.12 Q. The Zn content in *ehb1-1* was higher than in HA-EHB1 (Fig. 4.12 Q).

The Mn content of seeds is shown in figure 4.12 R, the seed Mn content of the HA-EHB1 plants was higher than in WT and *ehb1-1* seeds while the seed Mn contents of

WT and *ehb1-1* seeds were almost the same and no statistical difference could be seen between the two (Fig. 4.12 R.). Altogether, these results suggest that EHB1 suppresses the uptake of apoplastic Fe (Fig. 4.12 A-O.) and that EHB1 also affects the Fe content of the seeds.

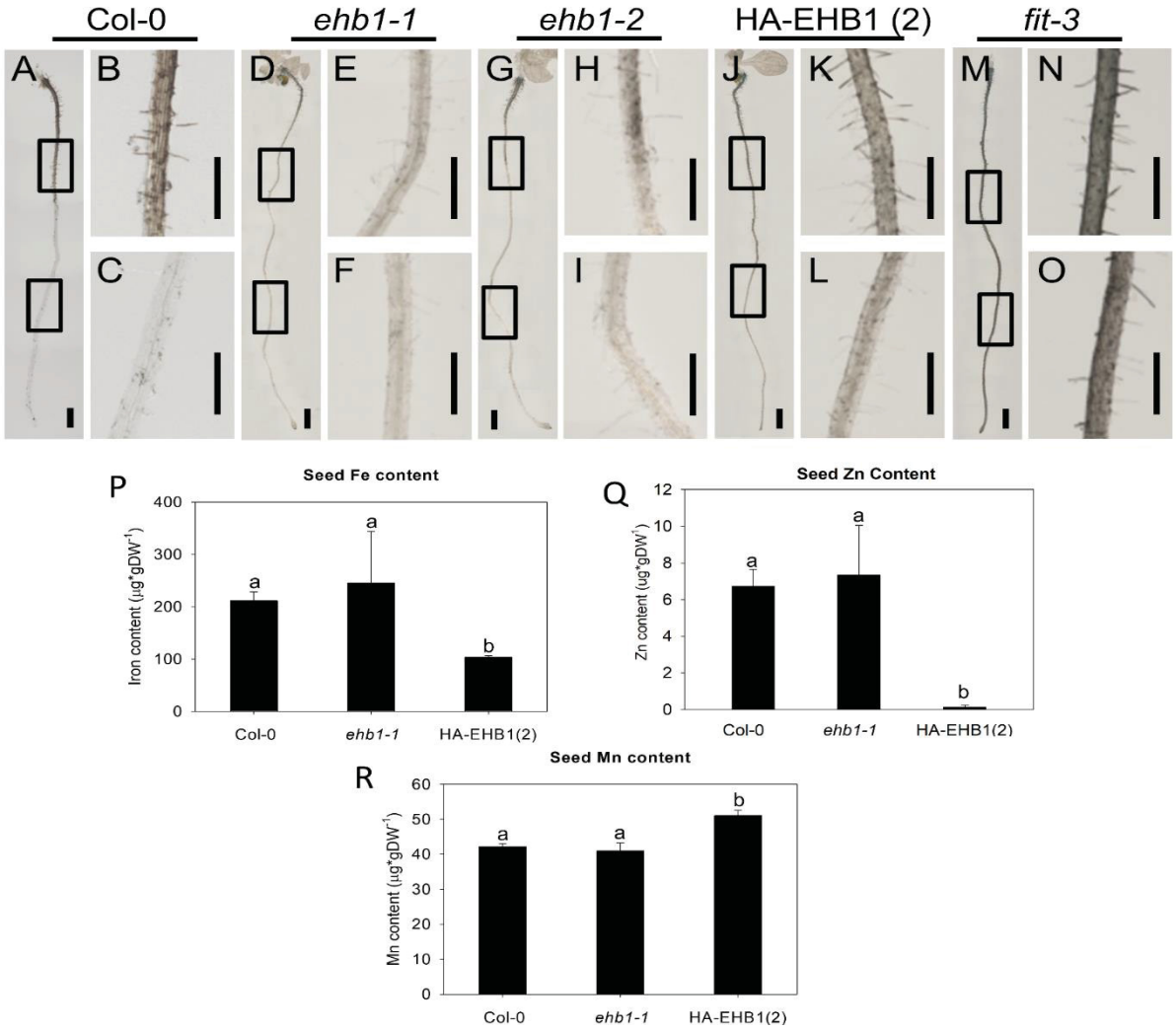

Figure 4.12. Effect of EHB1 on Iron import activity and iron storage in Arabidopsis. Visualization of iron (Fe^{3+}) in roots of Col-0, *ehb1-1*, *ehb1-2*, HA-EHB1(2) and *fit-3* plants grown for eight days under iron-sufficient conditions. For each genotype, an overview image of the root (A, Col-0; D, *ehb1-1*; G, *ehb1-2*; J, HA-EHB1(2) and M, *fit-3*) and three close-ups (B-C, Col-0; E-F, *ehb1-1*; H-I, *ehb1-2*; K-L, HA-EHB1(2) and N-O, *fit-3*) are shown. The dark staining along the roots shows the presence of iron. Results shown represent 3 independent repetitions. The experiment was performed on three biological repetitions. At least five plants per genotype were observed in each repetition. Bars = 2 mm. (P) Seed iron content of Col-0, *ehb1-1*, *ehb1-2* and HA-EHB1(2) plants. The seed iron content of *ehb1-1* is significantly higher than HA-EHB1(2). (Q) Seed Zn content of Col-0, *ehb1-1*, *ehb1-2* and HA-EHB1(2) plants. The seed Zn content of *ehb1-1* is significantly higher than HA-EHB1(2). (Q) Seed Mn content of Col-0, *ehb1-1*, *ehb1-2* and HA-EHB1(2) plants. The seed Mn content of HA-EHB1(2) is significantly higher than Col-0 and *ehb1-1*. The seeds were collected from the soil grown plants. Error bars represent SD, n=3. Letters indicate statistical significance obtained with one way ANOVA-Tukey's $P < 0.05$. The results were obtained from three replicates. DW: dry weight.

4.4.3 *EHB1* loss-of-function changes the expression pattern of iron deficiency-related genes

Whether reduced iron uptake in overexpression EHB1 (HA-EHB1) results in a feedback regulation of the expression of key iron uptake genes, to answer this question and to analyse the effect of *EHB1* on those key genes which are involved in iron uptake regulation (*IRT1, FRO2, FIT and FER1*) we used reverse transcription real-time quantitative PCR (RT-qPCR) to determine their expression. The gene expression was investigated in Col-0, *ehb1-1*, HA-EHB1 and *irt1* plant lines grown in the 2-week growth system (14 d +Fe and 3 d ± Fe). Expectedly and based on the previous studies (Vert et al., 2002; Colangelo and Guerinot, 2004; Jakoby et al., 2004), all the genes related to iron homeostasis were upregulated at –Fe condition and were downregulated at +Fe condition except *FER1* which is upregulated at +Fe instead of –Fe (Reyt et al., 2015).

EHB1 expression level tends to be downregulated at –Fe condition compared to +Fe condition in the tested genotypes suggesting that the iron status of the plant affect EHB1 gene expression. At –Fe, the expression of *EHB1* in *irt1* and WT was comparable however at +Fe in *irt1* mutant the expression was stronger than in the WT (Fig. 4.13 A.). The observed downregulation at –Fe is consistent with the proposed negative role of EHB1. We further investigated the role of EHB1 during iron-deficiency by evaluating the expression of marker genes related to Fe homeostasis. Most of these key genes are upregulated at –Fe condition in the *ehb1-1* loss-of-function mutant as compared to WT and *HA-EHB1* (Fig. 4.13 B-D.). *IRT1* (Fe transporter) expression was upregulated at –Fe in HA-EHB1 plant line. And the induction of *IRT1* was less pronounced in *ehb1-1* as compared to the WT (Fig. 4.13 B.). This could be explained by the fact that, in the presence of *EHB1* (*HA-EHB1* line) at –Fe condition most of the IRT1 is not actively functioning in the plant and because of this, plants might sense that they need more IRT1 that is why *IRT1* transcript is in abundance in HA-EHB1 and the observed reduced gene expression in *ehb1-1* might be a compensatory mechanism to suppress the overproduction of IRT1 (Fig. 4.13 B.).

On the other hand, the function of EHB1 might uncoupled the regulation of *FRO2* and *IRT1* because unlike *IRT1*, *FRO2* (Ferric reductase) expression was significantly higher in *ehb1-1* line as compared to WT and HA-EHB1 plants (Fig. 4.13 C.). This effect was consistent with the measured ferric reductase activity in these plants (Fig.

4.11 A.). The expression pattern of *FRO2* was similar in *irt1* and *ehb1-1* mutant lines (Fig. 4.13 C.).

In comparison to +Fe the expression of *FIT* (central transcriptional regulator) was upregulated in response to iron-deficiency in WT, *ehb1-1* mutant and HA-EHB1 (Fig. 4.13 D.). *FIT* expression was markedly increased in *irt1* plants as compared to WT under both + and –Fe conditions (Fig. 4.13 D.). It is known for *FER1* (iron-storage protein) that it responds positively to the amount of iron present in the plant (Reyt et al., 2015). The expression of *FER1* under the +Fe condition was significantly higher in *ehb1-1* plants as compared to WT and HA-EHB1 plants (Fig. 4.13 E.). This suggests that roots accumulate higher amounts of iron in the absence of EHB1. The observed elevated transcript abundance of *FER1* in the gene expression analysis fits well to the observed reduced iron uptake abilities in the presence of EHB1 (Fig. 4.12 P.). From these results it can be concluded that the expression pattern of some of the key genes involved in Fe homeostasis changes in the *ehb1* loss-of-function plant line (Fig. 4.13 B-E.). See Supplemental Fig. S10 for another repetition of the gene expression analysis.

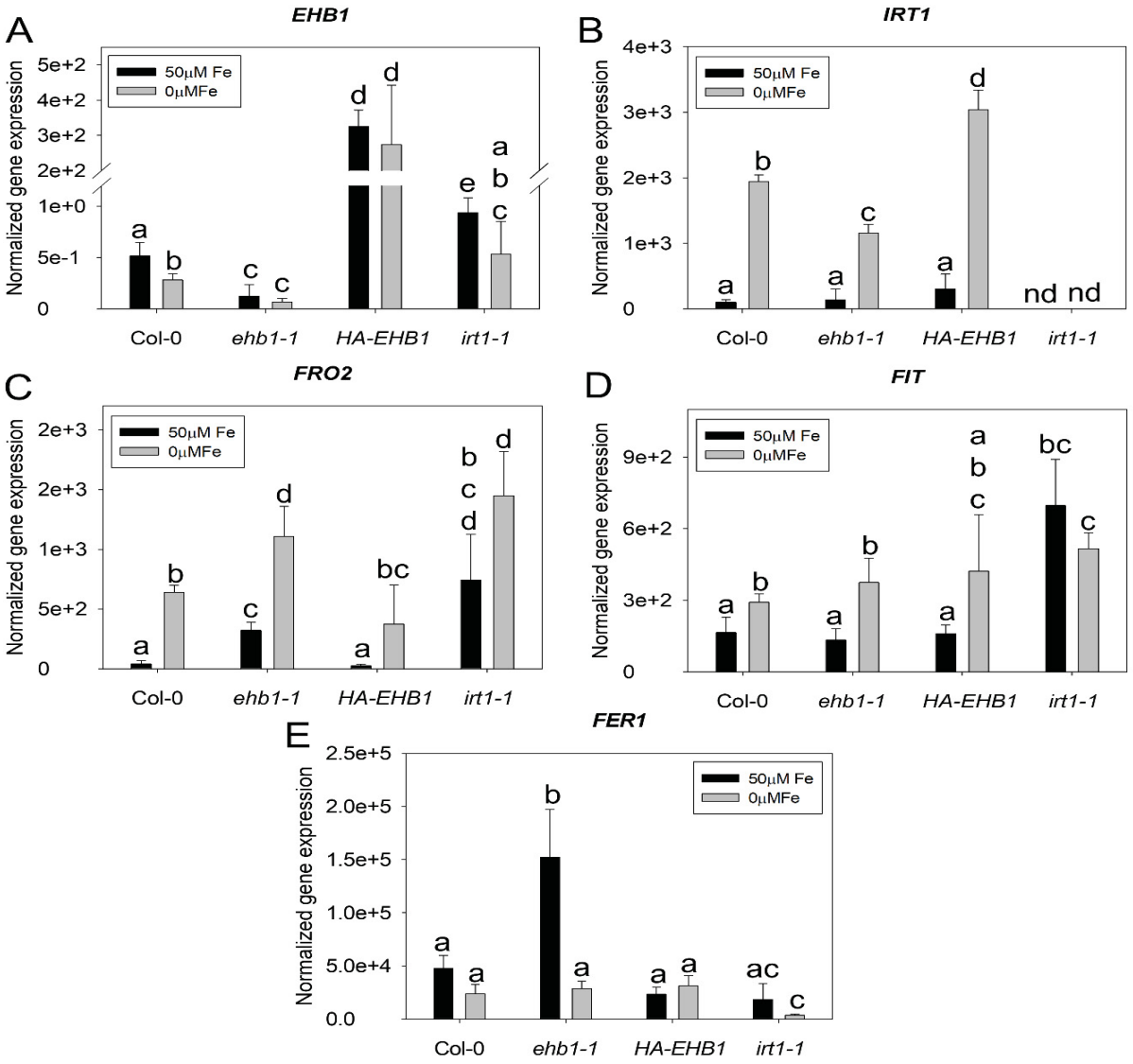

Figure 4.13. EHB1 loss of function changes the expression pattern of iron deficiency-related genes. Seeds were germinated and grown for 2-weeks growth system (14 d +Fe and 3 d ± Fe). Roots were harvested and processed to determine gene expression by quantitative RT-qPCR. The genes (A) *EHB1*, (B) *IRT1*, (C) *FRO2*, (D) *FIT* and (E) *FER1* were investigated. The represented results are from three biological repetitions. The experiment was repeated three times and the results obtained were comparable. Bars represent expression level under sufficient-iron (50 mM Fe; black) and deficient-iron (0 mM Fe; grey) conditions. Error bars represent SD of the mean (n = 3). Letters indicate statistical significance difference obtained with one way ANOVA-Tukey's $P < 0.05$.

5. Discussion

The ability of iron to change its oxidation state makes it an essential part of many biological processes, however, due to its presence oxidative damage can have an adverse effect on the cell. Therefore, for the cell, it is essential to have regulatory mechanisms for limiting iron import capacity that can ultimately overcome cell damage. Although IRT1 is not the only transporter which is capable of iron import at the root surface (Castaings et al., 2016), but its expression in the root hair cells of the early differentiation zone makes it the principal iron importer in Strategy I plants (Blum et al., 2014; Marquès-Bueno et al., 2016). The regulation of IRT1 is extremely important because the uncontrolled constitutive iron acquisition can harm the plant cell (Reyt et al., 2015).

Here, in search for the interacting regulatory proteins of iron uptake transporter IRT1, we have identified the small peripheral membrane protein EHB1 in a yeast two-hybrid screen (Y2H) of an iron-deficient root cDNA library as an interactor and negative regulator of IRT1. We showed that EHB1 interacts with IRT1 via its signature domain. We report that this interaction required the presence of calcium. We further identified specific parts of IRT1vr that are involved in interaction with EHB1. We could show that EHB1 can bind membrane phospholipids *in vitro*. Our physiological data show that EHB1 act as a negative regulator of the iron uptake machinery of the model plant *Arabidopsis thaliana*. We suggest that EHB1 negatively affects the activity of IRT1 and promotes its degradation in a calcium-dependent manner.

As mentioned EHB1 was identified in a Y2H screen as an interacting partner of IRT1vr, we have confirmed the protein-protein interaction between EHB1 and IRT1vr *in planta* via bimolecular fluorescence complementation (BiFC) and with co-immunoprecipitation. The *in planta* confirmation of the interaction was important to check if the interaction is happening directly at the interaction site in plant where the native surroundings are preserved, whereas in yeast the site of interaction is only nucleus (Xing et al., 2016).

Therefore, first, we performed BiFC to confirm the interaction between EHB1 and IRT1vr. The positive YFP signal in figure 4.1 A-C indicated that EHB1 interacts with IRT1vr *in planta* in this system, confirming the results obtained from the Y2H

experiment. This result is in agreement with results obtained by Rodriguez et al where they showed that members of the CAR family proteins interacted with PYR/PYL in the BiFC analysis (Rodriguez et al., 2014).

After this confirmation, we were interested to identify which domain/part of EHB1 is responsible for the protein-protein interaction. To this end, we deleted the C-terminally located predicted signature domain from EHB1 and generated a truncated EHB1-ΔSig which does not contain the signature domain. Crystallographic analysis of CAR4 shows that in addition to the C2 domain it contains a plant-specific conserved 43-amino acid long CAR signature domain that is likely used for interaction with other proteins by the CAR family members. We tested EHB1-ΔSig against IRT1vr in BiFC, Figure. 4.1. D-F showed that EHB1-ΔSig was no longer able to interact with IRT1vr, suggesting that deletion of signature domain abolishes the protein interacting ability of EHB1. This result is in agreement with Rodriguez et al. 2014, where they studied the interaction of CAR4-ΔSig with ABA receptors PYL1/PYL6. They reported that CAR4-ΔSig loses the ability to interact with PYL1/PYL6 (Rodriguez et al., 2014). Although we observe that EHB1 deletion construct EHB1-ΔSig did not interact with IRT1vr, we then went a step further and tested the interaction between IRT1vr and only the signature domain of EHB1 (EHB1-Sig). The positive YFP signal in the figure. 4.1. G-I suggests that EHB1-Sig interacts with IRT1vr. With these results, we confirm that EHB1 interact *in planta* with IRT1vr through its signature domain.

We also tested the C2 domain mutant EHB1-4X in BiFC for interaction with IRT1vr. EHB1-4X was able to interact with IRT1vr (Fig. 4.1 J-L.) suggesting that mutation in the C2 domain did not affect the interaction of EHB1 with IRT1vr. The possible reasons to explain this is that C2 domain is required for binding with membrane phospholipids and recruitment of proteins to targeted membranes, rather than for protein-protein interaction (Cho, 2001), and the signature domain which was needed for protein-protein interaction was still intact, So due to these reasons EHB1-4X retained the ability to interact with IRT1vr. Other plant proteins also use C2 domains for binding to membrane phospholipids, OsPBP1 involved in pollen fertility in rice binds membrane phospholipids (PC/PS) in a calcium-dependent manner via its C2 domain. Similarly, another rice small C2 domain protein OsERG1a also bind PC/PS in a calcium-dependent manner (Yang et al., 2008; Kang et al., 2013). Very recently

Liu et al, 2017, identified a 16 member family of multiple C2 domain and transmembrane region proteins (MCTPs) in Arabidopsis. QUIRKY (QKY, MCTP14) a membrane-anchored protein belongs to MCTPs family contains four C2 domains. QYK is localized to plasmodesmata and play an important role in tissue morphogenesis (Liu et al., 2017).

After the confirmation of EHB1 interacting domain, we were interested to identify the specific part of IRT1vr that is interacting with EHB1. As described in the results, it is predicted that IRT1vr contains three helices and two disordered regions (DR1 and DR2). Two of these three helices are bordering the transmembrane domains (III and IV) and the predicted metal-binding histidine motif is located in DR2 (Fig. 4.2 A.) (Ivanov and Bauer, 2017). We fragmented the whole cytosolic variable region of IRT1 into different pieces and subjected these deletion fragments to BiFC against EHB1 (Fig. 4.2.). All the deletion fragments (IRT1vrΔ1, IRT1vrΔ2, and IRT1vrΔHis) interacted with EHB1, except the fragment (IRT1vrΔ3). The deletion fragment IRT1vrΔ3 was lacking the helical regions that precede the membrane-spanning transmembrane domains III and IV, suggesting that, these helical regions are important for protein-protein interactions in the post-translational regulation of IRT1 (Fig. 4.3. G.). Our data provide the first direct evidence that the predicted helices in the variable region are involved in protein-protein interaction. In all the previous studies for the identification of IRT1 interacting proteins, the full-length whole variable region was tested. The presence of EHB1 close to the TM-III and TM-IV could affect the transport activity of IRT1 because the structural analysis of the ZIP family of transporter suggests that there are certain conserved amino acids and metals binding binuclear centres in close proximity of TM-III and TM-IV which are considered extremely important for the transport activity of IRT1 (Eng et al., 1998b; Rogers et al., 2000; Zhang et al., 2017). Due to the presence of EHB1, these sites may become hidden and dysfunctional.

For the interaction, IRT1 and EHB1 in Y2H and BiFC analysis, only variable region of IRT1 were tested. In the native situation (inside the cell) EHB1 should be able to interact with the full-length IRT1 protein. To address this question, we tested the interaction between EHB1 and IRT1 in Co-IP analysis.

The first attempt of the Co-IP was successful, both proteins HA-EHB1 and IRT1-GFP were expressed but the band for HA-EHB1 in the IP fraction was very weak (Fig. 4.4. A. IV.). After reviewing the published literature, Co-IP was performed in the presence of 100 µM calcium (Ca^{2+}). The Co-IP was successful, EHB1 was co-precipitate with IRT1 and the presence of 100 µM Ca^{2+} enhanced the co-precipitated EHB1 (Fig. 4.4 B. IV.). Calcium might cause structural rearrangement in EHB1 and stabilizes the protein at the membrane due to which EHB1-IRT1 interaction might become more stable. The Ca^{2+}-dependent lipid-binding protein (*AtCLB*) which negatively regulates the responses to abiotic stress in *Arabidopsis thaliana* binds phospholipids via C2 domain in a calcium-dependent manner (de Silva et al., 2011). This is consistent with the analysis of other members of the CAR family (CAR1 and CAR4) that they bind membrane phospholipids in a calcium-dependent manner in *in vitro* situation (Rodriguez et al., 2014; Diaz et al., 2016). Using lipid co-sedimentation assay and electron microscopy (EM) it has been shown that CAR4 can bind membrane phospholipids, and furthermore, that increase in calcium concentration leads to membrane insertion of the oligomerized CAR4 causing curvatures in the membrane (Diaz et al., 2016). With cell fractionation, we showed that EHB1 could exist as both soluble and membrane-associated. We could show that calcium enhances the association of EHB1 with membranes, which is pointing towards the importance of calcium for EHB1 membrane–binding (Fig. 4.7.). The stimulus-driven (wounding) relocalization from the cytoplasm to the plasma membrane of rice CAR family protein OsGAP1 has been shown (Cheung et al., 2010). EHB1 has been found associated with detergent-resistant Arabidopsis membranes in the preparations of leaf plasma membrane by using mass spectrometry (Demir et al., 2013). Furthermore, we showed the presence of EHB1 in the nucleus, the cytoplasm and colocalization with membrane proteins (Fig. 4.5. and supplemental Fig. S3. A-C). Such a subcellular localization is consistent with its effect on the IRT1 transporter and resembles the reported localization of other CAR-family proteins, using fluorescently labeled protein colocalization and biochemical fractionation dual localization of CAR1, CAR4, and CAR5 has been shown (Rodriguez et al., 2014). Dual localization at the plasma membrane and nucleus is reported for other small C2-domain proteins of plants (Wang et al., 2009).

In our study of special interest was the discovery that EHB1 showed a specific affinity for phosphoinositides, such as phosphatidylinositol (PI) and phosphatidylinositol 4 phosphate (PI(4)P). EHB1 was able to preferentially bind both these phospholipids both membrane-immobilized (membrane strips, Fig. 4.8 B.) and membrane form (liposomes, Fig. 4.9 C.). Phosphoinositides are low abundant lipids which represent only 1-2% of total phospholipids in living cells. PI(4)P is highly anionic and accumulates massively at the plant plasma membrane and contributes to generate electrostatic field at the plasma membrane (Simon et al., 2016; Platre and Jaillais, 2017). The surface charge generated at the plant plasma membrane due to the presence of PI(4)P plays a critical role in the plasma membrane localization of the regulatory proteins PINOID and BRI1 KINASE INHIBITOR1 (Simon et al., 2016). We showed that calcium is critically important for EHB1 association with the membrane. In the absence of calcium, EHB1 was mostly present in the cytosolic fraction while in the presence of calcium a significant amount of EHB1 was present in microsomal fraction as well (Fig. 4.7 A.). This phenomenon cannot be explained in the situation when EHB1 binds phosphoinositides *in vitro* (Fig. 4.9 C.). The dependence on calcium by EHB1 in binding to PI and PI(4)P that were observed in liposomes binding experiment was comparable and was not like the complete on-off situation which was seen in the fractionation experiment (Fig. 4.7 A.). This suggests that it could be that EHB1 targets additional membrane phospholipids.

We also tested the C2 domain mutant EHB1-4X for *in vitro* lipid binding. The mutation of four conserved aspartic acids in the CBLs did not abolish the ability of EHB1-4X to bind to PI and PI(4)P (Fig. 4.10 A.). This suggests that in addition to C2 domain there could be other sites in EHB1 which can be essential for phospholipid binding. Indeed it has been reported that members of CAR-family proteins in addition to calcium-dependent C2 domain, contains a positively charged lysine-rich polybasic lipid binding site which can bind to lipids independently and contribute to CARs stabilization on the membrane (Diaz et al., 2016). It has been reported for other C2-domain-containing proteins as well that they contain a lysine-rich polybasic cluster which can bind $PI(4,5)P_2$ both in the presence and absence of calcium (Guerrero-Valero et al., 2009; Groffen et al., 2010; Honigmann et al., 2013). The cationic lysine residues interact directly with the phosphate of inositol ring (Corbalan-Garcia and

Gómez-Fernández, 2014). Members of the CAR-family proteins are quite diverse in phospholipid binding, it has been shown for CAR1 and CAR4 that they bind phosphatidylcholine and phosphatidylserine (Rodriguez et al., 2014).

We report the involvement of calcium in the interaction between EHB1 and IRT1 which suggests a possible role of calcium bursts in the regulation of iron uptake. The role of calcium in the acquisition of iron by plants has not yet been clear but it has been reported that cytoplasmic concentration of calcium increases in response to iron-deficiency in roots (Tian et al., 2016). However, calcium signature is produced in response to different stresses which may vary in intensity and duration (Whalley and Knight, 2013; Steinhorst and Kudla, 2014). It has been shown that CARs are calcium sensors having basal phospholipid binding activity (Diaz et al., 2016), Therefore, specific short-term pulses of calcium waves might trigger the association of EHB1 with membrane and EHB1-IRT1 interaction sequentially. It is possible that EHB1 switch-off the iron uptake under certain specific conditions. Particularly, once the plant has acquired sufficient amounts iron, the iron uptake machinery needs to be switch-off to avoid excessive accumulation of iron. This is consistent with our data, we could show that the expression of *EHB1* enhances under iron-sufficient condition (Fig. 4.13 A.).

The physiological data that we conducted in this study are in agreement with the hypothesis that EHB1 is a negative regulator of the iron-uptake machinery of Arabidopsis. We could show that in the absence of EHB1 the iron reductase activity of FRO2 was strongly induced at –Fe as compared to WT, on the contrary, FRO2 activity was reduced under the same conditions in comparison to WT and *ehb1* alleles (Fig. 4.6 A.). The expression of the principal root-surface ferric reductase *FRO2* is upregulated upon iron-deficiency and its activity indirectly indicate the efficiency of iron uptake system mediated by IRT1 (Robinson et al., 1999; Colangelo and Guerinot, 2004), also the expression of *FRO2* and *IRT1* are coordinately controlled (Connolly et al., 2003). This step has been proposed as the rate-limiting step in iron acquisition by Strategy I plants (Robinson et al., 1999). It could also be possible that FRO2 and IRT1 proteins form a complex for the enhancement of iron import by IRT1. The possibility that EHB1 might directly affect the activity or the regulation of FRO2 cannot be ruled out. Our data is in agreement with this notion, as *FRO2* expression was strongly upregulated in the absence of EHB1 at –Fe condition

as compared to WT and HA-EHB1 plant lines (Fig. 4.13 C.). This effect was consistent with the measured ferric reductase activity in these plants (Fig. 4.11 C.).

We also investigated if the absence of EHB1 can have an effect on the chlorophyll content of young developing leaves. Our data showed that in sufficient Fe condition the chlorophyll content of young developing leaves was significantly higher in EHB1 mutant plants (*ehb1-1*) as compared to HA-EHB1 (Fig. 4.11 D.). Chlorophyll content of leaf is an important parameter which indicates the development of leaf chloroplast, the photosynthetic ability and general health of the plant (Ling et al., 2011). Plants respond to iron-deficiency by a marked decrease in photosynthetic activity due to compromise chlorophyll synthesis which leads to interveinal chlorosis in developing young leaves (Rodríguez-Celma et al., 2013b).

We also showed that the presence of EHB1 suppresses iron assimilation. We performed Perls-DAB staining for the visualization of apoplastic iron. The roots of *ehb1* mutant plants showed strongly decreased staining as compared to WT (Fig. 4.12 A-I.). On the other hand, HA-EHB1 showed enhanced staining in the early differentiation zone in comparison with WT (Fig. 4.12 J-L.) suggesting that the roots of *ehb1* loss-of-function plants were able to take up more iron from the apoplast than the roots of HA-EHB1 and WT. Modulation of IRT1 activity has been shown to affect the uptake of iron from apoplast (Ivanov et al., 2014). The iron content measurement reveals that the seeds of *ehb1* possess more iron as compared to HA-EHB1. Seeds are an important sink and the end point of the long-distance transported nutrients (Grillet et al., 2014). It has been reported that seed iron concentration is a useful indicator which helps in identifying the genotypes which possess high resistance to iron deficiency (Wiersma, 2012), And high seed iron content in wheat can improve resistance to chlorosis (Shen et al., 2002). Our results from the Perls-DAB staining and iron content measurement are consistent with iron reductase activity assay and gene expression analysis, which showed that in the absence of EHB1 the iron acquisition system is more active. This further ensures the role of EHB1 as a negative regulator of iron uptake system. The significantly decreased Zn content in HA-EHB1 (Fig. 4.12 Q.) could be explained if in addition to its negative affect on the transport activity of IRT1, EHB1 might also negatively affect the activity of other zinc transporters of the ZIP transporter family. However, this observation requires further investigation. We also observed a significant increase in seed Mn content of the

HA-EHB1 seeds in comparison to WT and *ehb1-1* seeds (Fig. 4.12 R.). The high Mn content in the seeds of HA-EHB1 can be explained by the fact that in addition to IRT1, metal transporters of the NRAMP family are involved in the uptake of Mn in Arabidopsis (Pittman, 2005; Sasaki et al., 2012). Hence, the high Mn content in HA-EHB1 could be due to the additive effect of the NRAMPs transporters (Fig. 4.12 R.).

Furthermore, to verify the direct connection between the negative effect of EHB1 on the iron acquisition and the function of IRT1, Dr. Rumen Ivanov in our group performed a yeast complementation assay. To this end, the *fet3fet4* mutant yeast strain was used as a model (Eide et al., 1996), This strain is incapable of iron import due to the lack of functional multicopper oxidase FET3 and a bivalent iron transporter FET4. It has been observed that IRT1 successfully complemented the iron import defective yeast strain *fet3fet4*. The addition of HA-EHB1 to the system reverted almost entirely this IRT1-mediated complementation. For control, wild-type yeast showed that EHB1 did not have any effect on its iron acquisition meaning that the EHB1 effect was direct and specific for inhibiting IRT1 activity. These results suggest that EHB1 is directly and negatively effecting IRT1-mediated iron import (Ivanov et al., unpublished).

Thus far, it is not so clear that how EHB1 inhibit the activity of IRT1. There could be two possibilities to explain this. The first possibility is based on the interaction site of IRT1, which involves the two helices in close proximity to the transmembrane domains (TM) III and IV in IRT1vr. A predicted aspartic acid (D136) lies at the end of TM-III is reported to be essential for iron import, mutation of this residue resulted in the elimination of iron and manganese transport by IRT1 (Rogers et al., 2000). In addition, there is conserved histidine (H197) and serine (S198) in TM-IV which binds metals and are necessary for the function of the transporter (Eng et al., 1998a; Rogers et al., 2000). Furthermore, structural analysis of *BbZIP* showed that it contains conserved substrate binding binuclear metal centers (M1 and M2) and metals chelating amino acid residues (^{177}HN*h*PEG^{182}) at TM-IV. A conserved glutamic acid (E181) on TM-IV functions to bridge M1 and M2. Additionally, the two conserved aspartic acids (D113 and D305) at the entrance cavity is crucial for metals recruitment and an absolutely invariant serine (S106) present at the bottom of the entrance cavity function in guiding metals during its import (Zhang et al., 2017).

These sites may become hidden and dysfunctional due to the presence of EHB1 in the proximity. Furthermore, EHB1 binding can force a conformational change in their orientation and make them incapable of transferring iron across the plasma membrane (Fig. 5.1 A.). A second possibility for the EHB1 to inhibit the activity of IRT1 is based on the finding that CAR4 can bend the membranes, it is shown that CAR4 causes tubulation in liposome membrane in a calcium-dependent manner *in vitro* (Diaz et al., 2016). Thus, it was proposed that it would initiate membrane curvatures in response to a stress-induced calcium signature, which would serve as a platform for signaling proteins to control ABA-mediated stress response (Diaz et al., 2016). In our case, EHB1 can cause membrane tubulation in a calcium-dependent manner thus promoting the endocytosis of IRT1. This will cause a reduction in the plasma membrane-localized IRT1 which ultimately will reduce the amount of available IRT1 protein for importing iron. The physiological data which we presented in this study is in agreement with this mechanism.

To summarize, we show that the peripheral membrane protein EHB1 can interact with the primary iron transporter IRT1. EHB1 is recruited to the plasma membrane (might be in a calcium-dependent manner) to inhibit the overaccumulation of iron in the cell. The presence of calcium promotes the interaction between EHB1 and IRT1 resulting in the inhibition of IRT1 activity by enhancing its degradation (Fig. 5.1 B.).

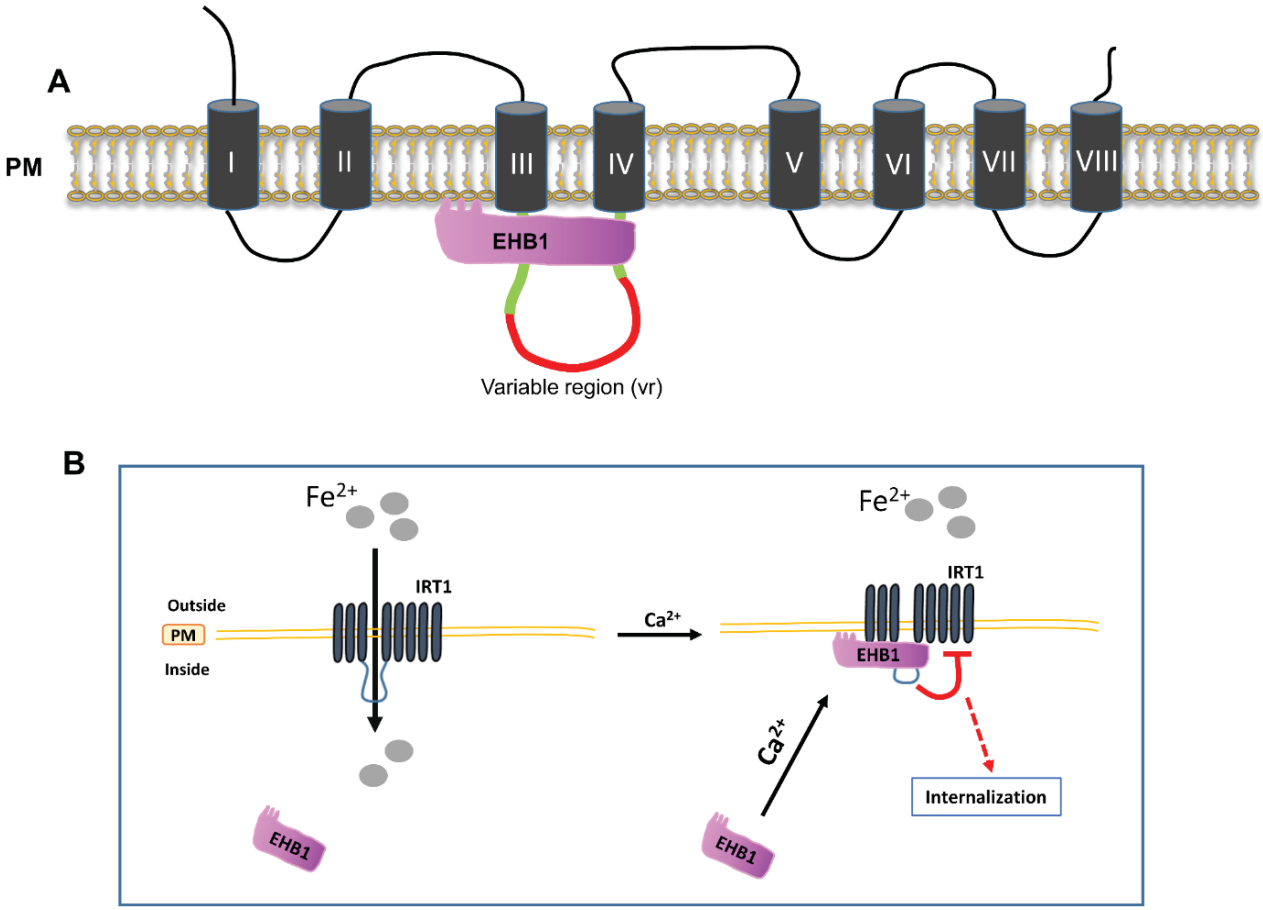

Figure 5.1. Model: Possibilities of how EHB1 might affect IRT1-mediated iron import.
(A) Schematic representation of EHB1 binding with IRT1, the two helices in IRT1vr which interacts with EHB1 are bordering the TM-III and IV and are shown in green, red color represents the rest of the VR. EHB1 is also shown as a cartoon, EHB1 bind to the plasma membrane via its C2 domain and interacts with IRT1vr through its signature domain. TM-III and IV which harbors conserved amino acids and metals binding centers important for metal import, due to the presence of EHB1 in close proximity these sites may become hidden and dysfunctional.
(B) IRT1 import iron from the rhizosphere to the inside of the root epidermal cells. Calcium signature might promote EHB1 binding with plasma membrane and IRT1. This interaction might cause membrane tubulation containing IRT1, which after internalization can lead to IRT1 degradation. And in this way, EHB1 might inhibit the activity of IRT1. PM: plasma membrane, TMs: transmembrane domains.

References

Abbaspour, N., Hurrell, R., and Kelishadi, R. (2014). Review on iron and its importance for human health. Journal of Research in Medical Sciences **19**.

Abdallah, H.B., and Bauer, P. (2016). Quantitative reverse transcription-qPCR-based gene expression analysis in plants. Plant Signal Transduction: Methods and Protocols**,** 9-24.

Aksoy, E., Jeong, I.S., and Koiwa, H. (2013). Loss of function of Arabidopsis C-terminal domain phosphatase-like1 activates iron deficiency responses at the transcriptional level. Plant physiology **161,** 330-345.

Alexandersson, E., Gustavsson, N., Bernfur, K., Karlsson, A., Kjellbom, P., and Larsson, C. (2008). Purification and proteomic analysis of plant plasma membranes. Organelle Proteomics**,** 161-173.

Ananthanarayanan, B., Das, S., Rhee, S.G., Murray, D., and Cho, W. (2002). Membrane targeting of C2 domains of phospholipase C-δ isoforms. Journal of Biological Chemistry **277,** 3568-3575.

Antala, S., Ovchinnikov, S., Kamisetty, H., Baker, D., and Dempski, R.E. (2015). Computation and functional studies provide a model for the structure of the zinc transporter hZIP4. Journal of Biological Chemistry **290,** 17796-17805.

Bai, J., Tucker, W.C., and Chapman, E.R. (2004). PIP2 increases the speed of response of synaptotagmin and steers its membrane-penetration activity toward the plasma membrane. Nature structural & molecular biology **11,** 36-44.

Barberon, M., Dubeaux, G., Kolb, C., Isono, E., Zelazny, E., and Vert, G. (2014). Polarization of IRON-REGULATED TRANSPORTER 1 (IRT1) to the plant-soil interface plays crucial role in metal homeostasis. Proceedings of the National Academy of Sciences **111,** 8293-8298.

Barberon, M., Zelazny, E., Robert, S., Conéjéro, G., Curie, C., Friml, J., and Vert, G. (2011). Monoubiquitin-dependent endocytosis of the iron-regulated transporter 1 (IRT1) transporter controls iron uptake in plants. Proceedings of the National Academy of Sciences **108,** E450-E458.

Bashir, K., Inoue, H., Nagasaka, S., Takahashi, M., Nakanishi, H., Mori, S., and Nishizawa, N.K. (2006). Cloning and characterization of deoxymugineic acid synthase genes from graminaceous plants. Journal of Biological Chemistry **281,** 32395-32402.

Bauer, P., and Blondet, E. (2011). Transcriptome analysis of ein3 eil1 mutants in response to iron deficiency. Plant signaling & behavior **6,** 1669-1671.

Behnia, R., and Munro, S. (2005). Organelle identity and the signposts for membrane traffic. Nature **438,** 597-604.

Benoist, B.d., McLean, E., Egll, I., and Cogswell, M. (2008). Worldwide prevalence of anaemia 1993-2005: WHO global database on anaemia. Worldwide prevalence of anaemia 1993-2005: WHO global database on anaemia.

Bittova, L., Sumandea, M., and Cho, W. (1999). A Structure-Function Study of the C2 Domain of Cytosolic Phospholipase A2 IDENTIFICATION OF ESSENTIAL CALCIUM LIGANDS AND HYDROPHOBIC MEMBRANE BINDING RESIDUES. Journal of Biological Chemistry **274,** 9665-9672.

Blum, A., Brumbarova, T., Bauer, P., and Ivanov, R. (2014). Hormone influence on the spatial regulation of IRT1 expression in iron-deficient Arabidopsis thaliana roots. Plant signaling & behavior **9,** e28787.

Bolte, S., and Cordelieres, F. (2006). A guided tour into subcellular colocalization analysis in light microscopy. Journal of microscopy **224,** 213-232.

Bonifacino, J.S., and Weissman, A.M. (1998). Ubiquitin and the control of protein fate in the secretory and endocytic pathways. Annual review of cell and developmental biology **14,** 19-57.

Borrill, P., Connorton, J.M., Balk, J., Miller, A.J., Sanders, D., and Uauy, C. (2014). Biofortification of wheat grain with iron and zinc: integrating novel genomic resources and knowledge from model crops. From soil to seed: micronutrient movement into and within the plant**,** 98.

Brewer, G.J. (2009). Risks of copper and iron toxicity during aging in humans. Chemical research in toxicology **23,** 319-326.

Briat, J.-F., Cellier, F., and Gaymard, F. (2006). Ferritins and iron accumulation in plant tissues. Iron Nutrition in Plants and Rhizospheric Microorganisms**,** 341-357.

Briat, J.-F., Curie, C., and Gaymard, F. (2007). Iron utilization and metabolism in plants. Current opinion in plant biology **10,** 276-282.

Briat, J.-F., Fobis-Loisy, I., Grignon, N., Lobréaux, S., Pascal, N., Savino, G., Thoiron, S., von Wirén, N., and Van Wuytswinkel, O. (1995). Cellular and molecular aspects of iron metabolism in plants. Biology of the Cell **84,** 69-81.

Briat, J., Cellier, F., and Gaymard, F. (2005). Ferritins and Iron Accumulation in Plant Tissues (Kluwer Academic Publishers).

Brose, N., and Rosenmund, C. (2002). Move over protein kinase C, you've got company: alternative cellular effectors of diacylglycerol and phorbol esters. Journal of cell science **115,** 4399-4411.

Brown, H.A., Gutowski, S., Moomaw, C.R., Slaughter, C., and Sternwels, P.C. (1993). ADP-ribosylation factor, a small GTP-dependent regulatory protein, stimulates phospholipase D activity. Cell **75,** 1137-1144.

Brumbarova, T., and Bauer, P. (2005). Iron-mediated control of the basic helix-loop-helix protein FER, a regulator of iron uptake in tomato. Plant Physiology **137,** 1018-1026.

Brumbarova, T., Bauer, P., and Ivanov, R. (2015). Molecular mechanisms governing Arabidopsis iron uptake. Trends in plant science **20,** 124-133.

Buckhout, T.J., Yang, T.J., and Schmidt, W. (2009). Early iron-deficiency-induced transcriptional changes in Arabidopsis roots as revealed by microarray analyses. BMC genomics **10,** 147.

Caesar, K., Elgass, K., Chen, Z., Huppenberger, P., Witthöft, J., Schleifenbaum, F., Blatt, M.R., Oecking, C., and Harter, K. (2011). A fast brassinolide-regulated response pathway in the plasma membrane of Arabidopsis thaliana. The Plant Journal **66,** 528-540.

Castaings, L., Caquot, A., Loubet, S., and Curie, C. (2016). The high-affinity metal Transporters NRAMP1 and IRT1 Team up to Take up Iron under Sufficient Metal Provision. Scientific reports **6,** 37222.

Chadick, J.Z., and Asturias, F.J. (2005). Structure of eukaryotic Mediator complexes. Trends in biochemical sciences **30,** 264-271.

Chalfant, C.E., Ogretmen, B., Galadari, S., Kroesen, B.-J., Pettus, B.J., and Hannun, Y.A. (2001). FAS activation induces dephosphorylation of SR proteins dependence on the de novo generation of ceramide and activation of protein phosphatase 1. Journal of Biological Chemistry **276,** 44848-44855.

Chapman, E.R., and Jahn, R. (1994). Calcium-dependent interaction of the cytoplasmic region of synaptotagmin with membranes. Autonomous function of a single C2-homologous domain. Journal of Biological Chemistry **269,** 5735-5741.

Chen, W.W., Yang, J.L., Qin, C., Jin, C.W., Mo, J.H., Ye, T., and Zheng, S.J. (2010). Nitric oxide acts downstream of auxin to trigger root ferric-chelate reductase activity in response to iron deficiency in Arabidopsis. Plant Physiology **154,** 810-819.

Cheung, M.-Y., Xue, Y., Zhou, L., Li, M.-W., Sun, S.S.-M., and Lam, H.-M. (2010). An ancient P-loop GTPase in rice is regulated by a higher plant-specific regulatory protein. Journal of Biological Chemistry **285,** 37359-37369.

Cho, W. (2001). Membrane targeting by C1 and C2 domains. Journal of Biological Chemistry **276,** 32407-32410.

Cho, W., and Stahelin, R.V. (2005). Membrane-protein interactions in cell signaling and membrane trafficking. Annu. Rev. Biophys. Biomol. Struct. **34,** 119-151.

Cho, W., and Stahelin, R.V. (2006). Membrane binding and subcellular targeting of C2 domains. Biochimica et Biophysica Acta (BBA)-Molecular and Cell Biology of Lipids **1761,** 838-849.

Cho, W., Bittova, L., and Stahelin, R.V. (2001). Membrane binding assays for peripheral proteins. Analytical biochemistry **296,** 153-161.

Clark, J.D., Lin, L.-L., Kriz, R.W., Ramesha, C.S., Sultzman, L.A., Lin, A.Y., Milona, N., and Knopf, J.L. (1991). A novel arachidonic acid-selective cytosolic PLA2 contains a Ca2+-dependent translocation domain with homology to PKC and GAP. Cell **65,** 1043-1051.

Cohen, C.K., Fox, T.C., Garvin, D.F., and Kochian, L.V. (1998). The role of iron-deficiency stress responses in stimulating heavy-metal transport in plants. Plant Physiology **116,** 1063-1072.

Colangelo, E.P., and Guerinot, M.L. (2004). The essential basic helix-loop-helix protein FIT1 is required for the iron deficiency response. The Plant Cell **16,** 3400-3412.

Connolly, E.L., and Guerinot, M.L. (1998). Reduction and uptake of iron in plants. In Plasma Membrane Redox Systems and their Role in Biological Stress and Disease (Springer), pp. 179-192.

Connolly, E.L., and Guerinot, M.L. (2002). Iron stress in plants. Genome biology **3,** reviews1024. 1021.

Connolly, E.L., Fett, J.P., and Guerinot, M.L. (2002). Expression of the IRT1 metal transporter is controlled by metals at the levels of transcript and protein accumulation. The Plant Cell **14,** 1347-1357.

Connolly, E.L., Campbell, N.H., Grotz, N., Prichard, C.L., and Guerinot, M.L. (2003). Overexpression of the FRO2 ferric chelate reductase confers tolerance to growth on low iron and uncovers posttranscriptional control. Plant Physiology **133,** 1102-1110.

Conte, S.S., and Walker, E.L. (2011). Transporters contributing to iron trafficking in plants. Molecular Plant **4,** 464-476.

Cooper, B., Clarke, J.D., Budworth, P., Kreps, J., Hutchison, D., Park, S., Guimil, S., Dunn, M., Luginbühl, P., and Ellero, C. (2003). A network of rice genes associated with stress response and seed development. Proceedings of the National Academy of Sciences **100,** 4945-4950.

Corbalan-Garcia, S., and Gómez-Fernández, J.C. (2014). Signaling through C2 domains: more than one lipid target. Biochimica Et Biophysica Acta (BBA)-Biomembranes **1838,** 1536-1547.

Corbalán-García, S., García-García, J., Rodríguez-Alfaro, J.A., and Gómez-Fernández, J.C. (2003). A new phosphatidylinositol 4, 5-bisphosphate-binding site located in the C2 domain of protein kinase Cα. Journal of Biological Chemistry **278,** 4972-4980.

Curie, C., Panaviene, Z., Loulergue, C., Dellaporta, S.L., Briat, J.-F., and Walker, E.L. (2001). Maize yellow stripe1 encodes a membrane protein directly involved in Fe (III) uptake. Nature **409,** 346-349.

Curie, C., Cassin, G., Couch, D., Divol, F., Higuchi, K., Le Jean, M., Misson, J., Schikora, A., Czernic, P., and Mari, S. (2009). Metal movement within the plant: contribution of nicotianamine and yellow stripe 1-like transporters. Annals of botany **103,** 1-11.

Dakora, F.D., and Phillips, D.A. (2002). Root exudates as mediators of mineral acquisition in low-nutrient environments. Plant and soil **245,** 35-47.

Das, S., Dixon, J.E., and Cho, W. (2003). Membrane-binding and activation mechanism of PTEN. Proceedings of the National Academy of Sciences **100,** 7491-7496.

Davletov, B.A., and Südhof, T. (1993). A single C2 domain from synaptotagmin I is sufficient for high affinity Ca2+/phospholipid binding. Journal of Biological Chemistry **268,** 26386-26390.

De Onis, M., Brown, D., Blossner, M., and Borghi, E. (2012). Levels and trends in child malnutrition. UNICEF-WHO-The World Bank joint child malnutrition estimates.

de Silva, K., Laska, B., Brown, C., Sederoff, H.W., and Khodakovskaya, M. (2011). Arabidopsis thaliana calcium-dependent lipid-binding protein (AtCLB): a novel repressor of abiotic stress response. Journal of experimental botany **62,** 2679-2689.

Demir, F., Horntrich, C., Blachutzik, J.O., Scherzer, S., Reinders, Y., Kierszniowska, S., Schulze, W.X., Harms, G.S., Hedrich, R., and Geiger, D. (2013). Arabidopsis nanodomain-delimited ABA

signaling pathway regulates the anion channel SLAH3. Proceedings of the National Academy of Sciences **110,** 8296-8301.

Diaz, M., Sanchez-Barrena, M.J., Gonzalez-Rubio, J.M., Rodriguez, L., Fernandez, D., Antoni, R., Yunta, C., Belda-Palazon, B., Gonzalez-Guzman, M., and Peirats-Llobet, M. (2016). Calcium-dependent oligomerization of CAR proteins at cell membrane modulates ABA signaling. Proceedings of the National Academy of Sciences **113,** E396-E405.

Dümmer, M., Michalski, C., Essen, L.-O., Rath, M., Galland, P., and Forreiter, C. (2016). EHB1 and AGD12, two calcium-dependent proteins affect gravitropism antagonistically in Arabidopsis thaliana. Journal of plant physiology **206,** 114-124.

Dunn, K.W., Kamocka, M.M., and McDonald, J.H. (2011). A practical guide to evaluating colocalization in biological microscopy. American Journal of Physiology-Cell Physiology **300,** C723-C742.

Durrett, T.P., Gassmann, W., and Rogers, E.E. (2007). The FRD3-mediated efflux of citrate into the root vasculature is necessary for efficient iron translocation. Plant physiology **144,** 197-205.

Eckhardt, U., Mas Marques, A., and Buckhout, T.J. (2001). Two iron-regulated cation transporters from tomato complement metal uptake-deficient yeast mutants. Plant molecular biology **45,** 437-448.

Edwards, A.S., and Newton, A.C. (1997). Regulation of protein kinase C βII by its C2 domain. Biochemistry **36,** 15615-15623.

Eide, D., Broderius, M., Fett, J., and Guerinot, M.L. (1996). A novel iron-regulated metal transporter from plants identified by functional expression in yeast. Proceedings of the National Academy of Sciences **93,** 5624-5628.

Eide, D.J. (2006). Zinc transporters and the cellular trafficking of zinc. Biochimica et Biophysica Acta (BBA)-Molecular Cell Research **1763,** 711-722.

Eng, B., Guerinot, M., Eide, D., and Saier, M. (1998a). Sequence analyses and phylogenetic characterization of the ZIP family of metal ion transport proteins. The Journal of membrane biology **166,** 1-7.

Eng, B., Guerinot, M., Eide, D., and Saier, J., MH. (1998b). Sequence analyses and phylogenetic characterization of the ZIP family of metal ion transport proteins. Journal of Membrane Biology **166,** 1-7.

Essen, L.-O., Perisic, O., Lynch, D.E., Katan, M., and Williams, R.L. (1997). A Ternary Metal Binding Site in the C2 Domain of Phosphoinositide-Specific Phospholipase C-δ1†. Biochemistry **36,** 2753-2762.

Fan, H., Zhang, Z., Wang, N., Cui, Y., Sun, H., Liu, Y., Wu, H., Zheng, S., Bao, S., and Ling, H.Q. (2014). SKB1/PRMT5-mediated histone H4R3 dimethylation of Ib subgroup bHLH genes negatively regulates iron homeostasis in Arabidopsis thaliana. The Plant Journal **77,** 209-221.

FAO, I. WFP (2015), The State of Food Insecurity in the World 2015. Meeting the 2015 international hunger targets: taking stock of uneven progress. Food and Agriculture Organization Publications, Rome.

Ferguson, K.M., Kavran, J.M., Sankaran, V.G., Fournier, E., Isakoff, S.J., Skolnik, E.Y., and Lemmon, M.A. (2000). Structural basis for discrimination of 3-phosphoinositides by pleckstrin homology domains. Molecular cell **6,** 373-384.

Ferreira, F., Jolliffe, D., and Prydz, E. (2015). The International Poverty Line Has Just Been Raised to $1.90 a Day, but Global Poverty Is Basically Unchanged. How Is That Even Possible? Let's Talk Development.

Ford, M.G., Mills, I.G., Peter, B.J., Vallis, Y., Praefcke, G.J., Evans, P.R., and McMahon, H.T. (2002). Curvature of clathrin-coated pits driven by epsin. Nature **419,** 361-366.

Fourcroy, P., Sisó-Terraza, P., Sudre, D., Savirón, M., Reyt, G., Gaymard, F., Abadía, A., Abadia, J., Álvarez-Fernández, A., and Briat, J.F. (2014). Involvement of the ABCG37 transporter in secretion of scopoletin and derivatives by Arabidopsis roots in response to iron deficiency. New Phytologist **201,** 155-167.

Fujiki, Y., HUBBARD, A., Fowler, S., and Lazarow, P.B. (1982). Isolation of Intracellular Membranes by Means of Sodium Carbonate Treatment: Application to Endoplasm is Reticu I um. The Journal of cell biology **93,** 97-102.

Gaither, L.A., and Eide, D.J. (2001). The human ZIP1 transporter mediates zinc uptake in human K562 erythroleukemia cells. Journal of Biological Chemistry **276,** 22258-22264.

García, M.J., Lucena, C., Romera, F.J., Alcántara, E., and Pérez-Vicente, R. (2010). Ethylene and nitric oxide involvement in the up-regulation of key genes related to iron acquisition and homeostasis in Arabidopsis. Journal of Experimental Botany**,** erq203.

García, M.J., Suárez, V., Romera, F.J., Alcántara, E., and Pérez-Vicente, R. (2011). A new model involving ethylene, nitric oxide and Fe to explain the regulation of Fe-acquisition genes in Strategy I plants. Plant Physiology and Biochemistry **49,** 537-544.

Giavalisco, P., Kapitza, K., Kolasa, A., Buhtz, A., and Kehr, J. (2006). Towards the proteome of Brassica napus phloem sap. Proteomics **6,** 896-909.

Gómez-Galera, S., Sudhakar, D., Pelacho, A.M., Capell, T., and Christou, P. (2012). Constitutive expression of a barley Fe phytosiderophore transporter increases alkaline soil tolerance and results in iron partitioning between vegetative and storage tissues under stress. Plant Physiology and Biochemistry **53,** 46-53.

Gómez-Galera, S., Rojas, E., Sudhakar, D., Zhu, C., Pelacho, A.M., Capell, T., and Christou, P. (2010). Critical evaluation of strategies for mineral fortification of staple food crops. Transgenic research **19,** 165-180.

Goñi, F.M. (2002). Non-permanent proteins in membranes: when proteins come as visitors (Review). Molecular membrane biology **19,** 237-245.

Graziano, M., and Lamattina, L. (2007). Nitric oxide accumulation is required for molecular and physiological responses to iron deficiency in tomato roots. The Plant Journal **52,** 949-960.

Greco, M., Chiappetta, A., Bruno, L., and Bitonti, M.B. (2012). In Posidonia oceanica cadmium induces changes in DNA methylation and chromatin patterning. Journal of experimental botany **63,** 695-709.

Green, L.S., and Rogers, E.E. (2004). FRD3 controls iron localization in Arabidopsis. Plant Physiology **136,** 2523-2531.

Grefen, C., and Blatt, M.R. (2012). Method summary. Biotechniques **53,** 311-314.

Grillet, L., Ouerdane, L., Flis, P., Hoang, M.T.T., Isaure, M.-P., Lobinski, R., Curie, C., and Mari, S. (2014). Ascorbate efflux as a new strategy for iron reduction and transport in plants. Journal of Biological Chemistry **289,** 2515-2525.

Groffen, A.J., Martens, S., Arazola, R.D., Cornelisse, L.N., Lozovaya, N., de Jong, A.P., Goriounova, N.A., Habets, R.L., Takai, Y., and Borst, J.G. (2010). Doc2b is a high-affinity Ca2+ sensor for spontaneous neurotransmitter release. Science **327,** 1614-1618.

Gropper, S.S., and Smith, J.L. (2012). Advanced nutrition and human metabolism. (Cengage Learning).

Gruber, B., and Kosegarten, H. (2002). Depressed growth of nonchlorotic vine grown in calcareous soil is an iron deficiency symptom prior to leaf chlorosis. Journal of Plant Nutrition and Soil Science **165,** 111.

Grusak, M.A. (1994). Iron transport to developing ovules of Pisum sativum (I. Seed import characteristics and phloem iron-loading capacity of source regions). Plant Physiology **104,** 649-655.

Guerinot, M.L. (2000). The ZIP family of metal transporters. Biochimica et Biophysica Acta (BBA)-Biomembranes **1465,** 190-198.

Guerrero-Valero, M., Ferrer-Orta, C., Querol-Audí, J., Marin-Vicente, C., Fita, I., Gómez-Fernández, J.C., Verdaguer, N., and Corbalán-García, S. (2009). Structural and mechanistic insights into the association of PKCα-C2 domain to PtdIns (4, 5) P2. Proceedings of the National Academy of Sciences **106,** 6603-6607.

Hall, B.P., and Guerinot, M.L. (2006). The role of ZIP family members in iron transport. In Iron Nutrition in Plants and Rhizospheric Microorganisms (Springer), pp. 311-326.

Heard, W., Sklenář, J., Tomé, D.F., Robatzek, S., and Jones, A.M. (2015). Identification of regulatory and cargo proteins of endosomal and secretory pathways in Arabidopsis thaliana by proteomic dissection. Molecular & Cellular Proteomics **14,** 1796-1813.

Henriques, R., Jásik, J., Klein, M., Martinoia, E., Feller, U., Schell, J., Pais, M.S., and Koncz, C. (2002). Knock-out of Arabidopsis metal transporter gene IRT1 results in iron deficiency accompanied by cell differentiation defects. Plant molecular biology **50,** 587-597.

Heucken, N., and Ivanov, R. (2018). The retromer, sorting nexins and the plant endomembrane protein trafficking. J Cell Sci **131,** jcs203695.

Hindt, M.N., and Guerinot, M.L. (2012). Getting a sense for signals: regulation of the plant iron deficiency response. Biochimica et Biophysica Acta (BBA)-Molecular Cell Research **1823,** 1521-1530.

Hirayama, T., Ohto, C., Mizoguchi, T., and Shinozaki, K. (1995). A gene encoding a phosphatidylinositol-specific phospholipase C is induced by dehydration and salt stress in Arabidopsis thaliana. Proceedings of the National Academy of Sciences **92,** 3903-3907.

Hoddinott, J., Maluccio, J.A., Behrman, J.R., Flores, R., and Martorell, R. (2008). Effect of a nutrition intervention during early childhood on economic productivity in Guatemalan adults. The lancet **371,** 411-416.

Holst, B., and Williamson, G. (2008). Nutrients and phytochemicals: from bioavailability to bioefficacy beyond antioxidants. Current opinion in biotechnology **19,** 73-82.

Honigmann, A., Van Den Bogaart, G., Iraheta, E., Risselada, H.J., Milovanovic, D., Mueller, V., Müllar, S., Diederichsen, U., Fasshauer, D., and Grubmüller, H. (2013). Phosphatidylinositol 4, 5-bisphosphate clusters act as molecular beacons for vesicle recruitment. Nature Structural and Molecular Biology **20,** 679.

Hotz, C., and Brown, K.H. (2004). Assessment of the risk of zinc deficiency in populations and options for its control. Food Nutr Bull **25,** 194-195.

Hötzer, B., Ivanov, R., Brumbarova, T., Bauer, P., and Jung, G. (2012). Visualization of Cu2+ uptake and release in plant cells by fluorescence lifetime imaging microscopy. The FEBS journal **279,** 410-419.

Hu, C.-D., and Kerppola, T.K. (2003). Simultaneous visualization of multiple protein interactions in living cells using multicolor fluorescence complementation analysis. Nature biotechnology **21,** 539.

Hu, C.-D., Chinenov, Y., and Kerppola, T.K. (2002). Visualization of interactions among bZIP and Rel family proteins in living cells using bimolecular fluorescence complementation. Molecular cell **9,** 789-798.

Ihemere, U., Narayanan, N., and Sayre, R. (2012). Iron biofortification and homeostasis in transgenic cassava roots expressing an algal iron assimilatory protein, FEA1. Frontiers in plant science **3,** 171.

Ishimaru, Y., Suzuki, M., Tsukamoto, T., Suzuki, K., Nakazono, M., Kobayashi, T., Wada, Y., Watanabe, S., Matsuhashi, S., and Takahashi, M. (2006). Rice plants take up iron as an Fe3+-phytosiderophore and as Fe2+. The Plant Journal **45,** 335-346.

Ivanov, R., and Bauer, P. (2016). Sequence and coexpression analysis of iron-regulated ZIP transporter genes reveals crossing points between iron acquisition strategies in green algae and land plants. Plant and Soil**,** 1-13.

Ivanov, R., and Bauer, P. (2017). Sequence and coexpression analysis of iron-regulated ZIP transporter genes reveals crossing points between iron acquisition strategies in green algae and land plants. Plant and Soil **418,** 61-73.

Ivanov, R., Brumbarova, T., and Bauer, P. (2012). Fitting into the harsh reality: regulation of iron-deficiency responses in dicotyledonous plants. Molecular Plant **5,** 27-42.

Ivanov, R., Brumbarova, T., Blum, A., Jantke, A.-M., Fink-Straube, C., and Bauer, P. (2014). SORTING NEXIN1 is required for modulating the trafficking and stability of the Arabidopsis IRON-REGULATED TRANSPORTER1. The Plant Cell **26,** 1294-1307.

Jakoby, M., Wang, H.-Y., Reidt, W., Weisshaar, B., and Bauer, P. (2004). FRU (BHLH029) is required for induction of iron mobilization genes in Arabidopsis thaliana. FEBS letters **577,** 528-534.

Jalewa, J., Joshi, A., McGinnity, T.M., Prasad, G., Wong-Lin, K., and Hölscher, C. (2014). Neural circuit interactions between the dorsal raphe nucleus and the lateral hypothalamus: an experimental and computational study. PloS one **9,** e88003.

Jeong, I.S., Fukudome, A., Aksoy, E., Bang, W.Y., Kim, S., Guan, Q., Bahk, J.D., May, K.A., Russell, W.K., and Zhu, J. (2013). Regulation of abiotic stress signalling by Arabidopsis C-terminal domain phosphatase-like 1 requires interaction with a K-homology domain-containing protein. PloS one **8,** e80509.

Johnson, J.E., Giorgione, J., and Newton, A.C. (2000). The C1 and C2 domains of protein kinase C are independent membrane targeting modules, with specificity for phosphatidylserine conferred by the C1 domain. Biochemistry **39,** 11360-11369.

Kahn, R.A., Yucel, J.K., and Malhotra, V. (1993). ARF signaling: a potential role for phospholipase D in membrane traffic. Cell **75,** 1045-1048.

Kampfenkel, K., Kushnir, S., Babiychuk, E., Inzé, D., and Van Montagu, M. (1995). Molecular characterization of a putative Arabidopsis thaliana copper transporter and its yeast homologue. Journal of Biological Chemistry **270,** 28479-28486.

Kang, C.H., Moon, B.C., Park, H.C., Koo, S.C., Chi, Y.H., Cheong, Y.H., Yoon, B.-D., Lee, S.Y., and Kim, C.Y. (2013). Rice small C2-domain proteins are phosphorylated by calcium-dependent protein kinase. Molecules and cells **35,** 381.

Kerkeb, L., Mukherjee, I., Chatterjee, I., Lahner, B., Salt, D.E., and Connolly, E.L. (2008). Iron-induced turnover of the Arabidopsis IRON-REGULATED TRANSPORTER1 metal transporter requires lysine residues. Plant Physiology **146,** 1964-1973.

Kikkawa, U., Kishimoto, A., and Nishizuka, Y. (1989). The protein kinase C family: heterogeneity and its implications. Annual review of biochemistry **58,** 31-44.

Kim, S.A., and Guerinot, M.L. (2007). Mining iron: iron uptake and transport in plants. FEBS letters **581,** 2273-2280.

Kim, S.A., Punshon, T., Lanzirotti, A., Li, L., Alonso, J.M., Ecker, J.R., Kaplan, J., and Guerinot, M.L. (2006). Localization of iron in Arabidopsis seed requires the vacuolar membrane transporter VIT1. Science **314,** 1295-1298.

Knauer, T., Dümmer, M., Landgraf, F., and Forreiter, C. (2011). A negative effector of blue light-induced and gravitropic bending in Arabidopsis. Plant physiology **156,** 439-447.

Kobayashi, T., and Nishizawa, N.K. (2012). Iron uptake, translocation, and regulation in higher plants. Annual review of plant biology **63,** 131-152.

Kobayashi, T., Nagasaka, S., Senoura, T., Itai, R.N., Nakanishi, H., and Nishizawa, N.K. (2013). Iron-binding haemerythrin RING ubiquitin ligases regulate plant iron responses and accumulation. Nature Communications **4**.

Kodama, Y., and Hu, C.-D. (2012). Review. Biotechniques **53,** 285-298.

Kohout, S.C., Corbalán-García, S., Torrecillas, A., Goméz-Fernandéz, J.C., and Falke, J.J. (2002). C2 domains of protein kinase C isoforms α, β, and γ: Activation parameters and calcium stoichiometries of the membrane-bound state. Biochemistry **41,** 11411-11424.

Kopka, J., Pical, C., Hetherington, A.M., and Müller-Röber, B. (1998). Ca 2+/phospholipid-binding (C 2) domain in multiple plant proteins: novel components of the calcium-sensing apparatus. Plant molecular biology **36,** 627-637.

Korshunova, Y.O., Eide, D., Clark, W.G., Guerinot, M.L., and Pakrasi, H.B. (1999). The IRT1 protein from Arabidopsis thaliana is a metal transporter with a broad substrate range. Plant molecular biology **40,** 37-44.

Kramer, D., Römheld, V., Landsberg, E., and Marschner, H. (1980). Induction of transfer-cell formation by iron deficiency in the root epidermis of Helianthus annuus L. Planta **147,** 335-339.

Kulkarni, S., Das, S., Funk, C.D., Murray, D., and Cho, W. (2002). Molecular basis of the specific subcellular localization of the C2-like domain of 5-lipoxygenase. Journal of Biological Chemistry **277,** 13167-13174.

Kurup, S., Runions, J., Köhler, U., Laplaze, L., Hodge, S., and Haseloff, J. (2005). Marking cell lineages in living tissues. The Plant Journal **42,** 444-453.

Kushnir, S., Babiychuk, E., Storozhenko, S., Davey, M.W., Papenbrock, J., De Rycke, R., Engler, G., Stephan, U.W., Lange, H., and Kispal, G. (2001). A mutation of the mitochondrial ABC transporter Sta1 leads to dwarfism and chlorosis in the Arabidopsis mutant starik. The Plant Cell **13,** 89-100.

Lahner, B., Gong, J., Mahmoudian, M., Smith, E.L., Abid, K.B., Rogers, E.E., Guerinot, M.L., Harper, J.F., Ward, J.M., and McIntyre, L. (2003). Genomic scale profiling of nutrient and trace elements in Arabidopsis thaliana. Nature biotechnology **21,** 1215-1221.

Landsberg, E.-C. (1986). Function of rhizodermal transfer cells in the Fe stress response mechanism of Capsicum annuum L. Plant Physiology **82,** 511-517.

Lanquar, V., Lelièvre, F., Bolte, S., Hamès, C., Alcon, C., Neumann, D., Vansuyt, G., Curie, C., Schröder, A., and Krämer, U. (2005). Mobilization of vacuolar iron by AtNRAMP3 and AtNRAMP4 is essential for seed germination on low iron. The EMBO journal **24,** 4041-4051.

Lawlor, D. (2004). Mengel, K. and Kirkby, EA Principles of plant nutrition (Oxford University Press).

Lee, J.-O., Yang, H., Georgescu, M.-M., Di Cristofano, A., Maehama, T., Shi, Y., Dixon, J.E., Pandolfi, P., and Pavletich, N.P. (1999). Crystal structure of the PTEN tumor suppressor: implications for its phosphoinositide phosphatase activity and membrane association. Cell **99,** 323-334.

Lemmon, M.A. (2008). Membrane recognition by phospholipid-binding domains. Nature reviews Molecular cell biology **9,** 99-111.

LEMMON, M.A., and FERGUSON, K.M. (2000). Signal-dependent membrane targeting by pleckstrin homology (PH) domains. Biochemical Journal **350,** 1-18.

Li, P., Qi, J.-L., Wang, L., Huang, Q.-N., Han, Z.-H., and Yin, L.-P. (2006). Functional expression of MxIRT1, from Malus xiaojinensis, complements an iron uptake deficient yeast mutant for plasma membrane targeting via membrane vesicles trafficking process. Plant science **171,** 52-59.

Lill, R., and Kispal, G. (2000). Maturation of cellular Fe–S proteins: an essential function of mitochondria. Trends in biochemical sciences **25,** 352-356.

Lin, Y.F., Liang, H.M., Yang, S.Y., Boch, A., Clemens, S., Chen, C.C., Wu, J.F., Huang, J.L., and Yeh, K.C. (2009). Arabidopsis IRT3 is a zinc-regulated and plasma membrane localized zinc/iron transporter. New Phytologist **182,** 392-404.

Lindsay, W. (1995). Chemical reactions in soils that affect iron availability to plants. A quantative approach. In Iron nutrition in soils and plants (Springer), pp. 7-14.

Ling, H.-Q., Bauer, P., Bereczky, Z., Keller, B., and Ganal, M. (2002). The tomato fer gene encoding a bHLH protein controls iron-uptake responses in roots. Proceedings of the National Academy of Sciences **99,** 13938-13943.

Ling, Q., Huang, W., and Jarvis, P. (2011). Use of a SPAD-502 meter to measure leaf chlorophyll concentration in Arabidopsis thaliana. Photosynthesis research **107,** 209-214.

Lingam, S., Mohrbacher, J., Brumbarova, T., Potuschak, T., Fink-Straube, C., Blondet, E., Genschik, P., and Bauer, P. (2011). Interaction between the bHLH transcription factor FIT and ETHYLENE INSENSITIVE3/ETHYLENE INSENSITIVE3-LIKE1 reveals molecular linkage between the regulation of iron acquisition and ethylene signaling in Arabidopsis. The Plant Cell **23,** 1815-1829.

Linka, N., Theodoulou, F.L., Haslam, R.P., Linka, M., Napier, J.A., Neuhaus, H.E., and Weber, A.P. (2008). Peroxisomal ATP import is essential for seedling development in Arabidopsis thaliana. The Plant Cell **20,** 3241-3257.

Liu, L., Li, C., Liang, Z., and Yu, H. (2017). Characterization of Multiple C2 Domain and Transmembrane Region Proteins in Arabidopsis. Plant physiology**,** pp. 01144.02017.

Livak, K. (1997). ABI Prism 7700 sequence detection system. User bulletin **2,** 1-36.

Long, T.A., Tsukagoshi, H., Busch, W., Lahner, B., Salt, D.E., and Benfey, P.N. (2010). The bHLH transcription factor POPEYE regulates response to iron deficiency in Arabidopsis roots. The Plant Cell **22,** 2219-2236.

López-Millán, A.F., Morales, F.n., Abadía, A., and Abadía, J. (2000). Effects of iron deficiency on the composition of the leaf apoplastic fluid and xylem sap in sugar beet. Implications for iron and carbon transport. Plant Physiology **124,** 873-884.

Lyons, G., Stangoulis, J., and Graham, R. (2003). High-selenium wheat: biofortification for better health. Nutrition Research Reviews **16,** 45-60.

Marquès-Bueno, M.M., Morao, A.K., Cayrel, A., Platre, M.P., Barberon, M., Caillieux, E., Colot, V., Jaillais, Y., Roudier, F., and Vert, G. (2016). A versatile Multisite Gateway-compatible promoter and transgenic line collection for cell type-specific functional genomics in Arabidopsis. The Plant Journal **85,** 320-333.

Marschner, H. (1995). Mineral Nutrition of Higher Plants Academic Press London Google Scholar.

Marschner, H. (2011). Marschner's mineral nutrition of higher plants. (Academic press).

Marschner, H., Römheld, V., and Kissel, M. (1986). Different strategies in higher plants in mobilization and uptake of iron. Journal of plant nutrition **9,** 695-713.

Martínez-Cuenca, M.-R., Primo-Capella, A., and Forner-Giner, M.A. (2017). Tolerance Response Mechanisms to Iron Deficiency Stress in Citrus Plants. In Stress Signaling in Plants: Genomics and Proteomics Perspective, Volume 2 (Springer), pp. 201-239.

Martz, F., Wilczynska, M., and Kleczkowski, L.A. (2002). Oligomerization status, with the monomer as active species, defines catalytic efficiency of UDP-glucose pyrophosphorylase. Biochemical Journal **367,** 295.

Mary, V., Ramos, M.S., Gillet, C., Socha, A.L., Giraudat, J., Agorio, A., Merlot, S., Clairet, C., Kim, S.A., and Punshon, T. (2015). Bypassing Iron Storage in Endodermal Vacuoles Rescues the Iron Mobilization Defect in the natural resistance associated-macrophage protein3natural resistance associated-macrophage protein4 Double Mutant. Plant physiology **169,** 748-759.

Mäser, P., Thomine, S., Schroeder, J.I., Ward, J.M., Hirschi, K., Sze, H., Talke, I.N., Amtmann, A., Maathuis, F.J., and Sanders, D. (2001). Phylogenetic relationships within cation transporter families of Arabidopsis. Plant Physiology **126,** 1646-1667.

Masuda, H., Kobayashi, T., Ishimaru, Y., Takahashi, M., Aung, M.S., Nakanishi, H., Mori, S., and Nishizawa, N.K. (2013). Iron-biofortification in rice by the introduction of three barley genes participated in mugineic acid biosynthesis with soybean ferritin gene. Frontiers in plant science **4,** 132.

Matsuoka, K., Furukawa, J., Bidadi, H., Asahina, M., Yamaguchi, S., and Satoh, S. (2014). Gibberellin-induced expression of Fe uptake-related genes in Arabidopsis. Plant and Cell Physiology **55,** 87-98.

Matthiadis, A., and Long, T.A. (2016). Further insight into BRUTUS domain composition and functionality. Plant Signaling & Behavior **11,** e1204508.

Maurer, F., Arcos, M.A.N., and Bauer, P. (2014). Responses of a triple mutant defective in three iron deficiency-induced Basic Helix-Loop-Helix genes of the subgroup Ib (2) to iron deficiency and salicylic acid. PloS one **9,** e99234.

Mazzucotelli, E., Belloni, S., Marone, D., De Leonardis, A., Guerra, D., Di Fonzo, N., Cattivelli, L., and Mastrangelo, A. (2006). The E3 ubiquitin ligase gene family in plants: regulation by degradation. Current genomics **7,** 509-522.

Medkova, M., and Cho, W. (1998). Mutagenesis of the C2 Domain of Protein Kinase C-α differential Roles of Ca2+ ligands and membrane binding residues. Journal of Biological Chemistry **273,** 17544-17552.

Meenakshi, J., Johnson, N.L., Manyong, V.M., DeGroote, H., Javelosa, J., Yanggen, D.R., Naher, F., Gonzalez, C., García, J., and Meng, E. (2010). How cost-effective is biofortification in combating micronutrient malnutrition? An ex ante assessment. World Development **38,** 64-75.

Meiser, J., Lingam, S., and Bauer, P. (2011). Posttranslational regulation of the iron deficiency basic helix-loop-helix transcription factor FIT is affected by iron and nitric oxide. Plant Physiology **157,** 2154-2166.

Mori, S., and Nishizawa, N. (1987). Methionine as a dominant precursor of phytosiderophores in Graminaceae plants. Plant and Cell Physiology **28,** 1081-1092.

Morrissey, J., and Guerinot, M.L. (2009). Iron uptake and transport in plants: the good, the bad, and the ionome. Chemical reviews **109,** 4553-4567.

Morsomme, P., Dambly, S., Maudoux, O., and Boutry, M. (1998). Single point mutations distributed in 10 soluble and membrane regions of the Nicotiana plumbaginifolia plasma membrane PMA2 H+-ATPase activate the enzyme and modify the structure of the C-terminal region. Journal of Biological Chemistry **273,** 34837-34842.

Moser, C.O. (1989). Gender planning in the Third World: meeting practical and strategic gender needs. World development **17,** 1799-1825.

Mukherjee, I., Campbell, N.H., Ash, J.S., and Connolly, E.L. (2006). Expression profiling of the Arabidopsis ferric chelate reductase (FRO) gene family reveals differential regulation by iron and copper. Planta **223,** 1178-1190.

Müller, O., and Krawinkel, M. (2005). Malnutrition and health in developing countries. Canadian Medical Association Journal **173,** 279-286.

Murata, Y., Ma, J.F., Yamaji, N., Ueno, D., Nomoto, K., and Iwashita, T. (2006). A specific transporter for iron (III)–phytosiderophore in barley roots. The Plant Journal **46,** 563-572.

Murray, D., and Honig, B. (2002). Electrostatic control of the membrane targeting of C2 domains. Molecular cell **9,** 145-154.

Nalefski, E.A., and Falke, J.J. (1996). The C2 domain calcium-binding motif: structural and functional diversity. Protein Science **5,** 2375-2390.

Nalefski, E.A., Sultzman, L.A., Martin, D.M., Kriz, R.W., Towler, P.S., Knopf, J.L., and Clark, J.D. (1994). Delineation of two functionally distinct domains of cytosolic phospholipase A2, a regulatory Ca (2+)-dependent lipid-binding domain and a Ca (2+)-independent catalytic domain. Journal of Biological Chemistry **269,** 18239-18249.

Nanmori, T., Taguchi, W., Kinugasa, M., Oji, Y., Sahara, S., Fukami, Y., and Kikkawa, U. (1994). Purification and characterization of protein kinase C from a higher plant, Brassica campestris L. Biochemical and biophysical research communications **203,** 311-318.

Naranjo-Arcos, M.A., and Bauer, P. (2016). Iron Nutrition, Oxidative Stress, and Pathogen Defense. In Nutritional Deficiency (InTech.

Neumann, G., and Römheld, V. (2007). The release of root exudates as affected by the plant physiological status. In The Rhizosphere: Biochemistry and Organic Substances at the Soil-Plant Interface, Second Edition (CRC Press), pp. 23-72.

Nishida, S., Mizuno, T., and Obata, H. (2008). Involvement of histidine-rich domain of ZIP family transporter TjZNT1 in metal ion specificity. Plant Physiology and Biochemistry **46,** 601-606.

Nishizuka, Y. (1988). The molecular heterogeneity of protein kinase C and its implications for cellular regulation. Nature **334,** 661-665.

Nozoye, T., Nagasaka, S., Kobayashi, T., Takahashi, M., Sato, Y., Sato, Y., Uozumi, N., Nakanishi, H., and Nishizawa, N.K. (2011). Phytosiderophore efflux transporters are crucial for iron acquisition in graminaceous plants. Journal of Biological Chemistry **286,** 5446-5454.

Organization, W.H. (2015). The global prevalence of anaemia in 2011.

Palmer, C.M., Hindt, M.N., Schmidt, H., Clemens, S., and Guerinot, M.L. (2013a). MYB10 and MYB72 are required for growth under iron-limiting conditions. PLoS genetics **9,** e1003953.

Palmer, C.M., Hindt, M.N., Schmidt, H., Clemens, S., and Guerinot, M.L. (2013b). MYB10 and MYB72 are required for growth under iron-limiting conditions. PLoS Genet **9,** e1003953.

Palmgren, M.G. (2001). Plant plasma membrane H+-ATPases: powerhouses for nutrient uptake. Annual review of plant biology **52,** 817-845.

Pascal, N., and Douce, R. (1993). Effect of iron deficiency on the respiration of sycamore (Acer pseudoplatanus L.) cells. Plant physiology **103,** 1329-1338.

Pavlovic, D., Nikolic, B., Djurovic, S., Waisi, H., Andjelkovic, A., and Marisavljevic, D. (2015). Chlorophyll as a measure of plant health: Agroecological aspects.

Pedas, P., Ladegaard, A.H., Schiller, M., Schjoerring, J.K., and Husted, S. (2009). Barley metal ion transport proteins involved in manganese acquisition and homeostasis.

Pérez-Massot, E., Banakar, R., Gómez-Galera, S., Zorrilla-López, U., Sanahuja, G., Arjó, G., Miralpeix, B., Vamvaka, E., Farré, G., and Rivera, S.M. (2013). The contribution of transgenic plants to better health through improved nutrition: opportunities and constraints. Genes & nutrition **8,** 29-41.

Perin, M.S., Fried, V.A., Mignery, G.A., Jahn, R., and Sudhof, T.C. (1990). Phospholipid binding by a synaptic vesicle protein homologous to the regulatory region of protein kinase C. Nature **345,** 260.

Perisic, O., Fong, S., Lynch, D.E., Bycroft, M., and Williams, R.L. (1998). Crystal structure of a calcium-phospholipid binding domain from cytosolic phospholipase A2. Journal of Biological Chemistry **273,** 1596-1604.

Peterson, D.A. (1991). Enhanced electron transfer by unsaturated fatty acids and superoxide dismutase. Free radical research communications **12,** 161-166.

Pical, C., Kopka, J., Müller-Röber, B., Hetherington, A., and Gray, J. (1997). Isolation of 2 cDNA clones for phosphoinositide-specific phospholipase C from epidermal peels (accession no. X95877) and guard cells (accession no. Y11931) of Nicotiana rustica (PGR 97–086). Plant Physiol **114,** 747.

Pires, N., and Dolan, L. (2010). Origin and diversification of basic-helix-loop-helix proteins in plants. Molecular biology and evolution **27,** 862-874.

Pittman, J.K. (2005). Managing the manganese: molecular mechanisms of manganese transport and homeostasis. New Phytologist **167,** 733-742.

Platre, M.P., and Jaillais, Y. (2017). Anionic lipids and the maintenance of membrane electrostatics in eukaryotes. Plant signaling & behavior **12,** e1282022.

Potocki, S., Valensin, D., Camponeschi, F., and Kozlowski, H. (2013). The extracellular loop of IRT1 ZIP protein—the chosen one for zinc? Journal of inorganic biochemistry **127,** 246-252.

Pourcher, M., Santambrogio, M., Thazar, N., Thierry, A.-M., Fobis-Loisy, I., Miège, C., Jaillais, Y., and Gaude, T. (2010). Analyses of sorting nexins reveal distinct retromer-subcomplex functions in development and protein sorting in Arabidopsis thaliana. The Plant Cell **22,** 3980-3991.

Qu, L.Q., Yoshihara, T., Ooyama, A., Goto, F., and Takaiwa, F. (2005). Iron accumulation does not parallel the high expression level of ferritin in transgenic rice seeds. Planta **222,** 225-233.

Ravet, K., Touraine, B., Kim, S.A., Cellier, F., Thomine, S., Guerinot, M.L., Briat, J.-F., and Gaymard, F. (2009). Post-translational regulation of AtFER2 ferritin in response to intracellular iron trafficking during fruit development in Arabidopsis. Molecular plant **2,** 1095-1106.

Rehrauer, H., Aquino, C., Gruissem, W., Henz, S.R., Hilson, P., Laubinger, S., Naouar, N., Patrignani, A., Rombauts, S., and Shu, H. (2010). AGRONOMICS1: a new resource for Arabidopsis transcriptome profiling. Plant Physiology **152,** 487-499.

Reyt, G., Boudouf, S., Boucherez, J., Gaymard, F., and Briat, J.-F. (2015). Iron-and ferritin-dependent reactive oxygen species distribution: impact on Arabidopsis root system architecture. Molecular plant **8,** 439-453.

Rizo, J., and Südhof, T.C. (1998). C2-domains, structure and function of a universal Ca2+-binding domain. Journal of Biological Chemistry **273,** 15879-15882.

Robinson, D.G., and Neuhaus, J.-M. (2016). Receptor-mediated sorting of soluble vacuolar proteins: myths, facts, and a new model. Journal of experimental botany **67,** 4435-4449.

Robinson, N.J., Procter, C.M., Connolly, E.L., and Guerinot, M.L. (1999). A ferric-chelate reductase for iron uptake from soils. Nature **397,** 694-697.

Rodríguez-Celma, J., Lin, W.-D., Fu, G.-M., Abadía, J., López-Millán, A.-F., and Schmidt, W. (2013a). Mutually exclusive alterations in secondary metabolism are critical for the uptake of insoluble iron compounds by Arabidopsis and Medicago truncatula. Plant Physiology **162,** 1473-1485.

Rodríguez-Celma, J., Pan, I.C., Li, W., Lan, P., Buckhout, T.J., and Schmidt, W. (2013b). The transcriptional response of Arabidopsis leaves to Fe deficiency. Frontiers in plant science **4**.

Rodriguez, L., Gonzalez-Guzman, M., Diaz, M., Rodrigues, A., Izquierdo-Garcia, A.C., Peirats-Llobet, M., Fernandez, M.A., Antoni, R., Fernandez, D., and Marquez, J.A. (2014). C2-domain abscisic acid-related proteins mediate the interaction of PYR/PYL/RCAR abscisic acid receptors with the plasma membrane and regulate abscisic acid sensitivity in Arabidopsis. The Plant Cell **26,** 4802-4820.

Rogers, E.E., and Guerinot, M.L. (2002). FRD3, a member of the multidrug and toxin efflux family, controls iron deficiency responses in Arabidopsis. The Plant Cell **14,** 1787-1799.

Rogers, E.E., Eide, D.J., and Guerinot, M.L. (2000). Altered selectivity in an Arabidopsis metal transporter. Proceedings of the National Academy of Sciences **97,** 12356-12360.

Römheld, V., and Kramer, D. (1983). Relationship between proton efflux and rhizodermal transfer cells induced by iron deficiency. Zeitschrift für Pflanzenphysiologie **113,** 73-83.

Roschzttardtz, H., Conéjéro, G., Divol, F., Alcon, C., Verdeil, J.-L., Curie, C., and Mari, S. (2013). New insights into Fe localization in plant tissues. Frontiers in plant science **4**.

Rout, G.R., and Sahoo, S. (2015). Role of iron in plant growth and metabolism. Reviews in Agricultural Science **3,** 1-24.

Sambrook, J., Fritsch, E.F., and Maniatis, T. (1989). Molecular cloning: a laboratory manual. (Cold spring harbor laboratory press).

Santi, S., and Schmidt, W. (2009). Dissecting iron deficiency-induced proton extrusion in Arabidopsis roots. New Phytologist **183,** 1072-1084.

Sasaki, A., Yamaji, N., Yokosho, K., and Ma, J.F. (2012). Nramp5 is a major transporter responsible for manganese and cadmium uptake in rice. The Plant Cell **24,** 2155-2167.

Sayre, R., Beeching, J.R., Cahoon, E.B., Egesi, C., Fauquet, C., Fellman, J., Fregene, M., Gruissem, W., Mallowa, S., and Manary, M. (2011). The BioCassava plus program: biofortification of cassava for sub-Saharan Africa. Annual review of plant biology **62,** 251-272.

Schachtman, D.P., and Schroeder, J.I. (1994). Structure and transport mechanism of a high-affinity potassium uptake transporter from higher plants. Nature **370,** 655.

Schiavo, G., Gu, Q.-M., Prestwich, G.D., Söllner, T.H., and Rothman, J.E. (1996). Calcium-dependent switching of the specificity of phosphoinositide binding to synaptotagmin. Proceedings of the National Academy of Sciences **93,** 13327-13332.

Schmid, N.B., Giehl, R.F., Döll, S., Mock, H.-P., Strehmel, N., Scheel, D., Kong, X., Hider, R.C., and von Wirén, N. (2014). Feruloyl-CoA 6′-hydroxylase1-dependent coumarins mediate iron acquisition from alkaline substrates in Arabidopsis. Plant Physiology **164,** 160-172.

Schmidt, T.G., and Skerra, A. (2007). The Strep-tag system for one-step purification and high-affinity detection or capturing of proteins. Nature protocols **2,** 1528.

Schouten, H.J., Krens, F.A., and Jacobsen, E. (2006). Cisgenic plants are similar to traditionally bred plants. EMBO reports **7,** 750-753.

Schuler, M., Rellán-Álvarez, R., Fink-Straube, C., Abadía, J., and Bauer, P. (2012). Nicotianamine functions in the phloem-based transport of iron to sink organs, in pollen development and pollen tube growth in Arabidopsis. The Plant Cell **24,** 2380-2400.

Schuler, M., Keller, A., Backes, C., Philippar, K., Lenhof, H.-P., and Bauer, P. (2011). Transcriptome analysis by GeneTrail revealed regulation of functional categories in response to alterations of iron homeostasis in Arabidopsis thaliana. BMC plant biology **11,** 87.

Scott, M.S., Calafell, S.J., Thomas, D.Y., and Hallett, M.T. (2005). Refining protein subcellular localization. PLoS computational biology **1,** e66.

Selote, D., Samira, R., Matthiadis, A., Gillikin, J.W., and Long, T.A. (2015). Iron-binding E3 ligase mediates iron response in plants by targeting basic helix-loop-helix transcription factors. Plant physiology **167,** 273-286.

Shao, X., Fernandez, I., Südhof, T.C., and Rizo, J. (1998). Solution structures of the Ca2+-free and Ca2+-bound C2A domain of synaptotagmin I: does Ca2+ induce a conformational change? Biochemistry **37,** 16106-16115.

Shen, J., Zhang, F., Chen, Q., Rengel, Z., Tang, C., and Song, C. (2002). Genotypic difference in seed iron content and early responses to iron deficiency in wheat. Journal of plant nutrition **25,** 1631-1643.

Shin, L.-J., Lo, J.-C., Chen, G.-H., Callis, J., Fu, H., and Yeh, K.-C. (2013). IRT1 degradation factor1, a ring E3 ubiquitin ligase, regulates the degradation of iron-regulated transporter1 in Arabidopsis. The Plant Cell **25,** 3039-3051.

Shojima, S., Nishizawa, N.-K., Fushiya, S., Nozoe, S., Irifune, T., and Mori, S. (1990). Biosynthesis of phytosiderophores in vitro biosynthesis of 2′-deoxymugineic acid from L-methionine and nicotianamine. Plant Physiology **93,** 1497-1503.

Simon, M.L.A., Platre, M.P., Marquès-Bueno, M.M., Armengot, L., Stanislas, T., Bayle, V., Caillaud, M.-C., and Jaillais, Y. (2016). A PtdIns (4) P-driven electrostatic field controls cell membrane identity and signalling in plants. Nature plants **2,** 16089.

Singer, S., and Nicolson, G.L. (1972). The fluid mosaic model of the structure of cell membranes. Membranes and Viruses in Immunopathology; Day, SB, Good, RA, Eds**,** 7-47.

Sivitz, A., Grinvalds, C., Barberon, M., Curie, C., and Vert, G. (2011). Proteasome-mediated turnover of the transcriptional activator FIT is required for plant iron-deficiency responses. The Plant Journal **66,** 1044-1052.

Sivitz, A.B., Hermand, V., Curie, C., and Vert, G. (2012). Arabidopsis bHLH100 and bHLH101 control iron homeostasis via a FIT-independent pathway. PloS one **7,** e44843.

Spiller, S., and Terry, N. (1980). Limiting factors in photosynthesis II. Iron stress diminishes photochemical capacity by reducing the number of photosynthetic units. Plant Physiology **65,** 121-125.

Stacey, M.G., Patel, A., McClain, W.E., Mathieu, M., Remley, M., Rogers, E.E., Gassmann, W., Blevins, D.G., and Stacey, G. (2008). The Arabidopsis AtOPT3 protein functions in metal homeostasis and movement of iron to developing seeds. Plant physiology **146,** 589-601.

Stahelin, R.V. (2009). Lipid binding domains: more than simple lipid effectors. Journal of lipid research **50,** S299-S304.

Stahelin, R.V., Subramanian, P., Vora, M., Cho, W., and Chalfant, C.E. (2007). Ceramide-1-phosphate binds group IVA cytosolic phospholipase a2 via a novel site in the C2 domain. Journal of Biological Chemistry **282,** 20467-20474.

Stahelin, R.V., Long, F., Diraviyam, K., Bruzik, K.S., Murray, D., and Cho, W. (2002). Phosphatidylinositol 3-phosphate induces the membrane penetration of the FYVE domains of Vps27p and Hrs. Journal of Biological Chemistry **277,** 26379-26388.

Stahelin, R.V., Long, F., Peter, B.J., Murray, D., De Camilli, P., McMahon, H.T., and Cho, W. (2003). Contrasting membrane interaction mechanisms of AP180 N-terminal homology (ANTH) and epsin N-terminal homology (ENTH) domains. Journal of Biological Chemistry **278,** 28993-28999.

Steinhorst, L., and Kudla, J. (2014). Signaling in cells and organisms—calcium holds the line. Current opinion in plant biology **22,** 14-21.

Stenmark, H., Aasland, R., and Driscoll, P.C. (2002). The phosphatidylinositol 3-phosphate-binding FYVE finger. Febs Letters **513,** 77-84.

Stephan, U.W., Schmidke, I., Stephan, V.W., and Scholz, G. (1996). The nicotianamine molecule is made-to-measure for complexation of metal micronutrients in plants. Biometals **9,** 84-90.

Stierhof, Y.-D., Viotti, C., Scheuring, D., Sturm, S., and Robinson, D.G. (2013). Sorting nexins 1 and 2a locate mainly to the TGN. Protoplasma**,** 1-6.

Sutton, R.B., and Sprang, S.R. (1998). Structure of the protein kinase Cβ phospholipid-binding C2 domain complexed with Ca 2+. Structure **6,** 1395-1405.

Sutton, R.B., Davletov, B.A., Berghuis, A.M., Sudhof, T.C., and Sprang, S.R. (1995). Structure of the first C2 domain of synaptotagmin I: a novel Ca2+/phospholipid-binding fold. Cell **80,** 929-938.

Taiz, L., and Zeiger, E. (2002). Plant Physiology. 3rd. Ed. Pub. Sinauer.

Taylor, K.M., and Nicholson, R.I. (2003). The LZT proteins; the LIV-1 subfamily of zinc transporters. Biochimica et Biophysica Acta (BBA)-Biomembranes **1611,** 16-30.

Terry, N., and Abadía, J. (1986). Function of iron in chloroplasts. Journal of Plant Nutrition **9,** 609-646.

Tian, Q., Zhang, X., Yang, A., Wang, T., and Zhang, W.-H. (2016). CIPK23 is involved in iron acquisition of Arabidopsis by affecting ferric chelate reductase activity. Plant Science **246,** 70-79.

Tiffin, L.O. (1966). Iron translocation I. Plant culture, exudate sampling, iron-citrate analysis. Plant Physiology **41,** 510.

Urzica, E.I., Casero, D., Yamasaki, H., Hsieh, S.I., Adler, L.N., Karpowicz, S.J., Blaby-Haas, C.E., Clarke, S.G., Loo, J.A., and Pellegrini, M. (2012). Systems and trans-system level analysis identifies conserved iron deficiency responses in the plant lineage. The Plant Cell **24,** 3921-3948.

Valentín-Berríos, S., González-Velázquez, W., Pérez-Sánchez, L., González-Méndez, R., and Rodríguez-del Valle, N. (2009). Cytosolic phospholipase A 2: a member of the signalling pathway of a new G protein α subunit in Sporothrix schenckii. BMC microbiology **9,** 100.

van Blitterswijk, W.J. (1998). Hypothesis: ceramide conditionally activates atypical protein kinases C, Raf-1 and KSR through binding to their cysteine-rich domains. Biochemical Journal **331,** 679.

Van der Ent, S., Verhagen, B.W., Van Doorn, R., Bakker, D., Verlaan, M.G., Pel, M.J., Joosten, R.G., Proveniers, M.C., Van Loon, L., and Ton, J. (2008). MYB72 is required in early signaling steps of rhizobacteria-induced systemic resistance in Arabidopsis. Plant Physiology **146,** 1293-1304.

Varotto, C., Maiwald, D., Pesaresi, P., Jahns, P., Salamini, F., and Leister, D. (2002). The metal ion transporter IRT1 is necessary for iron homeostasis and efficient photosynthesis in Arabidopsis thaliana. The Plant Journal **31,** 589-599.

Vasconcelos, M., Datta, K., Oliva, N., Khalekuzzaman, M., Torrizo, L., Krishnan, S., Oliveira, M., Goto, F., and Datta, S.K. (2003). Enhanced iron and zinc accumulation in transgenic rice with the ferritin gene. Plant Science **164,** 371-378.

Verdaguer, N., Corbalan-Garcia, S., Ochoa, W.F., Fita, I., and Gómez-Fernández, J.C. (1999). Ca2+ bridges the C2 membrane-binding domain of protein kinase Cα directly to phosphatidylserine. The EMBO journal **18,** 6329-6338.

Vert, G., Barberon, M., Zelazny, E., Séguéla, M., Briat, J.-F., and Curie, C. (2009). Arabidopsis IRT2 cooperates with the high-affinity iron uptake system to maintain iron homeostasis in root epidermal cells. Planta **229,** 1171-1179.

Vert, G., Grotz, N., Dédaldéchamp, F., Gaymard, F., Guerinot, M.L., Briat, J.-F., and Curie, C. (2002). IRT1, an Arabidopsis transporter essential for iron uptake from the soil and for plant growth. The Plant Cell **14,** 1223-1233.

von Wirén, N., Mori, S., Marschner, H., and Romheld, V. (1994). Iron inefficiency in maize mutant ys1 (Zea mays L. cv Yellow-Stripe) is caused by a defect in uptake of iron phytosiderophores. Plant Physiology **106,** 71-77.

Walker, E.L., and Connolly, E.L. (2008). Time to pump iron: iron-deficiency-signaling mechanisms of higher plants. Current opinion in plant biology **11,** 530-535.

Wang, H.-Y., Klatte, M., Jakoby, M., Bäumlein, H., Weisshaar, B., and Bauer, P. (2007). Iron deficiency-mediated stress regulation of four subgroup Ib BHLH genes in Arabidopsis thaliana. Planta **226,** 897-908.

Wang, N., Cui, Y., Liu, Y., Fan, H., Du, J., Huang, Z., Yuan, Y., Wu, H., and Ling, H.-Q. (2013). Requirement and functional redundancy of Ib subgroup bHLH proteins for iron deficiency responses and uptake in Arabidopsis thaliana. Molecular plant **6,** 503-513.

Wang, T., Pentyala, S., Rebecchi, M.J., and Scarlata, S. (1999). Differential association of the pleckstrin homology domains of phospholipases C-β1, C-β2, and C-δ1 with lipid bilayers and the βγ subunits of heterotrimeric G proteins. Biochemistry **38,** 1517-1524.

Wang, X. (1997). Molecular analysis of phospholipase D. Trends in Plant Science **2,** 261-266.

Wang, X., Li, Q., Niu, X., Chen, H., Xu, L., and Qi, C. (2009). Characterization of a canola C2 domain gene that interacts with PG, an effector of the necrotrophic fungus Sclerotinia sclerotiorum. Journal of experimental botany **60,** 2613-2620.

Welch, R.M., and Graham, R.D. (2005). Agriculture: the real nexus for enhancing bioavailable micronutrients in food crops. Journal of Trace Elements in Medicine and Biology **18,** 299-307.

Welch, R.M., Norvell, W.A., Schaefer, S.C., Shaff, J.E., and Kochian, L.V. (1993). Induction of iron (III) and copper (II) reduction in pea (Pisum sativum L.) roots by Fe and Cu status: Does the root-cell plasmalemma Fe (III)-chelate reductase perform a general role in regulating cation uptake? Planta **190,** 555-561.

Welters, P., Takegawa, K., Emr, S.D., and Chrispeels, M.J. (1994). AtVPS34, a phosphatidylinositol 3-kinase of Arabidopsis thaliana, is an essential protein with homology to a calcium-dependent lipid binding domain. Proceedings of the National Academy of Sciences **91,** 11398-11402.

Whalley, H.J., and Knight, M.R. (2013). Calcium signatures are decoded by plants to give specific gene responses. New Phytologist **197,** 690-693.

Wiener, M.C., and White, S.H. (1992). Structure of a fluid dioleoylphosphatidylcholine bilayer determined by joint refinement of x-ray and neutron diffraction data. III. Complete structure. Biophysical journal **61,** 434-447.

Wiersma, J.V. (2012). Is seed iron concentration predictive of resistance to iron deficiency in soybean? Crop science **52,** 471-481.

Wild, M., Davière, J.-M., Regnault, T., Sakvarelidze-Achard, L., Carrera, E., Diaz, I.L., Cayrel, A., Dubeaux, G., Vert, G., and Achard, P. (2016). Tissue-specific regulation of gibberellin signaling fine-tunes Arabidopsis iron-deficiency responses. Developmental cell **37,** 190-200.

Williams, M. (2010). Introduction to phytohormones. The Plant Cell **22,** 1-9.

Wishart, M.J., Taylor, G.S., and Dixon, J.E. (2001). Phoxy lipids: revealing PX domains as phosphoinositide binding modules. Cell **105,** 817-820.

Wu, C., Niu, Z., Tang, Q., and Huang, W. (2008). Estimating chlorophyll content from hyperspectral vegetation indices: Modeling and validation. Agricultural and forest meteorology **148,** 1230-1241.

Xing, S., Wallmeroth, N., Berendzen, K.W., and Grefen, C. (2016). Techniques for the analysis of protein-protein interactions in vivo. Plant physiology **171,** 727-758.

Yamaguchi-Iwai, Y., Dancis, A., and Klausner, R.D. (1995). AFT1: a mediator of iron regulated transcriptional control in Saccharomyces cerevisiae. The EMBO journal **14,** 1231.

Yamaguchi, T., Shirataki, H., Kishida, S., Miyazaki, M., Nishikawa, J., Wada, K., Numata, S.-I., Kaibuchi, K., and Takai, Y. (1993). Two functionally different domains of rabphilin-3A, Rab3A

p25/smg p25A-binding and phospholipid-and Ca (2+)-binding domains. Journal of Biological Chemistry **268,** 27164-27170.

Yang, C., and Kazanietz, M.G. (2003). Divergence and complexities in DAG signaling: looking beyond PKC. Trends in pharmacological sciences **24,** 602-608.

Yang, J.L., Chen, W.W., Chen, L.Q., Qin, C., Jin, C.W., Shi, Y.Z., and Zheng, S.J. (2013). The 14-3-3 protein GENERAL REGULATORY FACTOR11 (GRF11) acts downstream of nitric oxide to regulate iron acquisition in Arabidopsis thaliana. New Phytologist **197,** 815-824.

Yang, W.-Q., Lai, Y., Li, M.-N., Xu, W.-Y., and Xue, Y.-B. (2008). A novel C2-domain phospholipid-binding protein, OsPBP1, is required for pollen fertility in rice. Molecular plant **1,** 770-785.

Yang, Y., Ou, B., Zhang, J., Si, W., Gu, H., Qin, G., and Qu, L.J. (2014). The Arabidopsis Mediator subunit MED16 regulates iron homeostasis by associating with EIN3/EIL1 through subunit MED25. The Plant Journal **77,** 838-851.

Yi, Y., and Guerinot, M.L. (1996). Genetic evidence that induction of root Fe (III) chelate reductase activity is necessary for iron uptake under iron deficiency. The Plant Journal **10,** 835-844.

Yuan, Y., Wu, H., Wang, N., Li, J., Zhao, W., Du, J., Wang, D., and Ling, H.-Q. (2008). FIT interacts with AtbHLH38 and AtbHLH39 in regulating iron uptake gene expression for iron homeostasis in Arabidopsis. Cell research **18,** 385-397.

Yue, X., Li-Fong, S., HANSON, B., and Wanjin, H. (2001). The Phox homology (PX) domain, a new player in phosphoinositide signalling. Biochemical Journal **360,** 513-530.

Yung, Y.-L., Cheung, M.-Y., Miao, R., Fong, Y.-H., Li, K.-P., Yu, M.-H., Chye, M.-L., Wong, K.-B., and Lam, H.-M. (2015). Site-directed mutagenesis shows the significance of interactions with phospholipids and the G-protein OsYchF1 for the physiological functions of the rice GTPase-activating protein 1 (OsGAP1). Journal of Biological Chemistry **290,** 23984-23996.

Zamioudis, C., Hanson, J., and Pieterse, C.M. (2014). β-Glucosidase BGLU42 is a MYB72-dependent key regulator of rhizobacteria-induced systemic resistance and modulates iron deficiency responses in Arabidopsis roots. New Phytologist **204,** 368-379.

Zamyatnin, A.A., Solovyev, A.G., Bozhkov, P.V., Valkonen, J., Morozov, S.Y., and Savenkov, E.I. (2006). Assessment of the integral membrane protein topology in living cells. The Plant Journal **46,** 145-154.

Zelazny, E., and Vert, G. (2014). Plant nutrition: root transporters on the move. Plant physiology **166,** 500-508.

Zelazny, E., Barberon, M., Curie, C., and Vert, G. (2011). Ubiquitination of transporters at the forefront of plant nutrition. Plant signaling & behavior **6,** 1597-1599.

Zelazny, E., Santambrogio, M., Pourcher, M., Chambrier, P., Berne-Dedieu, A., Fobis-Loisy, I., Miège, C., Jaillais, Y., and Gaude, T. (2013). Mechanisms governing the endosomal membrane recruitment of the core retromer in Arabidopsis. Journal of Biological Chemistry **288,** 8815-8825.

Zhang, J., Liu, B., Li, M., Feng, D., Jin, H., Wang, P., Liu, J., Xiong, F., Wang, J., and Wang, H.-B. (2015). The bHLH transcription factor bHLH104 interacts with IAA-LEUCINE RESISTANT3 and modulates iron homeostasis in Arabidopsis. The Plant Cell **27,** 787-805.

Zhang, T., Liu, J., Fellner, M., Zhang, C., Sui, D., and Hu, J. (2017). Crystal structures of a ZIP zinc transporter reveal a binuclear metal center in the transport pathway. Science advances **3,** e1700344.

Zhang, Y., Wu, H., Wang, N., Fan, H., Chen, C., Cui, Y., Liu, H., and Ling, H.Q. (2014). Mediator subunit 16 functions in the regulation of iron uptake gene expression in Arabidopsis. New Phytologist **203,** 770-783.

Zhang, Y., Yao, B., Delikat, S., Bayoumy, S., Lin, X.-H., Basu, S., McGinley, M., Chan-Hui, P.-Y., Lichenstein, H., and Kolesnick, R. (1997). Kinase suppressor of Ras is ceramide-activated protein kinase. Cell **89,** 63-72.

Zhao, H., and Eide, D. (1996). The yeast ZRT1 gene encodes the zinc transporter protein of a high-affinity uptake system induced by zinc limitation. Proceedings of the National Academy of Sciences **93,** 2454-2458.

Zhu, C., Naqvi, S., Gomez-Galera, S., Pelacho, A.M., Capell, T., and Christou, P. (2007). Transgenic strategies for the nutritional enhancement of plants. Trends in plant science **12,** 548-555.

Zhu, C., Sanahuja, G., Yuan, D., Farré, G., Arjó, G., Berman, J., Zorrilla-López, U., Banakar, R., Bai, C., and Pérez-Massot, E. (2013). Biofortification of plants with altered antioxidant content and composition: genetic engineering strategies. Plant biotechnology journal **11,** 129-141.

Zimmermann, M.B., and Hurrell, R.F. (2007). Nutritional iron deficiency. The Lancet **370,** 511-520.

Supplemental Figures

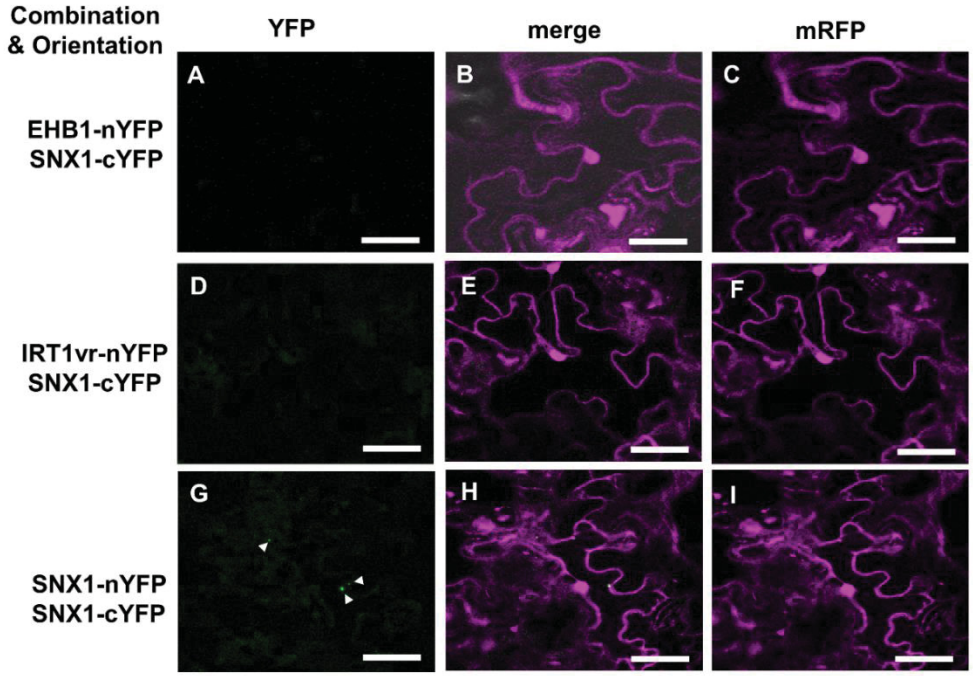

Supplemental Figure S1. Additional images for BiFC controls. CLSM images of leaf epidermal cells of *Nicotiana benthamiana* two days after transformation with *Agrobacterium* containing pBIFCt-2in1-CC. (A-F) Negative control: No YFP signal can be seen because Sorting Nexin-1(SNX1) did not interact with EHB1 and IRT1vr. (G-I) SNX1 interact with SNX1, positive YFP signal is indicated with white arrow heads. Bars, 20 µm.

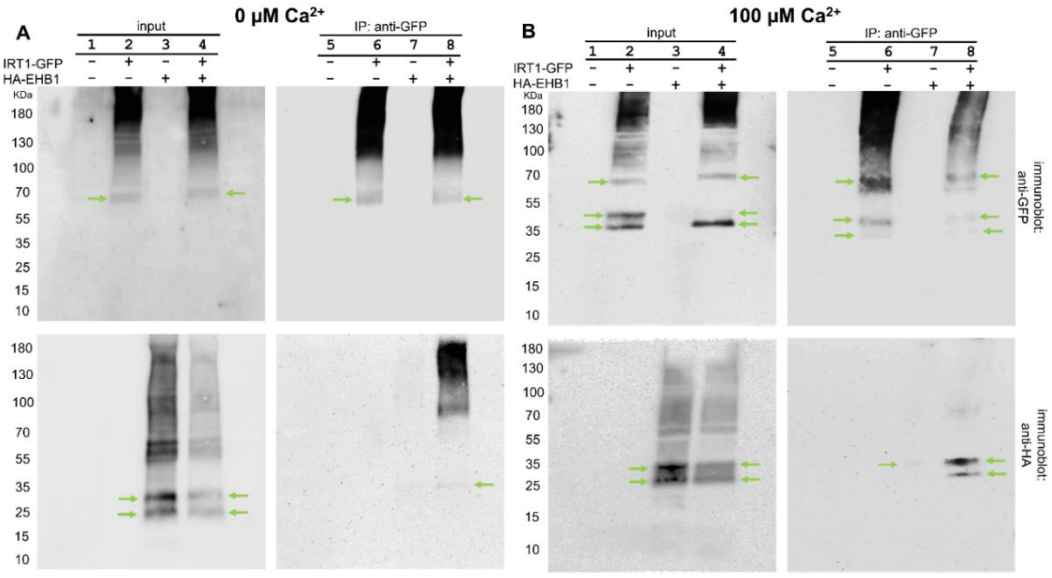

Supplemental Figure S2. Co-immunoprecipitation of IRT1-GFP and HA-EHB1. Full images of the Co-IP data shown in figure 4.4 in the main text. GFP trap assay. The presence of IRT1 and EHB1 proteins is detected both in input fractions (total protein extracts) and IP fraction. The indicated proteins IRT1-GFP (band at, 63 kDa) and HA-EHB1 (band at, 25 kDa) were transiently expressed in *Nicotiana benthamiana* and detected in an immunoblot with anti-GFP and anti-HA antibodies. The experiment was performed in the absence (0 µM) or presence (100 µM) calcium. (A) IP: anti-GFP in the absence of calcium, a weak bands can be seen in the IP fraction of anti-HA immunoblot, meaning that EHB1 was co-precipitated with IRT1. (B) IP: anti-GFP in the presence of calcium, a strong HA-EHB1 band can be seen in the IP fraction suggesting that HA-EHB1 was co-precipitated with IRT1-GFP. The second band in anti-HA immunoblot around 35 kDa could be a modified version of HA-EHB1 while the double bands around 36 kDa in anti-GFP immunoblot in B is free GFP. MW: molecular weight. KDa: kiloDaltons.

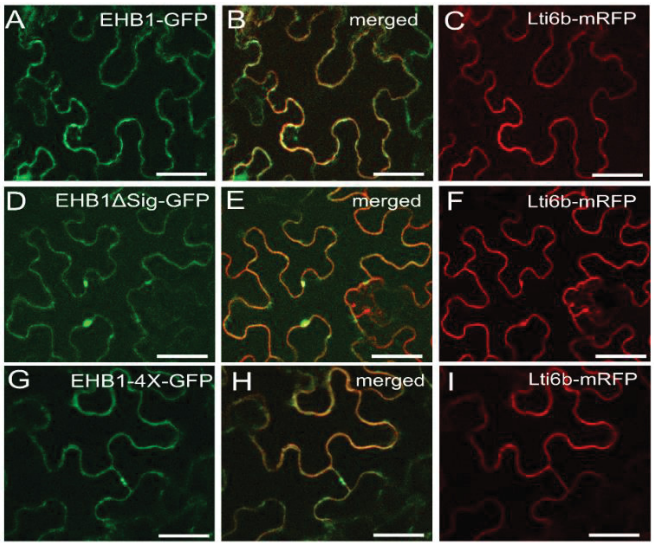

Supplemental Figure S3. Subcellular localization of EHB1-GFP, EHB1-ΔSig and EHB1-4x with plasma membrane protein Lti6b.
(A-C) Colocalization between EHB1-GFP (A) and Lti6b-mRFP (C).
(B) Yellow fluorescence signal shows colocalization due to the merger of A and C.
(D-F) Colocalization between EHB1-ΔSig-GFP (D) and Lti6b-mRFP (F)
(E) Yellow fluorescence signal shows colocalization due to the merger of D and F.
(G-I) Colocalization between EHB1-4X-GFP (G) and Lti6b-mRFP (I).
(H) Yellow fluorescence signal shows colocalization due to the merger of G and I.
Bars = 20 µm

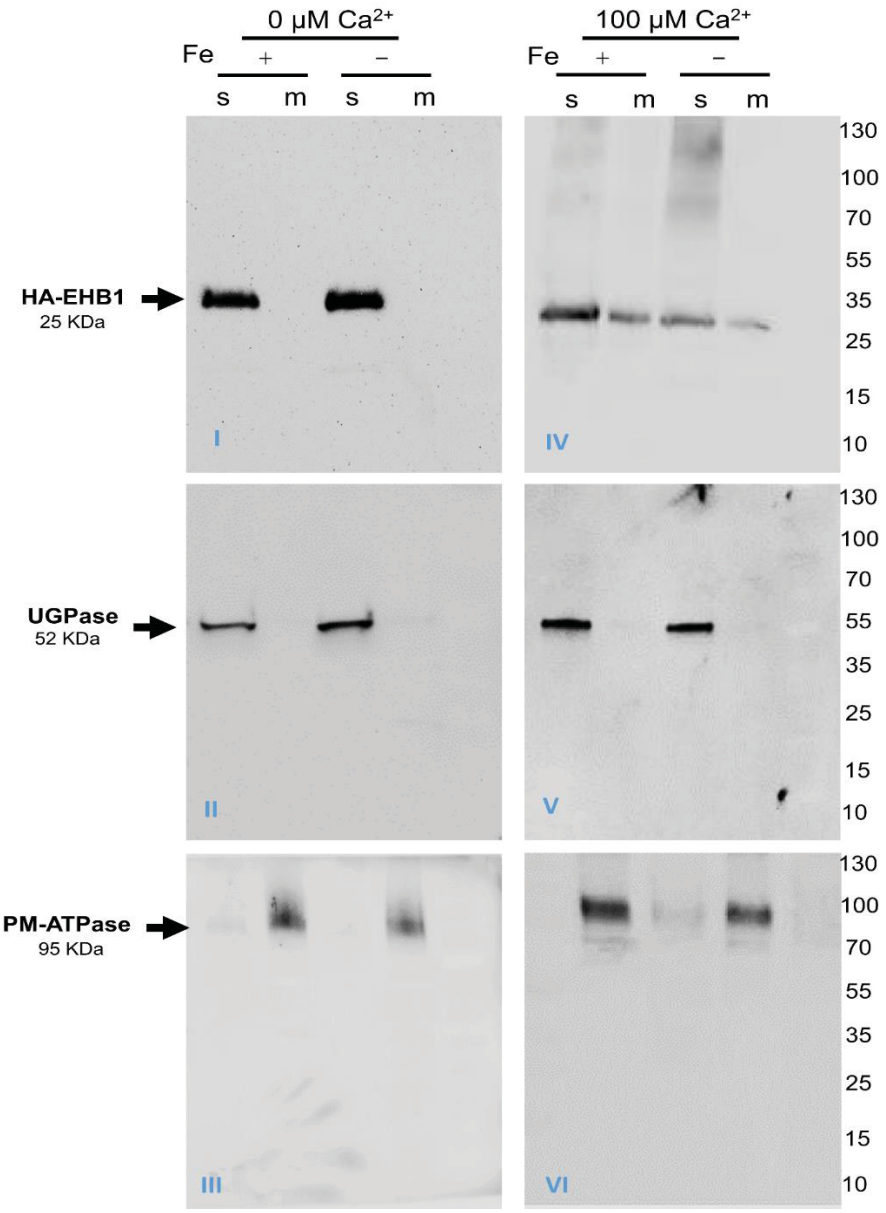

Supplemental Figure S4. EHB1 membrane-association. Full images of the cell fractionation data shown in figure 4.7 in the main text. Protein immunoblot showing the presence of EHB1 in soluble (s) and microsomal fraction (m) of the protein extract from 8 days old seedling expressing HA-EHB1. The experiment was performed in the absence (0 µM, I-III) and presence (100 µM, IV-VI) of calcium in the extraction buffer. The samples were probed with antibodies against (II and V) cytoplasmic marker UGPase (52 kDa), (III and VI) plasma membrane marker H^+ATPase (95 kDa) and to detect (I and IV) HA-EHB1 (25 kDa) antibody against HA tag was used. In the absence of calcium, significant amount of EHB1 is present in the cytosolic soluble fraction, while the presence of calcium enhanced the amount of EHB1 in microsomal fraction. + and – represent +Fe and –Fe, s: soluble. m: microsomal fraction. KDa: kiloDalton

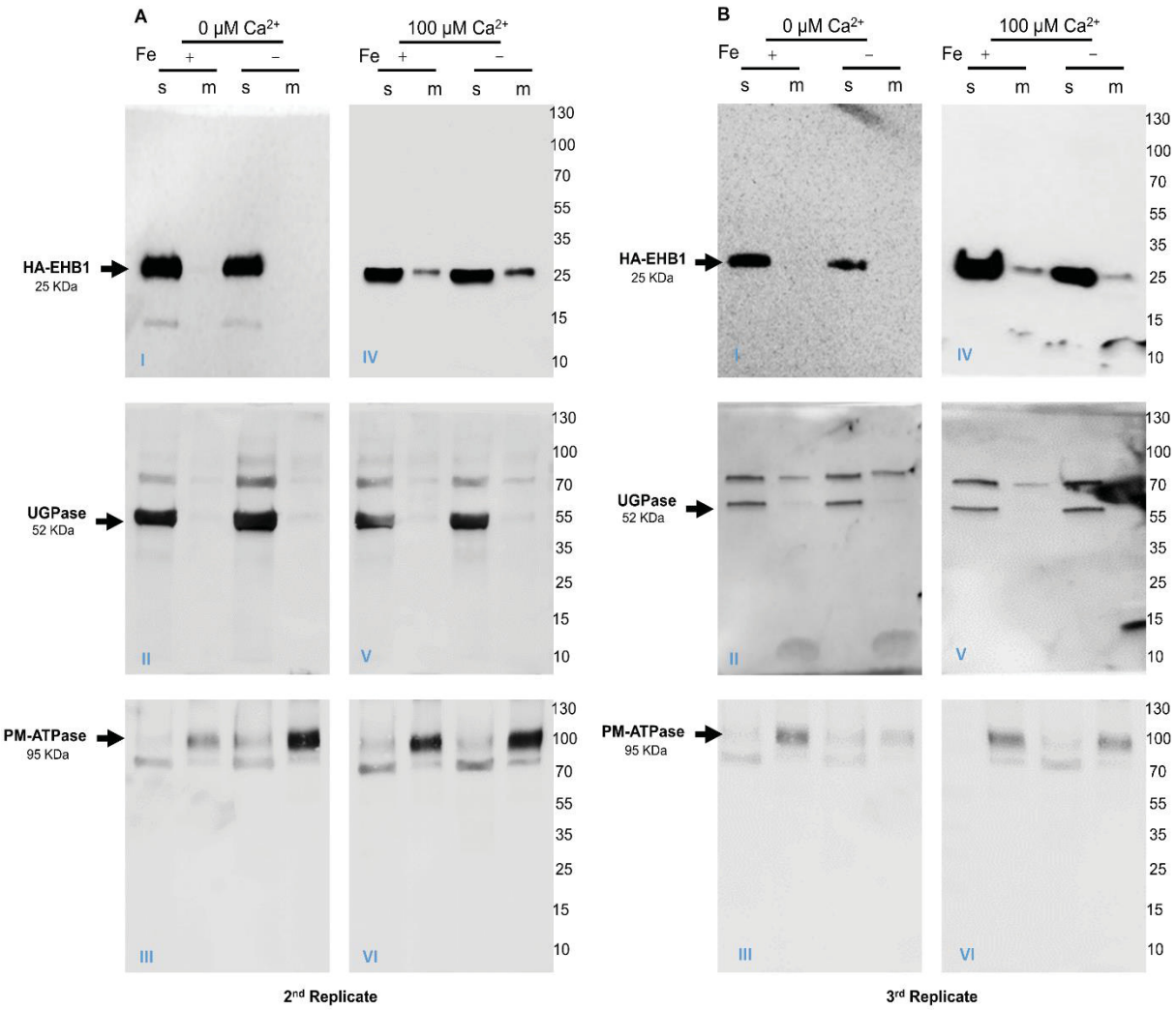

Supplemental Figure S5. EHB1 membrane-association 2nd and 3rd replicates. (A and B) Protein immunoblot showing the presence of EHB1 in soluble (s) and microsomal fraction (m) of the protein extract from 8 days old seedling expressing HA-EHB1. The experiment was performed in the absence (0 µM, I-III) and presence (100 µM, IV-VI) of calcium in the extraction buffer. The samples were probed with antibodies against (II and V) cytoplasmic marker UGPase (52 kDa), (III and VI) plasma membrane marker H^+ATPase (95 kDa) and to detect (I and IV) HA-EHB1 (25 kDa) antibody against HA tag was used. In the absence of calcium, significant amount of EHB1 is present in the cytosolic soluble fraction, while the presence of calcium enhanced the amount of EHB1 in microsomal fraction. The second band in s and m in II, III, V, and VI is binding immunoglobulin protein (BiP2, 73 kDa) probed with anti-BiP2 antibody. + and – represent +Fe and –Fe, s: soluble. m: microsomal fraction. KDa: kiloDalton

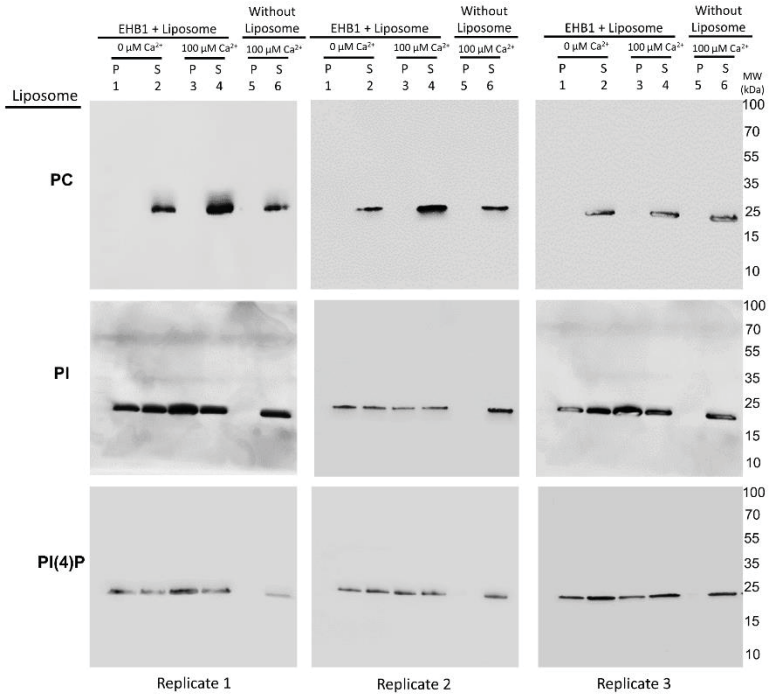

Supplemental Figure S6. Liposome binding assay for EHB1 binding to PI and PI(4)P three replicates. Following incubation with StrepII-EHB1, the liposomes were pelleted and the pellet (P, membrane), and soluble (S) fractions analyzed by immunoblot. Presence of StrepII-EHB1 in the membrane fraction (P) indicates binding. EHB1 bind to PI and PI(4)P both in the presence (100 µM) and absence (0 µM) of calcium. While it did not bind to PC. PC: phosphatidylcholine, PI: phosphatidylinositol, PI(4)P: phosphatidylinositol 4 phosphate. MW: molecular weight, P: pellet, S, soluble, KDa: kiloDalton

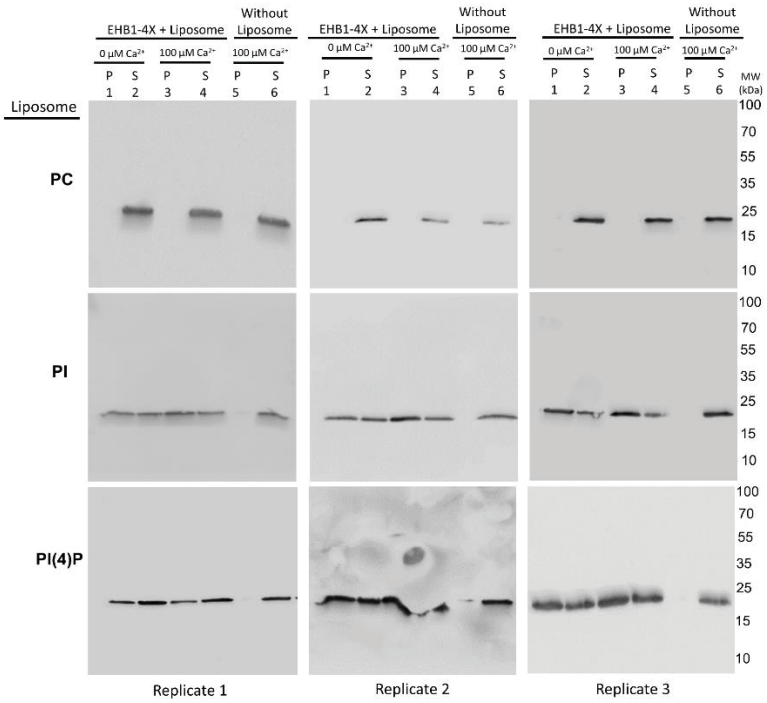

Supplemental Figure S7. Liposome binding assay for EHB1-4X binding to PI and PI(4)P three replicates. Following incubation with StrepII-EHB1-4X, the liposomes were pelleted and the pellet (P, membrane), and soluble (S) fractions analyzed by immunoblot. Presence of StrepII-EHB1-4X in the membrane fraction (P) indicates binding. EHB1-4X bind to PI and PI(4)P both in the presence (100 µM) and absence (0 µM) of calcium. While it did not bind to PC. PC: phosphatidylcholine, PI: phosphatidylinositol, PI(4)P: phosphatidylinositol 4 phosphate. MW: molecular weight, P: pellet, S, soluble, KDa: kiloDalton

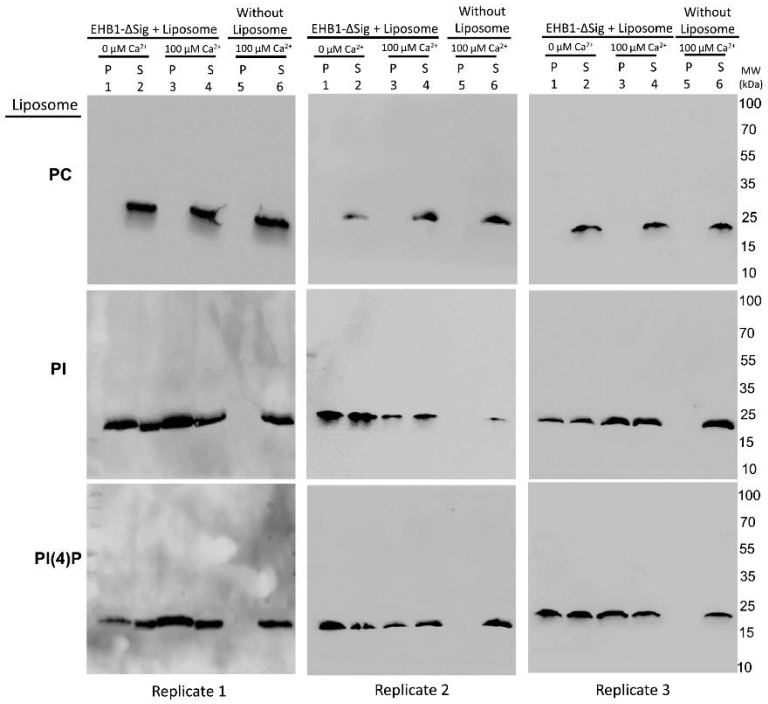

Supplemental Figure S8. Liposome binding assay for EHB1-ΔSig binding to PI and PI(4)P three replicates. Following incubation with StrepII-EHB1-ΔSig, the liposomes were pelleted and the pellet (P, membrane), and soluble (S) fractions analyzed by immunoblot. Presence of StrepII-EHB1-ΔSig in the membrane fraction (P) indicates binding. EHB1-ΔSig bind to PI and PI(4)P both in the presence (100 µM) and absence (0 µM) of calcium. While it did not bind to PC. PC: phosphatidylcholine, PI: phosphatidylinositol, PI(4)P: phosphatidylinositol 4 phosphate. MW: molecular weight, P: pellet, S, soluble, KDa: kiloDalton

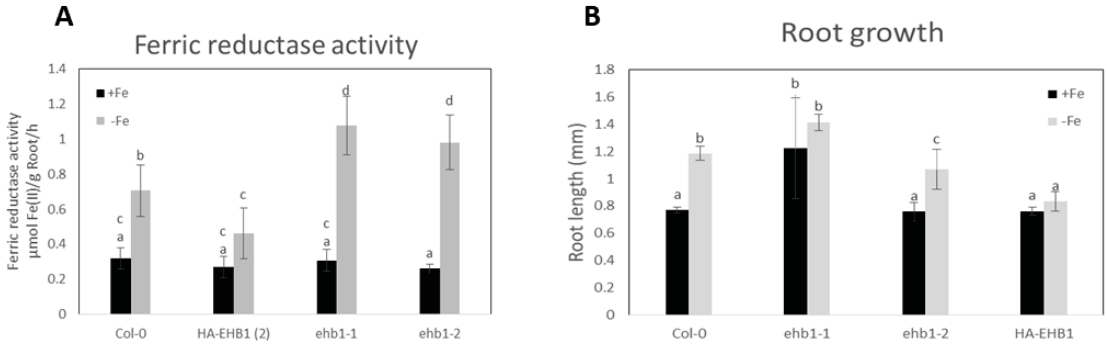

Supplemental Figure S9. Repetition of the data shown in figure 4.11. C and E in the main text.
(A) Iron reductase activity of 17 d old seedlings grown on ± Fe medium (14 d +Fe and 3 d ± Fe). The reductase activity of *ehb1-1* and *ehb1-2* is significantly higher than WT and HA-EHB1(2) at –Fe condition. Error bars represent standard deviation (SD) of the mean (n = 5). (B) Root lengths of Col-0, *ehb1-1*, *ehb1-2* and HA-EHB1 plants grown for 8 d under +Fe or –Fe conditions. Error bars represent SD of the mean (n = 15), root length was calculated using Jmicrovision-1.2.7. Roots of the EHB1 mutant *ehb1-1* and *ehb1-2* grows longer at –Fe condition. Letters indicate statistical significance obtained with one way ANOVA-Tukey's $P < 0.05$.

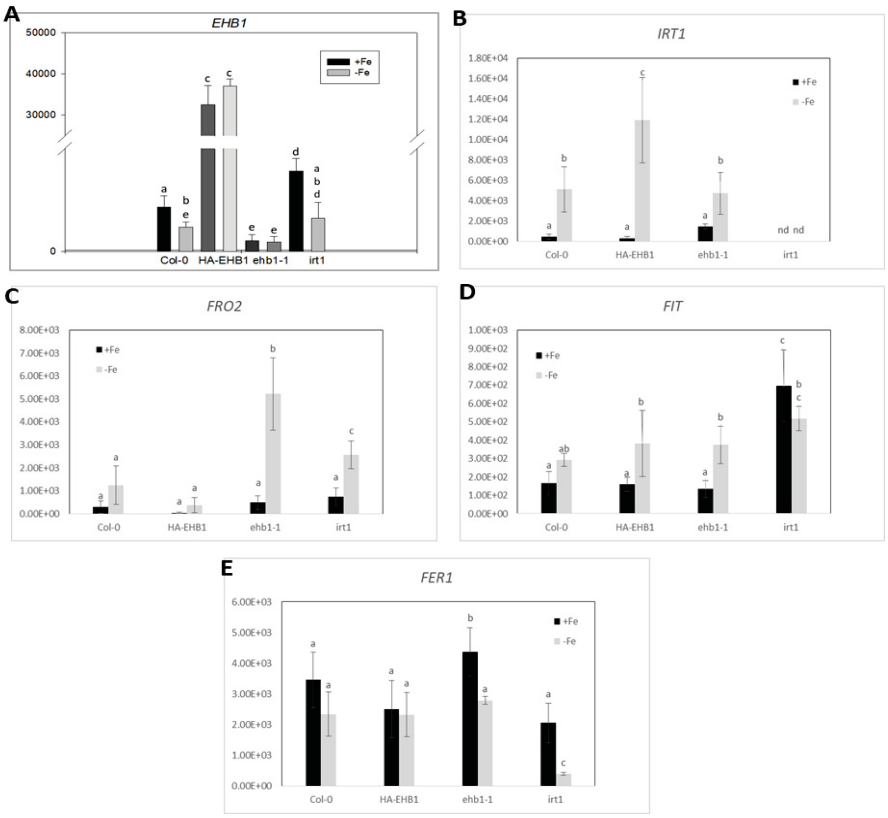

Supplemental Figure S10. Repetition of the data shown in figure 4.13 in the main text. Seeds were germinated and grown for 2-weeks growth system (14 d +Fe and 3 d ± Fe). Roots were harvested and processed to determine gene expression by quantitative RT-qPCR. The genes (A) *EHB1*, (B) *IRT1*, (C) *FRO2*, (D) *FIT* and (E) *FER1* were investigated. Bars represent expression level under sufficient-iron (50 mM Fe; black) and deficient-iron (0 mM Fe; grey) conditions. Error bars represent SD of the mean (n = 3). Letters indicate statistical significance difference obtained with one way ANOVA-Tukey's $P < 0.05$.